# Near-Ultraviolet Properties of a Large Sample of Type Ia Supernovae as Observed with the *Swift* UVOT

Peter A. Milne[1], Peter J. Brown[2], Peter W. A. Roming[2], Stephen T. Holland[3,4], Stefan Immler[3,4], Alexei V. Filippenko[5], Mohan Ganeshalingam[5], Weidong Li[5], Maximilian Stritzinger[6], Mark M. Phillips[6], Malcolm Hicken[7], Robert P. Kirshner[7], Peter J. Challis[7], Paolo Mazzali[8,9], Brian P. Schmidt[10], Filamena Bufano[3,11], Neil Gehrels[3], and Daniel Vanden Berk[2,12]

## ABSTRACT

We present ultraviolet (UV) and optical photometry of 26 Type Ia supernovae (SNe Ia) observed from March 2005 to March 2008 with the NASA *Swift* Ultraviolet and Optical Telescope (UVOT). The dataset consists of 2133 individual observations, making it by far the most complete study of the UV emission from SNe Ia to date. Grouping the SNe into three subclasses as derived from optical observations, we investigate the evolution of the colors of these SNe, finding a high degree of homogeneity within the normal subclass, but dramatic differences between that group and the subluminous and SN 2002cx-like groups. For the normal events, the redder UV filters on UVOT ($u$, $uvw1$) show more homogeneity

[1]University of Arizona, Steward Observatory, 933 N. Cherry Ave., Tucson, AZ 85719.

[2]Pennsylvania State University, Department of Astronomy & Astrophysics, University Park, PA 16802.

[3]NASA-Goddard Space Flight Center, Astrophysics Science Division, Codes 660.1 & 662, Greenbelt, MD 20771.

[4]Universities Space Research Association, Columbia, MD 21044.

[5]Department of Astronomy, University of California, Berkeley, CA 94720-3411.

[6]Las Campanas Observatory, Carnegie Observatories, Casilla 601, La Serena, Chile.

[7]Harvard-Smithsonian Center for Astrophysics, 60 Garden St., Cambridge, MA 02138.

[8]INAF, Observatorio Astronomico di Padova, Vicolo dell'Osservatorio 5, I-35122 Padova, Italy

[9]Max-Planck-Institut für Astrophysik, Karl-Schwartzschild-Str. 1, D-85748 Garching, Germany.

[10]Australian National University, Mt. Stromlo Observatory, The Research School of Astronomy and Astrophysics, Weston Creek, ACT 2611 Australia.

[11]Universita' degli Studi di Padova, Dipartmento di Astronomia, Padova, Italy 35122

[12]St. Vincent College, 300 Fraser Purchase Rd., Latrobe, PA 1560-2690.

than do the bluer UV filters ($uvm2$, $uvw2$). Searching for purely UV characteristics to determine existing optically based groupings, we find the peak width to be a poor discriminant, but we do see a variation in the time delay between peak emission and the late, flat phase of the light curves. The UV light curves peak a few days before the $B$ band for most subclasses (as was previously reported by Jha et al. 2006a), although the SN 2002cx-like objects peak at a very early epoch in the UV. That group also features the bluest emission observed among SNe Ia. As the observational campaign is ongoing, we discuss the critical times to observe, as determined by this study, in order to maximize the scientific output of future observations.

*Subject headings:* cosmology: distance scale — ISM: dust, extinction — galaxies: distances and redshifts — supernovae: general — ultraviolet: general

## 1. Introduction

A Type Ia supernova (SN Ia), driven by a thermonuclear explosion of a white dwarf generally near the Chandrasekhar limit, is an exceedingly luminous event ($L \approx 4 \times 10^9$ $L_\odot$), among the most powerful phenomena in the universe. This characteristic, combined with a relatively modest observed dispersion in the peak luminosity, has led to considerable interest in utilizing Type Ia supernovae (SNe Ia) to study the expansion history of the universe; see (Filippenko 2005) for a review. The factor of $\sim$10 variation in peak luminosity has been shown to correlate with observable features in the SN emission, making SNe Ia standardizable candles at the level of $\sim$8% in distance (see, e.g., Jha et al. 2007, and references therein). They have been used to measure the Hubble constant (e.g., Freedman et al. 2001; Riess et al. 2005; Riess et al. 2009), and were the first objects to clearly reveal the current acceleration of the universe (Riess et al. 1998; Perlmutter et al. 1999). There is also the desire to understand the progenitor systems, nucleosynthetic products, explosion mechanisms, and remnants of SNe Ia.

Based largely on the nature of the optical emission, SNe Ia have been categorized according to the width of the peak of their optical light curves (Phillips 1993; Hamuy et al. 1996b; 7; Phillips et al. 1999; Wang et al. 2003), their overall optical spectra (e.g., Filippenko et al. 1992a; Filippenko et al. 1992b; Phillips et al. 1992; Leibundgut et al. 1993), the velocity gradient of the Si II $\lambda$6355 absorption line (Benetti et al. 2005), the nature of "high velocity" absorption features in the early-epoch spectra (Mazzali et al. 2005), the width of the nebular emission lines (Mazzali et al. 1998), and so on. Decades of observational and theoretical investigations have led to the emerging understanding that there may be multiple paths for

a white dwarf in a binary star system to reach the critical mass for a thermonuclear runaway, and that advancing our understanding of these events depends, in part, on broadening the wavelength range of observations.

Observations at near-infrared (NIR) and ultraviolet (UV) wavelengths have led to an improved understanding of SNe Ia in a variety of ways. There are spectral features in the NIR and/or UV that either provide unique information or are less ambiguous than optical features alone. An appreciable fraction of the bolometric luminosity ($\leq 20\%$) is emitted outside the optical wavelength range (e.g., Wang et al. 2009a), making NIR/UV observations important to minimize the fraction of the bolometric luminosity that is extrapolated from the observed wavelength range.[1] The availability of ground-based NIR instruments has led to considerable progress in our understanding of SNe Ia in this wavelength range. Several of the major observational programs for SNe Ia include NIR observations of the nearest SNe Ia, notably the CfA Supernova Program which employs PAIRITEL (Bloom et al. 2006) and the Carnegie Supernova Project (CSP; Hamuy et al. 2006). NIR light curves are being studied to determine if the entire range of SN Ia events can be considered standard candles (Krisciunas et al. 2004; Wood-Vasey et al. 2008). Observations are also being expanded toward the bluest emission observable from the ground. Jha et al. (2006a) presented "CfA2," a $UBVRI$ study of 44 SNe Ia collected during the years 1997–2000, with an emphasis on the completeness of the $U$-band survey. Hicken et al. (2009) presented "CfA3," a $UBVRI$ study of an additional 185 SNe Ia. current, ongoing campaigns include $U$-band or $u$-band photometry, with the promise of dramatically increasing the number of SNe Ia with well-sampled $U$ or $u$ light curves.

Recognizing the importance of UV observations, SNe Ia have been observed with space-based UV satellites for over 30 years. The *International Ultraviolet Explorer (IUE)* observed 12 SNe Ia over 13 years (see Panagia 2007 for a summary), with the most extensive campaigns being 7 observations of SN 1990N (Jeffery et al. 1992) and 7 observations of SN 1992A (Kirshner et al. 1993; also see (Branch & Venkatakrishna 1986)). The *Hubble Space Telescope (HST)* has obtained UV spectra of 10 SNe Ia, with notable campaigns on SNe 1992A (Kirshner et al. 1993), 2001eh and 2001ep (Sauer et al. 2008), and 2005cf (Wang et al. 2009a). These observations have afforded insight into the nature of the UV emission from SNe Ia, and have been the basis for characterizing the UV portion of the bolometric luminosity. A theoretical understanding of the UV flux is slowly emerging, as radiative-transfer models are tested against these observations in an effort to reproduce the fundamental characteristics of the UV spectrum (Pauldrach et al. 1996; Fisher et al. 1997;

[1]This was well illustrated by observations of the peculiar SN 2000cx, where the $\gtrsim$400 day NIR emission exhibited a plateau, while the optical emission followed a linear decline (Sollerman et al. 2004).

Höflich et al. 1996; Mazzali et al. 2001; Lentz et al. 2001; Sauer et al. 2008). Foley et al. (2008b) present a collected study of *IUE* and *HST* observations, in particular finding a tentative correlation between light-curve peak width and a flux ratio of two UV wavelength bands, possibly providing a means of classifying SNe Ia based only on UV emission. Despite these successes, however, it is clear that our understanding of the UV emission in SNe Ia has been rather limited.

The Ultraviolet and Optical Telescope (UVOT; Roming et al. 2005) onboard the NASA *Swift* satellite (Gehrels et al. 2004) possesses a number of characteristics that make it useful for SN Ia studies. First, the telescope is one of only a handful capable of detecting UV emission from nearby SNe Ia.[2] For the very nearest subset, UV spectra have been obtained and will be presented by Bufano et al. (2009). Second, the primary science goal of the *Swift* mission, prompt follow-up observations of gamma-ray bursts (GRBs), permits a large fraction of the total time for secondary targets. UVOT can monitor a SN Ia daily for weeks, obtaining unprecedented temporal sampling of a variety of SNe Ia. Third, scheduling of targets can be arranged in less than 24 hours for important transients, including SNe. Indeed, SN 2006bp, a Type IIP SN, was observed within 24 hours of discovery, which was within 2.5 days after the explosion (Immler et al. 2007). This prompt scheduling led to the discovery of short-lived X-ray emission from SN 2006bp, a discovery that would not be possible with a less agile observatory, where all schedule changes require a much longer delay.

Between March 2005 and March 2008, UVOT observed 28 SNe Ia. In this paper, we work with the photometry of 25 of these events. In §2, we introduce the UVOT instrument and the analysis methods employed to accurately determine the UV emission from the observed SNe Ia. The SN Ia sample is detailed in §3, including the categorizations possible from ground-based optical observations. In §4, we fit the light curves of the well-observed events, comparing their UV behavior to parameters that have been defined in the past based upon the optical emission. Section 5 presents the UV to optical, as well as UV to UV, colors of all the SNe Ia included in this study. We discuss in §6 how these observations have improved the understanding of SNe Ia. The absolute UV magnitudes of our SNe Ia at peak brightness are not given in this paper; instead, the peak apparent magnitudes derived here contribute to a companion paper (Brown et al. 2010, hereafter B10) that explores the UV emission from SNe Ia as a potential standard candle.

---

[2]GALEX is another UV telescope that has observed SNe during the period of these UVOT observations (Gezari et al. 2008; Gal-Yam et al 2008). See Roming et al. (2009) for a review of 4 current UV-capable missions.

## 2. UVOT Analysis and Photometry

The UVOT has an aperture of 30-cm, and is equipped with a photon-counting detector sensitive to emission in the 1600–8000 Å wavelength range. The effective UVOT field of view is $17' \times 17'$, with a point-spread function (PSF) of $\sim 2''$ full width at half-maximum intensity (FWHM). UVOT features six filters, with three in the UV wavelength range ($uvw2$, $\lambda_c \approx 1928$ Å; $uvm2$, $\lambda_c \approx 2246$ Å; $uvw1$, $\lambda_c \approx 2600$ Å) and three in the optical ($u$, $b$, $v$). The filter transmission curves are shown in Figure 1, compared to the *HST* $F220W$ and $F250W$ filters.

The $uvw1$ filter transmission peaks at a wavelength similar to that of the *HST* $F250W$ and $F275W$ filters; however, the $uvw1$ filter has greater sensitivity to redder-wavelength emission. For the *HST* SN 1992A spectrum, this $uvw1$ "red leak" leads to 52% of the emission emanating from wavelengths longer than 3000 Å compared to 36% and 46% for the $F250W$ and $F275W$ filters, respectively. The $uvw2$ filter transmission peaks at ∼1900 Å, but also has sensitivity to redder-wavelength emission. Using the *HST* SN 1992A spectrum, the $uvw2$ red leak leads to 44% of the emission emanating from wavelengths longer than 3000 Å compared to 10% for the *HST* $F220W$ filter. Due to the observed tendency of SN emission to peak toward the red edge of each filter, the filter center is not the ideal wavelength for characterizing each filter. As extinction further reddens the SN emission, highly extinguished SNe Ia suffer the most from this effect. For our study, we treat the highly extinguished SNe Ia separately in order to minimize this effect. UV photometry of SN 2005cf shows encouraging agreement between UVOT and *HST* filters ($F250W/uvw1$, $F220W/uvm2$; Wang et al. 2009a).

In our companion paper (B10), a spectrum of SN 1992A (Fig. 1) is employed to approximately remove the red leak from the $uvw1$ and $uvw2$ filters, creating $uvw1_{rc}$ and $uvw2_{rc}$ pseudofilters. That paper concentrates on the absolute near-UV magnitudes of SNe Ia, which justifies the additional effort to create pseudofilters. Here we present the original photometry with a note of caution that, especially for the $uvw2$ filter, the light collected is not entirely near-UV emission.

The $uvm2$ filter is a medium-bandpass filter optimized for the 2000–2500 Å wavelength range. This filter has the advantage of having a sharp red cutoff, so it has the largest fraction (99%) of its total emission blueward of 3000 Å for the *HST* SN 1992A spectrum. The disadvantage of this filter is that the narrow bandpass leads to lower signal-to-noise ratios for our SN sample. As the $uvw2$ and $uvm2$ filters feature a high degree of overlap, we will emphasize the comparison and contrast between the features seen in each filter.

The UVOT $u$-band filter detects bluer emission than ground-based $U$-band filters. Al-

though the instrumental filter transmission curves are similar for ground-based systems with optimal blue sensitivity, the atmospheric absorption of light toward the blue edge of the ground-based $U$ band results in the UVOT $u$ band being more sensitive to light in the $\sim$3000–3500 Å range. As atmospheric conditions change by site and by night, comparisons between ground-based $U$-band systems are particularly difficult (Suntzeff 1996). One goal for future investigations is to attempt such comparisons by determining whether the differences between spectral responses can account for the differences between UVOT $u$-band photometry and photometry in the $U$ band from various ground-based systems, employing S-corrections (see Stritzinger et al. 2002).

In this work, we include ground-based $U$-band photometry for a handful of SNe Ia to give the reader the ability to compare our findings with previous studies. In situations where the same SN was observed with both the ground-based $U$ and UVOT $u$ systems, we briefly discuss the level of agreement between the two photometric sets, and we use this to estimate how much UVOT $u$ and ground-based $U$ photometry can differ.

The UVOT $b$ and $v$ filters are largely comparable to ground-based $B$ and $V$ systems. As this paper concentrates on the UV filters, we will present S-corrections between UVOT filters and ground-based systems elsewhere.

A large fraction of the observed SNe occurred in regions where emission from the host galaxy was an important consideration. The methodology of host-galaxy removal is different for the UVOT detector than for standard CCD photometry, due to the photon-counting nature of the UVOT detector. After obtaining a post-SN image, rather than subtracting that image from the science images, the $3''$ aperture is placed at the location of the SN in the post-SN image and the counts attributed to the host galaxy are subtracted from the SN counts. This is dictated by coincidence loss (similar to pile-up in X-ray instruments), which makes it critical to account for the full number of counts in each pixel in every image. See Brown et al. (2009) for a complete description of the method employed.

The majority of our SN photometry comes from Brown et al. (2009). UVOT photometry of SN 2007ax is from Kasliwal et al. (2008), while UVOT photometry of SN 2008ha is from Foley et al. (2009) and UVOT photometry of SN 2007gi is from Wang et al. (in preparation). In Appendix A, we present new UVOT photometry for SNe 2005mz, 2007on, 2007sr, 2008A, 2008Q, and 2008ec following the same photometric procedure and galaxy subtraction as in Brown et al. (2009).

## 3. UVOT SN Ia Sample

Between March 2005 and March 2008, *Swift* UVOT observed 28 SNe Ia, and we have chosen to include 25 of those 28 in this study. SNe 2005bc and 2005gj were detected at a single epoch in the UV filters, and are not included here. SN 2007bm suffered from high extinction, with the additional difficulty of the host-galaxy count rate being very high in the $b$ and $v$ bands. It is excluded from this work, but UVOT photometry will be combined with ground-based photometry for inclusion in a future study that uses SNe Ia to probe extinction (see §5.1.4).

### 3.1. SN Ia Subclasses

It has long been recognized that there exists diversity in both the light curves and optical spectra among the events categorized as SNe Ia (see Filippenko 1997 for a review). Subsequent to the recognition of this diversity, there was the development of a single-parameter categorization that placed individual events along a continuum of SNe Ia. This single parameter has been based upon the light-curve shape ($\Delta m_{15}(B)$: (Phillips 1993; Hamuy et al. 1996b); $\Delta$: (7; Jha et al. 2006b); stretch: (Goldhaber et al. 2001)); $C_{12}$: (Wang et al. 2003)), spectral features (Nugent et al. 1995; Hachinger et al. 2008), and colors at peak ($B-V$: (Phillips et al. 1999; Garnavich et al. 2004); $U-B$: (Jha et al. 2006a)), with a high level of correlation between the various techniques. The large majority of SNe Ia have been suitably categorized by these parameters, but there have been notable outliers from single-parameter categorization (e.g., Li et al. 2001; Li et al. 2003).

Of the SNe Ia that are suitably categorized by a single parameter, we will present the events according to their $B$-band decline in the first 15 days after maximum brightness, the $\Delta m_{15}(B)$ value. This parameter has the benefit of simplicity, and our categorization does not require high precision. We separate normal and superluminous events from subluminous events at $\Delta m_{15}(B) \approx 1.6$ mag; the fast-declining SNe Ia are typically subluminous (e.g., SN 1991bg, Filippenko et al. 1992b; Leibundgut et al. 1993). We do not discriminate between normal and superluminous events (e.g., SN 1991T, Filippenko et al. 1992a; Phillips et al. 1992). None of the SNe in this study are of the peculiar "overluminous" group (possibly super-Chandrasekhar mass; Howell et al. 2006; Hicken et al. 2007); however, SN 2009dc (Yamanaka et al. 2009) is a member of that group and it will be included in our follow-up studies. We note that a number of observed characteristics of SNe Ia show that the normal and/or superluminous events vary relatively little, whereas subluminous events can differ appreciably. Examples of this are the peak $B-V$ colors (Garnavich et al. 2004), the late-time optical light curves (Milne, The, & Leising 2001), and the peak $U-B$ col-

ors (Jha et al. 2006a). The subluminous events are redder than normal events, and feature lower expansion velocities, lower $^{56}$Ni yields, stronger Ti II lines, lower ionization, and possibly higher intrinsic polarization (Filippenko et al. 1992b; Leibundgut et al. 1993; Howell et al. 2001; Garnavich et al. 2004).

There are indications of variations within the group of "normal" SNe Ia. It has been suggested that the velocity of the absorption lines of intermediate-mass elements in the spectra near peak brightness might permit subdivision of the normal subclass (Benetti et al. 2004; Benetti et al. 2005; Wang et al. 2006; Wang et al. 2008). This subdivision distinguishes high-velocity (HV) normal SNe Ia from normal-velocity normal SNe Ia, with the inference that the HV group might have different progenitor properties and/or the presence of circumstellar matter (CSM) surrounding the SN event. Wang et al. (2009b) applied this method to a large sample of normal SNe Ia, including a majority of the normal events in this study.

As mentioned above, some SNe Ia are not suitably categorized by these single parameters. Their anomalous nature can reveal itself in light curves explainable by none of the range of templates, or by spectral characteristics that do not match expectations based upon the light-curve shapes. In particular, SN 2002cx (Filippenko 2003; Li et al. 2003) has emerged as the namesake event for an emerging subclass of SNe Ia. SN 2002cx-like events are characterized by high-ionization iron lines in the premaximum spectra, but low expansion velocities and low peak luminosities (Jha et al. 2006b; Phillips et al. 2007; Valenti et al. 2009; Foley et al. 2009). Furthermore, the $R$ and $I$-band light curves did not feature the normal secondary maxima. It has been suggested that this subclass of SNe Ia may be due to a deflagration, rather than a delayed detonation (Phillips et al. 2007). Alternatively, perhaps SN 2002cx-like events are not of thermonuclear origin, but rather a variety of stripped-envelope, core-collapse events (Valenti et al. 2009, but see Foley et al. 2009).

### 3.2. SN Ia Sample

All of the SNe presented in this study were also observed with ground-based telescopes. Those observations have been used with the UVOT data to categorize the SNe in this sample. The Carnegie Supernova Project (CSP) observed SNe 2005am, 2005hk, 2005ke, 2007co, 2007cq, 2007cv, 2007gi, and 2007on. The Harvard-Smithsonian Center for Astrophysics supernova program (CfA) observed SNe 2005am, 2005cf, 2005hk, 2005ke, 2005mz, 2006ej, 2007S, 2007af, 2007ax, 2007co, 2007cq, 2007cv, and 2008A. Using the 0.76-m Katzman Automatic Imaging Telescope (KAIT; Filippenko et al. 2001; Filippenko 2003) at Lick Observatory, the U. C. Berkeley SN group observed SNe 2005am, 2005cf, 2006dm, 2006ej, 2007co, 2007cq, and 2008ha. The Australian National University observed SN 2005df; that

photometry is presented in Appendix B.

Tables 1 and 2 show the basic optical parameters for each SN Ia included in this study. When multiple $\Delta m_{15}(B)$ values were available, we use the average of the values in Tables 1 and 2. Fifteen of the SNe have $\Delta m_{15}(B)$ values (hereafter referred to as "decline rates") less than 1.6 mag, by far the largest group. Two more SNe Ia do not have known $\Delta m_{15}(B)$ values, one was spectroscopically categorized as a member of the normal subclass (2006E), the other as a member of the SN 2002cx-like subclass (2008A). Five have faster decline rates, with a few of the SNe with undetermined decline rates being likely members of this subclass based upon spectroscopic properties. The optically brightest events, in terms of apparent magnitude, were SNe 2005cf, 2005df, and 2007af; they are three of the best-studied SNe Ia in the sample. The high-velocity normal SNe Ia are listed in column 4 as "NHV," the normal-velocity normal SNe Ia as "NNN," and the normal SNe Ia with undetermined absorption velocity features as "N."

## 4. Fitting Light Curves

For the best-sampled subset of the UVOT SN Ia dataset, the fitting of functions to the multi-band light curves permits the direct study of individual events. We explore specifically the UV light curves compared to the optical light-curve shapes for the purpose of probing the SN Ia events. The derived peak magnitudes contribute to the absolute-magnitude study presented by B10. We also emphasize considerations related to the utilization of SNe Ia as very high-redshift distance indicators. Observations of SNe Ia at very high redshifts sample little or none of the rest-frame optical wavelength range, so individual events must be categorized according to their rest-frame UV emission. In this section, we explore possible indicators of SN Ia subclass from UV emission.

### 4.1. Fitting with Functions

Fifteen SNe Ia were determined to be adequately observed in the UVOT $uvw1$ filter to warrant fitting the light curves with functions. Seven SNe Ia were well observed in the $uvw2$ filter, ten in the $u$ and $b$ filters, and twelve in the $v$ filter.

The complete function chosen contains four terms: a Gaussian rise to peak, an initial Gaussian decline, a middle-epoch linear decline, and a late-epoch linear decline (Fig. 2). In total, eight parameters are used for the complete function ("cmplt"), as follows:

$$m = \begin{cases} A_0 - 2.5\log_{10}(\exp(A_1(t-t_p)^2)) & \text{(before peak)} & t \le t_p, \\ A_0 - 2.5\log_{10}(\exp(A_2(t-t_p)^2)) & \text{(Gaussian decline)} & t_p \le t \le t_{br1} \\ A_0 - 2.5\log_{10}(\exp(A_2(t_{br1}-t_p)^2)) + A_3(t-t_{br1}) & & \\ & \text{(steep linear decline)} & t_{br1} \le t \le t_{br2} \\ A_0 - 2.5\log_{10}(\exp(A_2(t_{br1}-t_p)^2)) + A_3(t_{br2}-t_{br1}) & & \\ \qquad +A_4 * (t-t_{br2}) & \text{(late linear decline)} & t \ge t_{br2}. \end{cases}$$

The fitting function is not physically motivated; it was chosen with the goal of approximating the light curves with the minimum number of parameters. We follow the methodology of Contardo, Leibundgut, & Vacca (2000), who note that Pinto & Eastman (2000) predict a Gaussian shape for the peak in models with constant opacity and $^{56}$Ni buried well within the ejecta. The fitted light curves are shown in Figures 3–8. Tables 3, 4, and 5 show parameters derived from those fits.

For many of the SNe, the campaigns were incomplete, being sparsely sampled in one of the four epochs. For these SNe, the adopted model either eliminated the late-epoch linear decline ("mid": $A_4$ term) or both linear declines ("peak": $A_3$ and $A_4$ terms). SNe poorly sampled at peak but well observed post-peak were fitted with "fix-peak" models, where the $A_1$ and $A_2$ terms were fixed to be 0.013 and 0.008, respectively ("FXPKLATE": fit $A_0$, $A_3$, and $A_4$; "FXPK": fit $A_0$ and $A_3$). SNe only observed at late epochs were fit with a straight line ("LINEAR"). For all models, the fitted parameters were not constrained, but SNe Ia that were best fitted with models in which the peak, first time break, and second time break were not positively separated in time were fit instead with "fix-peak" models. In all cases, we attribute the fitting problems to be a result of sparse sampling, and we treat those SNe in §4.2. Removing a decline epoch results in elimination of two parameters. The model used for each SN is listed in Table 3. We note that for SN 2005ke, the dataset was truncated about 25 days after the late break for fitting, as the light-curve shape differs appreciably from the function shown above.

The $uvw1$, $uvw2$, and $u$ bands all peak days earlier than the $b$ band. This can be seen by comparing (in Tables 3 and 4) columns 2, 7, and 13 with column 18. (Jha et al. 2006a) report that the $U$ band peaks $2.3 \pm 0.4$ days before the $b$ band for their sample of 44 SNe Ia. We find similar early peaking for a smaller sample. One SN Ia stands out as peaking much earlier (5.6 days), SN 2005hk. The UV peaks of SN 2005hk were not well constrained at early epochs, but were definitely earlier than the normal SNe Ia. We will show in §5 that this is consistent with the UV color curves, where the bluest emission was seen in the first observations.

Using the information obtained from fitting the normal SNe Ia (Fig. 3), we fixed the peak parameters to fit the $uvw1$ light curves of four normal SNe Ia either observed only

post-peak (SNe 2005am, 2006ej, 2006E) or observed before the peak phase, but not within 5 days of the peak (SN 2006dd). The resulting fitted light curves are shown in Figure 4. The light curves either exhibit a late break, or constrain such a break to being later than 20 days past maximum brightness.

#### *4.1.1. The $\Delta m_{15}(i)$ Parameter*

As a check of the fitting outputs for UVOT data, in the lower-right panel of Figure 9 we compare the $\Delta m_{15}(b)$ values from fitting the UVOT data to the $\Delta m_{15}(B)$ values from ground-based telescopes (see Tables 1 and 2 for references). There is reasonable agreement between the two methods, as the mean $\Delta m_{15}(b)$ - $\Delta m_{15}(B)$ (i.e., UVOT minus literature) value of $-0.02 \pm 0.12$ mag is consistent with zero.

Extending the comparisons of the UVOT study to other ground-based studies, the UVOT $v$-band values in the $\Delta m_{15}(b)$ versus $\Delta m_{15}(v)$ plane (Fig. 9, upper-right panel) agree well with the (Hamuy et al. 1996b) templates and with 101 SNe Ia in the CfA3 study. Comparing $\Delta m_{15}(b)$ versus $\Delta m_{15}(u)$ (Fig. 9, lower-left panel), we see that the UVOT $u$-band data largely agree with the 53 CfA3 SNe Ia and with the P. Nugent (2009, private communication) $U$-band templates for superluminous, normal, and subluminous SNe Ia. The CfA3 study suggests a correlation between $\Delta m_{15}(B)$ and $\Delta m_{15}(U)$. As the UVOT dataset generally agrees with the CfA3 dataset in terms of $\Delta m_{15}(B)$ and $\Delta \mathrm{m}_{15}(U)$, that suggestion is largely supported, albeit with increased scatter for the fast-declining events.

The comparison between $\Delta m_{15}(B)$ and $\Delta m_{15}(uvw1)$ can only be performed with UVOT data (Fig. 9, upper-left panel). This comparison is particularly interesting, as the peak width has been the dominant method used to determine SN Ia subclass for high-redshift SN searches. The trends are generally the same as seen for $\Delta m_{15}(B)$ versus $\Delta m_{15}(u)$, although for this comparison, SN 2005ke stands out with a relatively slow $uvw1$ decline rate. The decline rates are not as well distributed in $\Delta m_{15}(uvw1)$, appearing to clump at 1.3 and 1.6 mag.

For the goal of characterizing the SN subclass via purely UV observables, $\Delta m_{15}(uvw1)$ would be inadequate. This is of particular importance for the cosmological utilization of SNe Ia at high redshifts, where rest-frame UV emission would be shifted into optical or even NIR wavelength ranges. Although the peak width has been the dominant method used to determine SN Ia subclass for high-redshift SN searches for rest-frame optical emission, these light curves suggest that single-band UV light-curve peak widths would be inadequate to categorize precisely a given SN Ia.

The 5-day rise to peak and decline from peak are shown in Figure 10; clearly, within 5 days of peak brightness the light curves rise faster than they fall. There are no other obvious tendencies in the rise and decline rates relative to the optical decline rates, as correlation with the $\Delta m_{15}(B)$ parameter is not apparent to the statistical precision of these data (Fig. 10, upper-left and lower-left panels). There is the appearance of an inverse correlation between the 5-day rise and the 5-day decline (Fig. 10, lower-right panel), but many more SNe Ia need to be observed to further explore that possibility.

#### *4.1.2. Late Break to a Shallow Decline*

The delays between the peak in the $uvw1$ filter and the late break (at which time the light curves flatten) are shown in Figure 11. The normal SNe Ia have delays that cluster around ∼28 days, whereas the subluminous SNe 2005ke and 2007on and the SN 2002cx-like SN 2005hk break at far earlier epochs. This characteristic could be used to distinguish between normal SNe Ia and these other two subclasses if only rest-frame UV emission can be observed. Such an approach has been used in the optical wavelength range before (Pskovskii 1984; Hamuy et al. 1996b); it was even employed on one SN in our dataset, SN 2007ax, for the $B$ band (Kasliwal et al. 2008). Figure 12 shows $uvw1$-band light curves of SNe 2005ke and 2007on compared with those of a selection of normal SNe Ia. All SNe have been normalized to the same magnitude at $B_{\rm peak}$. The two subluminous SNe Ia have different light-curve shapes, but both break at earlier epochs than do the normal SNe Ia. SN 2005ke has a light-curve shape similar to that of the normal SNe Ia before the break, while SN 2007on has a narrower light curve peak before the break. SN 2005df is interesting in featuring a late break, but breaking to a shallow slope similar to that of SN 2007on.

The initial and late linear slopes, parameterized as $\beta$ and $\gamma$ respectively (Pskovskii 1984), have only been measured for a few SNe Ia (Table 5). A detailed study of the late-time light curves will be performed in a future work. It is worth noting that to date, no SN has been observed in the UV sufficiently well to determine $\gamma_1$ (50–150 days) and $\gamma_2$ (later than 150 days), a splitting of the late-time decline shown in the Salvo et al. (2001) study of SN 1996X.

One unfortunate aspect of utilizing the late-break delay to determine SN Ia subclass is the fact that the SN has faded from peak by as much as 4 mag before the existence of the late break is apparent. For magnitude-limited surveys, it might not be possible to observe a SN at "peak + 4" mag. This problem is similar to the problems that arise by trying to estimate the extinction via the Lira (1995) relation, where the SNe must be observed 60 or more days after the peak. Nonetheless, there is a clear difference between the subclasses in

this observed parameter, making it useful if no other observable can be found to perform the same task. The "$R_{\rm UV}$" ratio suggested by Foley et al. (2008b) is another potential observable. A worthwhile project would be to obtain both parameters, as well as optical information, for a collection of SNe Ia to test the accuracy of each as a SN subclass predictor. The appreciable scatter evident in Figure 11 suggests that the timing of the late break might only be useful to eliminate subluminous events from a sample.

#### *4.1.3. Limits of Stretch Fitting*

The stretch method has been employed in the optical bands to show that the light curves of a large range of SNe Ia can be explained as a function of only the timescale of the light-curve evolution. (Jha et al. 2006a) used stretch to fit $U$-band light curves of a collection of SNe Ia from $-10$ to $+40$ days relative to $B_{\rm peak}$ in the SN rest frame, following the formalism of Goldhaber et al. (2001). We have shown that the peak widths and late-break times of these SNe in the $uvw1$ filter do not support the idea that the entire range of normal to subluminous events can be explained with the stretch of a single, characteristic light-curve shape during that entire epoch. This is supported by the color evolution shown in Figure 16, which suggests that stretch can be suitably employed on the normal subclass (as they have similar color evolution and stretch has been employed with the $V$ band). However, the other subclasses have very different color evolution, so fitting with stretch would be at best approximate. Hicken et al. (2009) arrived at a similar conclusion with the $U$-band dataset of CfA3. The fact that the Nugent $U$-band templates cross, due to the flatness of the late-time light curves for the subluminous subclass, is further grounds for rejecting the use of stretch for the entire range of SN Ia events in the $U$ band or UV. That being said, subluminous SNe Ia are not large outliers in relations that compare the $U$-band stretch with other values as presented by (Jha et al. 2006a). We do not attempt to characterize exact ranges of SN subclass and epoch where stretch would be appropriate, as this will be better addressed at a later date with a larger sample.

### 4.2. Fitting Normal SNe Ia to a Mean Template

The similarity of the UV light curves of the normal SNe Ia suggests that a single, mean template could be generated for each filter. There are a number of advantages to creating a mean template, and comparing that against individual SNe Ia and light-curve templates in other filters: (1) the combined dataset better samples the range of epochs than any individual SN, (2) the templates can be analyzed for structure beyond that revealed in the function

fitting performed earlier in this section, (3) individual SNe can be compared to search for subtle variations from the mean behavior, and (4) the mean template can be used to estimate the peak magnitude and peak date for SNe with gaps in their sampling. Determining peak magnitudes and dates via template fitting has the drawback that it assumes the individual SN evolves exactly as the mean template, an assumption that is not fully supported by the available light curves. The subluminous and SN 2002cx-like subclasses are not included, as there is adequate evidence of differences from the light-curve fitting, and from the color curves that we will present in the next section.

The $uvw1$-band mean template is shown in Figure 13. It was calculated from $-12$ days to $+50$ days relative to $uvw1$ maximum, by including data within 2.5 days of each time point and weighting the data with inverse proportion to the time separation and the photometric error bar. The mean template was created iteratively by allowing individual SNe to move in time and magnitude to afford the best fit to the mean shape. The mean template features a steep rise to peak, and a long period of linear (in magnitudes) decline (from a few days after peak to roughly 30 days after peak). There are suggestions that the later decline is not uniform in all events, but overall the mean template represents the subclass very well.

We further explore the shape of the $uvw1$ mean template by fitting it to the Nugent $U$-band template for normal SNe Ia (Fig. 15, top panel). The rise to peak is steeper for the $uvw1$ filter, but the decline from peak is fairly similar. There are a few bumps and dips in the $uvw1$ template not present in the Nugent $U$-band template; we will continue to observe SNe Ia at these epochs to determine whether such features are characteristic of normal SNe Ia. The narrower peak of the $uvw1$ template compared to the Nugent $U$-band template also manifests itself in the $uvw1$-$u$ color curves shown in the next section. This feature might be the net effect of iron-peak elements in the emitting region.

The $uvw2$ mean template is shown in Figure 14. It was calculated with an algorithm similar to that used to generate the $uvw1$ mean template. The dominant features are the same as for the $uvw1$ template. Beyond $+20$ days, the scatter is appreciable, as SNe Ia are difficult to detect in that filter when the SN is faint. The shape of the $uvw2$ mean template is similar to the Nugent $U$-band normal SN Ia template until $+15$ days. This might be symptomatic of the higher degree of red leak in the $uvw2$ filter, causing $u$-band emission to drive the basic shape of the light curve.

Table 6 shows peak magnitudes and dates derived from fitting these SNe to the mean templates. The $uvw1$ peak dates are compared with the $B$-band peak dates, revealing that the $B$ band peaks more than 1.5 days after the $uvw1$ band. The mean delay (ignoring SN 2005hk) is roughly equal to the $2.3 \pm 0.4$ day $U$-peak to $B$-peak delay found by Jha et al. (2006), as was also seen from functional fitting in §4.1. SN 2005hk has a delay in excess

of the other SNe Ia. It appears that SN 2002cx-like SNe Ia peak many days earlier in the UV than in the $B$ band. This is potentially a useful diagnostic for theoretical simulations of that SN explosion type. We will explore this further when we look at the colors of SN 2008A compared to SN 2005hk.

## 5. Colors

The *Swift* SN Ia sample was not observed with a uniform cadence; consequently, the light curves are very heterogeneous in terms of the epochs of observation. To study the color curves of the SNe Ia in our sample, we require an estimate of the $B$-band peak date for each SN; these values are listed in Tables 1 and 2. Extinction can be important, so our initial comparisons concentrate on low-extinction SNe. SN 2005df is included only in the $uvw2 - uvw1$ colors, as UVOT obtained no $ubv$ data for that SN.

### 5.1. Colors Relative to the $v$ Band

First, we show comparisons relative to the *Swift* $v$ band. This was motivated by the desire to allow comparisons and contrasts with the commonly used $B - V$ color index. In addition, comparisons with the $v$ band permit the maximal separation between the UV filters and the optical emission observable with UVOT.

#### *5.1.1. Colors Relative to v: Normal SNe Ia*

The $uvw1 - v$, $uvw2 - v$, $u - v$, and $b - v$ color curves for the twelve SNe Ia considered to be normal with $E(B - V) < 0.20$ mag are shown in Figure 16. Most striking is the high degree of homogeneity among this large collection of SNe in the $uvw1 - v$ and $u - v$ color curves. All show an initial, dramatic shift toward bluer emission until reaching a "blue peak" roughly 5 days before the $b$-band peak. This peak is followed immediately by a shift toward redder emission until ∼20 days past $b$-band peak. This trend is also present in the $b - v$ color curve, but the individual color curves have a larger offset in this index. After +20 days, the $b - v$ color curve settles onto the slope that is the basis of the Lira (1995) relation, while in the bluer filters the transition is to a fairly flat evolution. For context, the Mazzali et al. (2008) study of the normal SN 2004eo reports that at -11 days, the photospheric velocity is 12,000 km s$^{-1}$, which corresponds to an enclosed mass of ∼1.1 M$_\odot$. They report abundant iron-peak elements, in particular providing line blocking in the UV. That study suggests

that iron-peak elements are in the photosphere well before the blue peak.

UV emission in SNe Ia at early times is the product of reverse fluorescence in metal lines (Mazzali 2000). In regions near the photosphere the UV opacity is so large that essentially no UV photons can escape, as they are absorbed in lines of metals (mostly iron-group ions) and reemitted at optical wavelengths. At layers well above the photosphere, the inverse process can occur if metals are sufficiently abundant: red photons are absorbed in metal lines and reemitted in the UV, since the UV radiation field in those layers is negligible. Thus the initial shift toward bluer emission could mark the onset of the reverse fluorescence process, and it indicates the presence of metals at velocities well above the photosphere. The subsequent shift toward redder emission is a cooling phase, where the majority of emission tends to the red. The sharpness of the "blue peak" in the $u$ and $uvw1$ filters is a feature that invites theoretical investigation.

Concentrating on the near-peak epoch, the individual events do exhibit variations (Fig. 17), with the $uvw2-v$ color exhibiting more variations than the $uvw1-v$ or $u-v$ color curves. Perhaps this is a direct probe of variations in the distribution of iron-peak elements in the outer layers of the ejecta. We will explore this further in §5.1.4.

### *5.1.2. Colors Relative to v: Subluminous SNe Ia*

Five subluminous SNe Ia were observed by UVOT, with SN 2005ke and 2007on being by far the best studied. Their color curves are shown in Figure 18; the color curves for the normal SNe Ia have been replaced by a shaded region. Clearly, the evolution is far different for this subclass than for normal SNe Ia. Whereas the normal SNe Ia are becoming bluer from $-10$ to $-5$ days relative to the $b$ peak, the subluminous SNe Ia are becoming redder, reaching a "red peak" at +5 to +10 days. For context, the Hachinger et al. (2009) study of the subluminous SN 2005bl report that at -6 days, the photospheric velocity is 8400 km s$^{-1}$, which corresponds to an enclosed mass of $\sim$0.7 M$_\odot$. They report that oxygen dominates the zone, with no evidence of iron. Indeed, there is no evidence of iron in the -3 day spectrum for that event. The color evolution in these events as well as the tomography of these events differs from normal events.

After +10 days, the color indices become bluer, either matching the colors of the normal SNe Ia ($b-v$, $u-v$), or even becoming bluer at late epochs ($uvw1-v$). SN 2005ke and 2007on evolve with similar patterns, with SN 2007on being bluer at all epochs. SNe 2005mz, 2006mr, and 2007ax add few data points, but they generally support the trends exhibited

by SN 2005ke.[3] The $B - V$ evolution has been explored in previous studies. Indeed, other investigations contain SNe Ia that bridge the gap between very subluminous events like SN 1991bg (Filippenko et al. 1992b; Leibundgut et al. 1993) and transitionally subluminous events (SN 1986G is a well-studied example; Phillips et al. 1987). The earliest observations of both SNe 2005ke and 2007on hint at a "blue peak" at roughly −9 days. It is fortunate that although only two subluminous SNe Ia have been well sampled with UVOT, both modes of the bimodal distribution claimed by Krisciunas et al. (2009) have one event. Additional early-time observations are needed to test the suggestion that even very subluminous SNe Ia also have a blue peak, but it occurs at such an early epoch that it is seldom detected.

The existence of a red peak is apparent in all four colors. In the $b - v$ color, the peak is slightly redder than an extrapolation of the Lira (1995) relation to earlier epochs. This is readily apparent in $B - V$ curves shown in previous studies (Phillips et al. 1999; Garnavich et al. 2004). The red-peaked nature is more dramatic in the UV$-v$ colors, making that wavelength range ideal for the study of the physics that drives that phenomenon.

Of particular interest is the color evolution from +5 to +30 days relative to the $b$-band peak. SN 2005ke was reported by *Swift* to exhibit a UV excess, the start of which (at ∼+16 days) was correlated in time with the weak detection of X-ray emission with XRT (Immler et al. 2006). The SN 2005ke light curves remain brighter than those of normal SNe Ia for more than 40 days, when normalized to the peak magnitude. The slopes of the color curves of SN 2005ke do not appear to change at +16 days, with linear evolution from +5 to +25 days. Indeed, it is the normal SNe Ia that appear to experience an inflection point between +15 and +20 days. If there is an excess of emission due to the SN shock interacting with CSM, it would need to produce emission such that the multi-band color evolution continues in a manner similar to that of the earlier-epoch intrinsic SN emission. These puzzling findings call into question whether the differences between the $uvw1$, $uvw2$, and $u$-band light curves of SN 2005ke versus those of normal SNe Ia are caused by shocked CSM emission. Alternatively, Kasliwal et al. (2008) present observations of SN 2007ax and suggest a photospheric origin for the flat late-time decline.

### *5.1.3. Colors Relative to V: SN 2002cx-Like SNe Ia*

Four SNe Ia that are considered members of the "SN 2002cx-like" subclass have been observed (see (Jha et al. 2006b) for a description of this subclass and Foley et al. 2009 for

[3]The ∼+30 day $uvw1 - v$ color point for SN 2007ax was obtained by interpolating two Super-LOTIS $V$-band data points from (Kasliwal et al. 2008).

observations of the very subluminous, SN 2002cx-like SN 2008ha). The color curves are illustrated in Figure 19; as in Figure 18, the normal SNe Ia are shown as a shaded region, and external data for other members of this class are included. The color curves for three of the four SNe are notable by being bluer than those of normal SNe Ia at the pre-peak epochs and by following a steeper slope during the reddening phase. The slope of the three SNe in $uvw1 - v$ is consistent with a straight line from $-7$ to $+10$ days (Fig. 20). The very linear evolution is a characteristic that must be reproduced by simulations of this subclass of SNe Ia. The colors of SN 2008ha are much redder than those of the other three objects, a characteristic unlikely to be due to extinction, as Foley et al. (2009) measured only upper limits for interstellar Na I D absorption. They assumed zero host-galaxy extinction, and corrected for $A_V = 0.25$ mag of Milky Way extinction. The SN 2008ha optical light curves were reported to be well fit by those of the other SN 2002cx-like SNe when a stretch was applied to the timescale, but this is not an explanation for the red color seen in Figure 19. The UVOT observations were obtained near optical peak, and would not be affected appreciably by a stretch of $\sim$0.75 centered at peak light.

The SN 2002cx-like subclass is characterized by the early appearance of iron-peak elements in the pre-peak spectra, but with narrow lines, a suggested characteristic of a deflagration explosion (Phillips et al. 2007). It is possible that the very blue colors at early epochs for SNe 2005hk and 2008A are a consequence of reverse fluorescence from these iron-peak elements, but this is speculative until demonstrated by theoretical simulations.

### *5.1.4. Extinction Correction*

The homogeneity of the near-peak color evolution of the normal SNe Ia in $uvw1 - v$ and $u - v$ invites further investigation, as this feature could be used to determine rest-frame UV extinction. Specifically, we test two hypotheses: (1) the color evolution from $-12$ to $+12$ days relative to $B_{\rm peak}$ can be fitted with two lines, and (2) the color evolution is the same for all normal SNe Ia in that color. We provide no basis for these hypotheses, presenting them *ad hoc*, but these tests allow us to simultaneously study SN Ia emission and the net wavelength dependence of extinction. SN 2008Q is excluded from this preliminary investigation, due to its very blue color and anomalous light-curve shapes. The follow-up study that will concentrate on using SNe Ia as probes of UV extinction will address SN 2008Q in detail.

In Figure 21, we display the residuals of the low-extinction SNe (i.e., small values of $E(B-V)$) to a best-fit two-line evolution (upper two panels). The standard deviation about that fit is $\sigma = 0.134$ mag. We then include higher-extinction SNe to the sample (third panel),

and apply a reddening correction that allows the value of $R_{uvw1} - R_V$ to be a fitted parameter for each individual SN.[4] We bounded $R_{uvw1} - R_V$ such that $0.0 \leq R_{uvw1} - R_V \leq 5.0$. In Table 7, we show the optimal $R_{uvw1} - R_V$ values for the three SNe Ia with $E(B-V) > 0.20$ mag. The $R_{uvw1} - R_V$ values range from 1.09 to 1.93, and result in the larger group (which includes the higher-extinction SNe) having a standard deviation comparable to that of the low-extinction subset, 0.138 mag versus 0.134 mag.

Figure 22 displays the $u - v$ color curves following the same procedures as in Figure 21. The standard deviation of the low-extinction SNe without reddening correction is 0.098 mag. The correction decreases the standard deviation for the larger group that includes the higher-extinction SNe from 0.675 mag to 0.104 mag. The $R_u - R_V$ values range from 0.81 to 2.17 (Table 7).

Whereas the variations in the $uvw1 - v$ colors are suggestive of being dominated by the effects of extinction, the $uvw2 - v$ light curves appear to vary in shape as well as vertical offset (Fig. 17). Applying the same approach as done for $uvw1 - v$ and $u - v$, we investigate the idea that the differences are purely due to extinction (Fig. 23). The residuals of most SNe appear to deviate little, or slightly toward the red relative to the two-line fit a few days before $B$-band peak. By contrast, some objects (SNe 2006dm and 2007cq) appear to deviate toward the blue during the same epoch. Neither group represents the extremes of $E(B-V)$, so it seems unlikely that the differences are related to reddening. Rather, this appears to be an intrinsic difference among normal SNe Ia. The $R_{uvw2} - R_v$ values range from 1.20 to 1.63 (Table 7). The standard deviation of the low-extinction SNe without reddening correction is 0.249 mag. The correction decreases the standard deviation for the larger group that includes the higher-extinction SNe from 0.611 mag to 0.230 mag.

Collectively, this shows that the $uvw1-v$ and $u-v$ color curves can be well characterized by two lines that form a blue peak. For the $uvw2 - v$ color curves, the characterization is more approximate. Application of a reddening correction optimized for each individual SN reduces the scatter of the total sample to the same order as the low-extinction subset. These preliminary findings show that using SN Ia color curves to probe the UV extinction in other galaxies has promise. The limit to this technique will be the intrinsic variations in the UV$-v$ colors, and more work is required to further explore the possibilities. In particular, it is important to have multiple low-extinction SNe of the same variety as each high-extinction event to isolate extinction as the cause of color differences. We note that this sample is biased in that two of the highest-extinction events are toward the luminous (broad-peaked light curve) extreme of SNe Ia, with spectral features that are similar to those of SN 1991T.

[4]Note that $E(uvw1 - V) = A_{uvw1} - A_V = (R_{uvw1} - R_V) \times E(B-V)$.

It will be important to observe multiple SN 1991T-like SNe Ia that have low extinction.

### *5.1.5. $uvm2 - v$ Colors*

In Figure 24 we show the $uvm2 - v$ colors for 15 SNe Ia. Twelve of these are normal SNe Ia, but SNe 2005ke and 2007on are members of the subluminous subclass and SN 2005hk belongs to the SN 2002cx-like subclass. Among the normal SNe Ia, the $uvm2 - v$ colors for SNe 2005am, 2005cf, 2007af, and 2007gi are initially red, in agreement with the $uvw2 - v$ colors (dashed line). The $uvm2 - v$ colors for SNe 2006ej, 2007cq, and 2008Q are initially blue, transitioning to redder emission after the peak (dot-dashed line). Many of the red-colored group are normal-velocity normal SNe Ia, while SN 2006ej is HV and in the blue group. However, SN 2007gi is red, but of the HV group, and a number of SNe Ia have yet to be categorized as HV or NN. Whether there is a correlation between HV categorization and UV colors remains uncertain and will be explored in future papers.

By contrast, the SN 2005ke and SN 2005hk $uvm2 - v$ color curves appear to match the trends seen in the $u$, $uvw1$, and $uvw2$ filters. SN 2005ke reddens to reach a red peak 5–10 days after $B_{\rm peak}$, followed by a blueward shift to colors as blue as those of the normal SNe Ia after +25 days. SN 2005hk is initially very blue, but quickly reddens to fall within the range of normal events. The fact that this evolution is observed for a range of color curves suggests that the SN 2002cx-like color curves are not dominated by specific absorption or emission features, but by emission over a wider wavelength range.

We investigate further the UV emission from normal SNe Ia by comparing the $uvw2 - v$ and $uvm2 - v$ color curves. The near-peak $uvw2 - v$ color curves (Fig. 17) show that a few SNe Ia (SNe 2007cq and 2008Q) are significantly bluer from −7 to +5 days relative to the time of $B$-band maximum than the larger collection of SNe Ia. These same SNe are blue in the $uvm2 - v$ color curves (Fig. 24) and evolve toward redder emission, while the larger group has less color evolution, evolving toward bluer emission. Perhaps more interestingly, three SNe Ia (SNe 2006dm, 2006ej, and 2008ec) are initially as blue as that first group in the $uvw2 - v$ color curves, but abruptly shift to a redder color curve that matches that of the larger group. By contrast, the $uvm2 - v$ color curve of SN 2006ej remains similar to that of the bluer SNe at all epochs, exhibiting no jump toward redder emission, while SNe 2006dm and 2008ec have color curves somewhat intermediate to the blue and the red groups of SNe Ia, evolving toward bluer emission.

We quantify these tendencies in Figure 25. The upper panel shows the mean $uvw2 - v$ color from −5 to −3 days relative to $B$ maximum (abcissa) versus the mean $uvw2 - v$ color

in the interval $t = -3$ to $+2$ days (ordinate). Most SNe Ia are above the equality line, meaning that there is some evolution toward redder emission, but SNe 2006ej and 2006dm are notable in the larger shift toward redder emission. SN 2008ec is below the equality line, but we note that that SN experiences the redward jump mentioned above at an earlier epoch, making this SN poorly represented in this figure. The lower panel again displays the mean $uvw2 - v$ color from $-5$ to $-3$ days relative to $B_{\rm peak}$ on the abcissa, but shows the mean $uvm2 - v$ color in the interval $t = -5$ to $+2$ days (ordinate). The larger interval was chosen to accomodate the poorer sampling in the $uvm2$ filter. The general trend for the SNe Ia with redder $uvw2 - v$ color to also emit with redder $uvm2 - v$ color is apparent, and this is in line with expectations based on the fact that the $uvw2$ and $uvm2$ filters have considerable overlap in their bandpasses. SN 2008ec appears to deviate from this general trend, but we note that the color curves shown in Figure 17 appear to evolve on an earlier time-scale than the other SNe Ia. This might be evidence of an incorrect estimate of the B-band peak date, which was derived from UVOT data. Shifting the color curves by +2 days puts SN 2008ec in better agreement with the other SNe Ia, and would alter the values shown in Figure 25. Our attempt to quantify tendencies in UV color evolution is crude, and biased by the variations in the sampling of individual events, but the existence of basic trends beyond the scatter in the observations is apparent.

## 5.2. Other Color Curves

### *5.2.1. $uvw1 - b$ Color Curves*

Figure 26 shows the $uvw1 - b$ color curves with the SNe Ia broken into the same three subclasses as for the $v$-band comparisons. The general curve features are similar to those of the $v$-band comparisons: the normal SNe Ia exhibit a blue peak and a late flattening, the subluminous SNe Ia are redder transitioning to bluer, and the SN 2002cx-like SNe Ia are initially very blue, rapidly becoming redder. It is readily apparent that there is considerable divergence in the normal color curves after +5 days. SNe 2005am, 2006ej, and 2007cq are bluer at the later epochs than SNe 2005cf, 2006dm, 2007af, and 2007cv by $\sim$0.5 mag. SN 2008Q is a blue outlier. The transition to the later, flatter epoch is at approximately +10 days, whereas in $uvw1 - v$ the inflection was at +15 to +20 days. The differences between the peak and +15 day color should be studied in tandem with Figure 9, which shows clumping in the $\Delta m_{15}(uvw1)$ vs. $\Delta m_{15}(B)$ plane.

### *5.2.2. $u - b$ Color Curves*

Figure 27 illustrates the $u-b$ colors with the SNe Ia broken into the same three subclasses as for the $v$-band comparisons. The general curve features are similar to those of the $v$-band and $uvw1 - b$ comparisons: the normal SNe Ia exhibit a blue peak and a late flattening, the subluminous SNe Ia are redder from $-10$ to $+20$ days, and the SN 2002cx-like SNe Ia are initially very blue, rapidly becoming redder.

### *5.2.3. $uvw1 - u$ Color Curves*

The $uvw1 - u$ colors permit a comparison of UVOT $uvw1$ photometry with ground-based $U$-band photometry. The color curves (Fig. 28) have two interesting features. First, the normal SNe Ia show a gradual shift toward bluer emission during the entire epoch of the $uvw1 - v$ "Z"-shaped evolution, though this gradual trend is moderated by appreciable scatter. Second, the subluminous SNe Ia become bluer from the earliest epochs to the latest epochs. No clear trend is apparent for the SN 2002cx-like subclass, which would benefit from observations of additional events.

### *5.2.4. $uvw2 - uvw1$ Color Curves*

Finding purely rest-frame UV indicators of SN Ia subclass is important for the study of SNe Ia at very high redshifts. Foley et al. (2008b) suggest a $R_{\rm UV}$ ratio, comparing wavelength bands at 2900 Å and 2770 Å; the ratio increases with increasing MLCS-$\Delta$ (i.e., the low-luminosity events have the largest $R_{\rm UV}$ ratio). The UVOT filters are not ideally suited to study such a ratio, but we can show the $uvw2-uvw1$ color curves. As seen in Figure 29, the UV emission becomes slightly bluer for the normal SNe Ia, but with considerable scatter. The subluminous SNe Ia appear to exhibit a shallower shift toward blue emission. The SN 2002cx-like SNe Ia are not sampled sufficiently well to yield information regarding the temporal evolution of this color index.

## 6. Summary

We present a UVOT study of the UV and optical emission from 26 SNe Ia, collected during 2005–2008. The normal SNe Ia exhibit definite similarities in the UV$-v$ colors, particularly in the $uvw1-v$ and $u-v$ colors. The colors rapidly become bluer from the earliest

epochs until $\sim -5$ days relative to $B$-band maximum, followed by a redward shift until $\sim$+20 days. At the later epochs, the color change is modest. By contrast, the subluminous subclass features redder emission initially, becoming still redder until $\sim$+20 days, at which time it becomes bluer, roughly matching the colors of the normal SNe Ia. Members of the SN 2002cx-like subclass are initially very blue, but rapidly redden, with a slope steeper than the evolution seen among the normal SNe Ia.

The $uvw1$ light curves of normal and subluminous SNe Ia exhibit less variation in the peak shapes than seen in the $B$ or $b$ bands. This relative lack of variation makes discrimination between subclasses more difficult in the UV emission than in the $B$ or $b$-band emission. The SN 2002cx-like SNe do exhibit a steeper decline from peak than the normal or subluminous SNe Ia, thus appearing different in peak shape than these latter subclasses. The SN 2002cx-like $uvw1 - v$ color evolution is linear from $-8$ days to +30 days relative to $B$-band peak.

The subluminous SNe Ia do differ from the normal SNe Ia in the earlier transition to a late-time, flatter light curve. This difference could be utilized to discriminate this subclass from normal SNe Ia when only rest-frame UV emission can be observed.

The UV emission peaks at earlier epochs than the $B$-band emission, roughly two days earlier for normal events. This UV to $B$-band delay is consistent with the $U$-band study by Jha et al. (2006). The SN 2002cx-like SN 2005hk peaked anomalously early in the UV, and the other SN 2002cx-like object, SN 2008A, is consistent with a very large UV to $B$-band peak delay.

Compared with a $U$-band template for normal SNe Ia, the $uvw1$ mean template rises more steeply to the peak, but declines at a similar rate. The $uvw2$ mean template for normal SNe Ia is very similar to the $U$-band template.

These features require further study to determine how they constrain the physics of SN Ia explosions. The nature of the $uvw1$ and $uvw2$ filters is such that they can be contaminated to some extent by redder emission; this dictates that interpretation of these findings must include folding theoretical spectra through the UVOT filter response. Bearing that in mind, the data presented here introduce interesting challenges for SN Ia theory.

The UVOT instrument has been observing, and will continue to observe, additional SNe Ia. Based upon the findings presented in this work, as well as the new questions introduced in this work, the ongoing observational campaign will focus on the critical epochs described in the text to maximize the scientific yield of future UVOT observations. In particular, more SN 2002cx-like, subluminous, and transitional subluminous SNe must be observed. Observations of all subclasses at very early epochs are critical, but such early

detections of SNe Ia are always a challenge. The normal subclass exhibits dramatic color evolution during the week preceding $B$-band maximum. Dense sampling (daily, or even twice daily) during that week with high signal-to-noise ratio photometry in the four bluest filters would be important to further investigate that emission. Subluminous SNe Ia evolve to a red peak, and back toward the blue during the first three weeks after $B_{\rm peak}$. Regular sampling (daily or every two days) with high-quality detections would optimize that study. For all subclasses, late-time observations every 3–5 days would permit measurement of the late-break time and slope.

The results presented here invite additional investigations. Intermediate-redshift surveys have also observed rest-frame UV emission. Comparisons between those data and UVOT observations of nearby SNe Ia would be important to conduct. The generation of bolometric light curves of various subclasses of SNe Ia will benefit through better estimation of the UV contributions to the optical and NIR emission. This will be particularly powerful for SNe Ia simultaneously observed in all three wavelength ranges.

Our study of the absolute magnitudes of these SNe Ia is presented in a companion paper (Brown et al. 2010). The cosmological application of the combined studies is clear, as high-redshift surveys will study UV emission redshifted into the optical and NIR wavelength ranges. In addition, very nearby SNe Ia will be observed with the UVOT UV grism, continuing spectral studies first presented by Bufano et al. (2008). Multi-wavelength SN Ia observing campaigns that include UVOT observations should continue for years to come.

We thank the Mission Operations team at Penn State University for scheduling so many UVOT SN Ia observations on short notice. We are grateful to Stephane Blondin for his efforts on behalf of the CfA Supernova Program, and X. Wang for categorization of NHV and NNN SNe Ia. P.A.M. would like to thank K. Krisciunas for assistance in obtaining information on specific supernovae. The research of A.V.F.'s supernova group at UC Berkeley is supported by National Science Foundation (NSF) grants AST–0607485 and AST-0908886, the TABASGO Foundation, US Department of Energy SciDAC grant DE-FC02-06ER41453, US Department of Energy grant DE-FG02-08ER41563, and *Swift* Guest Investigator grant NNX09AG54G. The work at PSU is sponsored NASA contract NAS5-00136. KAIT and its ongoing operation were made possible by donations from Sun Microsystems, Inc., the Hewlett-Packard Company, AutoScope Corporation, Lick Observatory, the NSF, the University of California, the Sylvia & Jim Katzman Foundation, and the TABASGO Foundation. Supernova research at the Harvard College Observatory is supported in part by the NSF through grants AST–0606772 and AST–0907903.

Table 1: Optical Parameters for the SN Ia Sample: 2005 and 2006

| SN | Discovery CBET | Host Galaxy | Sub-Class[c] | $\Delta m_{15}(B)$ [mag][d] | $t(B)_{\rm peak}$ [days] | $B_{\rm peak}$ [mag][e] | Ref[a] | $E(B-V)$ [mag][f] | Ref.[ab] | $\Delta$ | Ref. |
|---|---|---|---|---|---|---|---|---|---|---|---|
| 2005am[g] | 113 | NGC 2811 | NNN | 1.51(04) | 3437.1 | 13.91 | 1 | 0.075(014) | 1-M31 | 0.456(045) | 1 |
| | | | | 1.73(05) | 3435.5 | 13.79(04) | 2 | 0.07(02) | 2-M17 | 0.40(09) | 2 |
| | | | | 1.48(02) | 3433.5 | 13.857(003) | 3 | 0.06 | 3-P | | |
| 2005cf | 158 | MCG | NNN | 1.11 | 3534.0 | 13.54 | 4 | 0.097 | 4-Av | — | |
| | | -1-39-3 | | 1.03(01) | 3533.9 | 13.65 | 1 | 0.143(019) | 1-M31 | −0.127(017) | 1 |
| | | | | 1.05(03) | 3533.7 | 13.63(02) | 5 | 0.09(03) | 5-Av | — | |
| | | | | 1.06(08) | 3533.9 | 13.54(07) | 2 | 0.22(04) | 2-M17 | −0.15(08) | 2 |
| 2005df[h] | 192 | NGC 1559 | N | 1.2 | 3598.3 | 12.32 | 6 | 0.03 | 6-M31 | -0.12 | 6 |
| 2005hk | 268,269 | UGC 272 | 02cx | 1.56 | 3685.1 | 15.91 | 7 | 0.09 | 8-NaD | — | |
| | | | | 1.47(14) | | 15.91(05) | 2 | 0.48(03) | 2-M17 | −0.31(05) | 2 |
| 2005ke[i] | 287 | NGC 1371 | sub | 1.76(01) | 3699.2 | 14.882(005) | 3 | 0.06 | 3-P | — | |
| | | | | 1.66(06) | 3699.2 | 14.95(05) | 2 | 0.06(02) | 2-M17 | 1.55(03) | 2 |
| | | | | | | | | 0.12 | T | | |
| | | | | | | | | 0.27 | P | | |
| 2005mz | 347 | NGC 1275 | sub | 1.96(14) | 3745.9 | 16.88(11) | 2 | 0.32(05) | 2-M17 | 1.36(07) | 2 |
| 2006E[j] | 8658 | NGC 5338 | N | — | — | — | 14 | — | — | — | — |
| 2006X | 8667 | NGC 4321 | NHV | 1.10(12) | — | 14.05(02) | 2 | 1.50(02) | 2-M17 | −0.10(04) | 2 |
| | | | | 1.17(05)[k] | 3786.2 | 15.40(03) | 13 | 1.42(04) | 13-Av | | |
| 2006dd | 553,723 | NGC 1316 | NNN | 1.34 | 3918.8 | 12.18 | 9 | 0.08 | 9-P | 0.01 | 9 |
| | | | | | | | | 0.26 | T | | |
| 2006dm | 569,570 | MCG | NNN | 1.28 | 3928.6 | 16.18 | T | 0.005 | T | | |
| | | -01-60-21 | | 1.53(06) | 3929.0 | 16.13 | 1 | 0.060(014) | 1-M31 | 0.550(042) | 1 |
| | | | | | | | | 0.01 | P | | |
| 2006ej | 603 | NGC 191 | NHV | 1.38(11) | 3976.9 | 15.88 | 1 | 0.050(009) | 1-M31 | 0.277(045) | 1 |
| | | | | | 3973.6 | 15.90 | 12 | 0.03 | 12-M17 | 0.19(08) | 12 |
| | | | | | | | | 0.36 | T | | |
| 2006mr | 723 | NGC 1316 | sub | 1.82(02) | 4049. | | 3 | 0.00 | 3-P | | |

[a]REFERENCES. — (1) KAIT, this work, (2) CfA3, Hicken et al. 2009, (3) CSP, Folatelli et al. 2010, (4) Pastorello et al. 2007, (5) Wang et al. 2009a, (6) ANU, Appendix B, this work, (7) Phillips et al. 2007, (8) Chornock et al. 2007, (9) Krisciunas 2009, private communication, (10) Simon et al. 2007, (11) Kasliwal et al. 2008, (12) Blondin 2009, private communication, (13) Wang et al. 2008, (T) UVOT tail observations, this work, and (P) UVOT peak observations, this work.

[b]Extinction estimates are from MLCS2k2 with $R_V = 3.1$ (M31), MLCS2k2 with $R_V = 1.7$ (M17), Lira tail relation (L), Phillips peak color relation (P), Na I D absorption (NaD), and average of multiple methods (Av).

[c]Utilizing the results of Wang et al. 2009b, the normal SNe are further divided into the following categories. NHV = normal SN with high-velocity absorption features, NNN = normal SN without high-velocity features, N = normal SN where existence of high-velocity features has not been determined, sub = subluminous SN Ia, and 02cx-like = SN 2002cx-like SN Ia (as explained in §3.1).

[d]Uncertainties are in parentheses, and are given in units of 0.01 mag.

[e]Apparent magnitudes, no correction for Milky Way extinction.

[f]Total of Milky Way extinction plus host-galaxy extinction.

[g]Preliminary photometry was presented by Brown et al. 2005.

[h]Only observed in UVOT UV filters ($uvw1$, $uvm2$, $uvw2$).

[i]Preliminary photometry was presented by Immler et al. 2005.

[j]SN 2006E was spectrally identified to be a SN Ia.

[k]The true $\Delta m_{15}(B) = 1.31 \pm 0.05$ mag differs from the observed value for this highly reddened SN.

Table 2: Optical Parameters for the SN Ia Sample: 2007 and 2008

| SN | Discovery CBET | Host Galaxy | Sub-Class[c] | $\Delta m_{15}(B)$ [mag][d] | $t(B)_{\rm peak}$ [days] | $B_{\rm peak}$ [mag][e] | Ref[a] | $E(B-V)$ [mag][f] | Ref.[ab] | $\Delta$ | Ref. |
|---|---|---|---|---|---|---|---|---|---|---|---|
| 2007S | 829 | UGC 5378 | N91T | 0.88(08) | — | 15.82(03) | 2 | 0.53(03) | 2-M17 | −0.32(04) | 2 |
| | | | | 0.91 | 4143.5 | 15.95 | T | 0.45 | Av | | |
| | | | | 0.80 | — | — | 3 | | | | |
| 2007af | 865 | NGC 5584 | NNN | 1.11 | 4173.2 | 13.34 | T | 0.15 | Av | — | |
| | | | | 1.20(05) | — | 13.13(03) | 2 | 0.17(03) | 2-M17 | −0.04(05) | 2 |
| | | | | | 4174.3 | — | 10 | 0.13 | 10-Av | −0.04(02) | 10 |
| 2007ax | 904 | NGC 2577 | sub | 1.90 | 4187.3 | 16.3 | 11 | 0.05 | 11-Av | — | |
| | | | | | 4186.0 | | | 0.19(03) | 12-M17 | 1.33(07) | 12 |
| 2007co | 977,978 | MCG | NHV | 1.06(02) | 4264.9 | 16.94 | 1 | 0.161(025) | 1-M31 | −0.079(076) | 1 |
| | | +05-43-16 | | 1.14(09) | — | 16.43(08) | 2 | 0.34(04) | 2-M17 | −0.04(08) | 2 |
| | | | | | | | | 0.26 | P | | |
| 2007cq | 980 | Anon. Gal. | N91T | 1.02(03) | 4280.8 | 16.34 | 1 | 0.123(012) | 1-M31 | −0.024(027) | 1 |
| | | | | 1.17(18) | 4281. | 15.82(07) | 2 | 0.17(03) | 2-M17 | 0.05(07) | 2 |
| 2007cv | 989 | IC 2587 | N | 1.31 | 4290.2 | 15.29 | ? | 0.19 | 2 | — | |
| 2007gi | 1017 | NGC 4036 | NHV | 1.31(09) | 4327. | 13.25(04) | 15 | 0.17(04) | 15-Av | | 15 |
| 2007on | 1121 | NGC 1404 | sub | 1.89 | —- | —- | 3 | — | | | |
| 2007sr | 1172 | NGC 4038 | NHV | 0.97(01) | 4448.8 | | 13 | 0.18(02) | 13 | — | |
| 2008A | 1193 | NGC 634 | 02cx | — | 4476. | — | — | — | 2 | | |
| 2008Q | 1228 | NGC 524 | NNN | 1.39 | 4505.5 | 13.81 | P | 0.07 | P | | |
| 2008ec | 1437 | NGC 7469 | NNN | 1.06 | 4672.4 | 15.84 | P | 0.22 | PT-ave | | |
| 2008ha | 1567 | UGC 12682 | 02cx | 2.17(02) | 4783.2 | 18.23(01) | 14 | 0.076 | 14 | — | |

[a]REFERENCES. — (1) KAIT, this work, (2) CfA3, Hicken et al. 2009, (3) CSP, Folatelli et al. 2010, (4) Pastorello et al. 2007, (5) Wang et al. 2009a, (6) ANU, private communication, (7) Phillips et al. 2007, (8) Chornock et al. 2007, (9) Krisciunas 2009, private communication, (10) Simon et al. 2007, (11) Kasliwal et al. 2008, (12) Blondin 2009, private communication, (13) Schweizer et al. 2008, (14) Foley et al. 2009b, (15) Zhang et al. 2009, (T) UVOT tail observations, this work, and (P) UVOT peak observations, this work.

[b]Extinction estimates are from MLCS2k2 with $R_V = 3.1$ (M31), MLCS2k2 with $R_V = 1.7$ (M17), Lira tail relation (L), Phillips peak color relation (P), Na I D absorption (NaD), and average of multiple methods (Av).

[c]Utilizing the results of Wang et al. 2009b, the normal SNe are further divided into the following categories. NHV = normal SN with high-velocity absorption features, NNN = normal SN without high-velocity features, N = normal SN where existence of high-velocity features has not been determined, sub = subluminous SN Ia, and 02cx-like = SN 2002cx-like SN Ia (as explained in §3.1).

[d]Uncertainties are in parentheses, and are given in units of 0.01 mag.

[e]Apparent magnitudes, no correction for Milky Way extinction.

[f]Total of Galactic extinction plus host-galaxy extinction.

Table 3: Parameters Derived from UVOT UV Observations: Early Epochs

| | Function-fitted $uvw1$ Parameters | | | | | | | |
|---|---|---|---|---|---|---|---|---|
| SN | Model[a] | $\chi^2/DOF$ | $t(\mathrm{pk})_{uvw1}$ | $uvw1^b_{\max}$ | $R_{5d}(uvw1)^c$ | $\Delta m_5(uvw1)^d$ | $\Delta m_{15}(uvw1)^d$ | $t(\mathrm{LB})^f_{uvw1}$ |
| | (1) | (2) | (3) | (4) | (5) | (6) | (7) | (8) |
| 2005am | FXPKLT | 0.42 | 3435.3 | 15.34(–) | — | — | — | 3465.0 |
| 2005cf | CMPLT | 0.24 | 3531.0 | 15.11(07) | 1.20 | 0.10 | 1.25 | 3557.7 |
| 2005df | CMPLT | 0.54 | 3597.4 | 13.92(07) | 0.49 | 0.16 | 1.32 | 3626.4 |
| 2005hk | MID | 0.81 | 3678.4 | 16.90(10) | — | 0.15 | 1.69 | 3696.6 |
| 2005ke | MID | 1.11 | 3696.7 | 17.09(08) | 0.73 | 0.24 | 1.49 | 3707.4 |
| 2006dm | MID | 0.54 | 3926.2 | 17.63(09) | 0.71 | 0.29 | 1.62 | — |
| 2006ej | FXPK | 0.45 | 3974.5 | 16.91(–) | — | — | — | — |
| 2007S | MID | 0.66 | 4141.1 | 17.83(13) | 0.42 | 0.13 | 1.11 | — |
| 2007af | CMPLT | 1.05 | 4172.0 | 14.74(07) | 0.62 | 0.49 | 1.64 | 4203.9 |
| 2007co | MID | 0.75 | 4264.1 | 18.81(15) | 0.06 | 0.13 | 1.31 | — |
| 2007cv | MID | 0.69 | 4288.5 | 16.83(08) | 0.83 | 0.37 | 1.56 | — |
| 2007on | CMPLT | 2.11 | 4414.73 | 14.34(05) | 1.97 | 0.23 | 1.80 | 4439.9 |
| 2008Q | MID | 0.29 | 4501.99 | 14.84(05) | 1.13 | 0.23 | 1.63 | — |
| 2008ec | MID | 0.55 | 4669.28 | 17.31(11) | 1.01 | 0.20 | 1.31 | — |

| | Function-fitted $uvw2$ Parameters | | | | Function-fitted $u$ Parameters | | | | |
|---|---|---|---|---|---|---|---|---|---|
| SN | Model[a] | $\chi^2/DOF$ | $t(\mathrm{pk})_{uvw2}$ | $uvw2^b_{\max}$ | Model[a] | $\chi^2/DOF$ | $t(\mathrm{peak})_U$ | $U^a_{\max}$ | $\Delta m_{15}(U)^d$ |
| | (9) | (10) | (11) | (12) | (13) | (14) | (15) | (16) | (17) |
| 2005am | — | — | — | — | FXPKLT | 0.79 | 3435.8 | 13.55(05) | — |
| 2005cf | MID | 0.79 | 3533.0 | 16.86(08) | CMPLT | 0.39 | 3530.9 | 13.41(05) | 1.17 |
| 2005df | CMPLT | 0.87 | 3598.9 | 15.61(07) | — | — | — | — | — |
| 2005hk | — | — | — | — | CMPLT | 6.87 | 3680.3 | 15.49(08) | 1.90 |
| 2005ke | MID | 1.13 | 3697.7 | 18.41(11) | MID | 1.08 | 3695.3 | 15.52(07) | 1.79 |
| 2006dm | — | — | — | — | CMPLT | 0.11 | 3926.0 | 15.99(07) | 1.71 |
| 2006ej | — | — | — | — | FXPKLT | 1.31 | 3974.1 | 15.47(06) | — |
| 2007S | — | — | — | — | MID | 1.01 | 4143.0 | 15.86(07) | 1.38 |
| 2007af | CMPLT | 0.82 | 4170.0 | 16.53(09) | CMPLT | 0.96 | 4170.1 | 13.16(07) | 1.29 |
| 2007co | — | — | — | — | MID | 0.91 | 4263.9 | 16.99(07) | 1.56 |
| 2007cv | MID | 2.22 | 4287.8 | 18.60(12) | MID | 3.20 | 4288.4 | 15.08(06) | 1.88 |
| 2007on | CMPLT | 2.03 | 4414.7 | 15.65(05) | CMPLT | 1.39 | 4415.0 | 12.93(05) | 2.08 |
| 2008Q | MID | 1.04 | 4502.3 | 16.43(05) | MID | 3.15 | 4501.5 | 13.39(05) | 1.54 |
| 2008ec | — | — | — | — | CMPLT | 1.42 | 4669.9 | 15.62(07) | 1.53 |

[a]Light-curve model used in fitting.

[b]Uncertainties are in parentheses, and are given in units of 0.01 mag.

[c]Change in magnitude in the 5 days before the peak to the peak date.

[d]Change in magnitude from the peak date to 5 days after peak.

[e]Change in magnitude from the peak date to 15 days after peak.

[f]The date of the late break, JD−2,450,000.

Table 4: Parameters Derived from UVOT Optical Observations: Early Epochs

| | Function-Fitted $b$ Parameters | | | | | Function-Fitted $v$ Parameters | | | | |
|---|---|---|---|---|---|---|---|---|---|---|
| SN | Model (18) | $\chi^2/DOF$ (19) | $t(\mathrm{peak})_B$ (20) | $B_{\max}$ (21) | $\Delta m_{15}(B)^d$ (22) | Model (23) | $\chi^2/DOF$ (24) | $t(\mathrm{peak})_V$ (25) | $V_{\max}$ (26) | $\Delta m_{15}(V)^d$ (27) |
| 2005am | — | | [3437.5] | — | — | MID | 5.01 | 3439.0 | 13.83(05) | 0.49 |
| 2005cf | — | | [3534.0] | — | — | CMPLT | 0.95 | 3532.0 | 13.62(05) | 0.35 |
| 2005hk | CMPLT | 2.31 | 3684.3 | 15.90(07) | 1.52 | MID | 0.99 | 3688.1 | 15.72(05) | 0.75 |
| 2005ke | CMPLT | 0.86 | 3698.0 | 14.93(07) | 1.74 | CMPLT | 1.00 | 3699.8 | 14.21(05) | 1.07 |
| 2006dm | CMPLT | 0.57 | 3928.7 | 16.17(07) | 1.28 | CMPLT | 0.53 | 3930.6 | 16.13(07) | 0.86 |
| 2006ej | FXPKLT | 1.87 | 3977.2 | 15.89(07) | — | — | — | — | — | — |
| 2007S | CMPLT | 0.34 | 4143.7 | 15.94(07) | 0.77 | CMPLT | 0.58 | 4145.6 | 15.53(07) | 0.61 |
| 2007af | MID | 1.41 | 4172.3 | 13.39(07) | 1.05 | CMPLT | 0.53 | 4175.9 | 13.25(05) | 0.58 |
| 2007co | MID | 0.48 | 4263.1 | 16.86(07) | 0.96 | MID | 0.20 | 4265.2 | 16.69(07) | 0.63 |
| 2007cv | CMPLT | 0.20 | 4290.0 | 15.30(07) | 1.39 | MID | 0.29 | 4291.9 | 15.15(05) | 0.76 |
| 2007on | CMPLT | 1.04 | 4418.6 | 13.14(07) | 1.70 | CMPLT | 0.65 | 4420.4 | 13.06(05) | 0.92 |
| 2008Q | MID | 0.27 | 4504.7 | 13.85(07) | 1.39 | MID | 0.45 | 4505.1 | 13.80(05) | 0.66 |
| 2008ec | CMPLT | 0.88 | 4672.5 | 15.83(07) | 1.06 | CMPLT | 0.61 | 4673.6 | 15.70(07) | 0.58 |

[a] Light-curve model used in fitting.

[b] Uncertainties are in parentheses, and are given in units of 0.01 mag.

[c] Change in magnitude in the 5 days before the peak to the peak date.

[d] Change in magnitude from the peak date to 5 days after peak.

[e] Change in magnitude from the peak date to 15 days after peak.

[f] The date of the late break, JD−2,450,000.

Table 5: Parameters Derived from UVOT Observations: Late Epochs

| | $uvw1$-Band Parameters | | | $u$-Band Parameters | | |
|---|---|---|---|---|---|---|
| SN | $\beta^a_{uvw1}$ | $t(\mathrm{LB})^b_{uvw1}$ | $\gamma(uvw1)^c$ | $\beta^a_u$ | $t(\mathrm{LB})^b_u$ | $\gamma(u)^c$ |
| 2005am | 12.04(0.07) | 3461.5(0.5) | 3.88(0.39) | — | — | — |
| 2005cf | 13.15(0.36) | 3559.0(0.9) | 3.38(0.51) | — | — | — |
| 2005df | 8.55(0.96) | 3626.5(0.8) | 2.52(0.05) | — | — | — |
| 2005hk | — | — | — | 17.66(0.65) | 3706.7(1.0) | 1.44(0.36) |
| 2006E | — | — | 2.12(0.07) | — | — | — |
| 2006dd | 14.52(0.27) | 3944.1(0.7) | 3.62(0.13) | — | — | — |
| 2006dm | 12.68(3.27) | — | — | 13.56(0.97) | 3952.8(0.9) | 3.86(0.65) |
| 2006ej | 11.92(1.76) | — | — | — | — | — |
| 2007S | 10.85(0.67) | — | — | 10.60(0.23) | 4172.2(1.5) | 3.40(0.65) |
| 2007af | 12.73(0.14) | 4199.8(0.4) | 3.41(0.11) | 13.05(0.06) | 4200.9(0.1) | 2.91(0.03) |
| 2007co | 9.35(1.98) | — | — | — | — | — |
| 2007cv | 11.87(0.07) | — | — | — | — | — |
| 2007on | 6.88(0.58) | 4439.5(1.4) | 3.52(0.11) | 10.77(0.35) | 4440.7(0.3) | 3.42(0.07) |
| 2007sr | 11.68(0.11) | — | — | — | — | — |
| 2008ec | — | — | — | 13.13(0.71) | 4702.1(2.4) | -0.12(1.93) |

| | $b$-Band Parameters | | | $v$-Band Parameters | | |
|---|---|---|---|---|---|---|
| SN | $\beta^a_b$ | $t(\mathrm{LB})^b_b$ | $\gamma(b)^c$ | $\beta^a_v$ | $t(\mathrm{LB})^b_v$ | $\gamma(v)^c$ |
| 2005hk | 11.54(0.78) | 3709.1(0.6) | 1.59(0.16) | — | — | — |
| 2005ke | 4.67(0.12) | 3730.9(1.0) | 2.03(0.11) | 6.69(0.44) | 3728.6(1.4) | 3.23(0.10) |
| 2006dm | 10.89(0.15) | 3960.0(0.6) | 1.76(0.40) | 7.56(0.20) | 3962.8(1.8) | 3.43(0.62) |
| 2007S | 9.47(0.21) | 4177.9(0.3) | 1.52(0.41) | 5.38(0.05) | 4174.6(1.8) | 4.57(0.12) |
| 2007af | 9.91(0.06) | 4208.0(0.2) | 1.61(0.02) | 6.10(0.03) | 4215.9(0.3) | 2.61(0.02) |
| 2007cv | 12.53(1.15) | 4312.1(1.1) | 4.65(0.41) | — | — | — |
| 2007on | 11.84(1.41) | 4441.9(1.6) | 3.00(0.15) | 8.91(0.34) | 4445.5(1.0) | 3.71(0.17) |
| 2008ec | 11.01(1.28) | 4703.2(1.1) | 2.53(0.65) | 6.21(0.32) | 4703.6(0.3) | 4.67(0.46) |

[a]The initial linear slope in mag per 100 days.

[b]The date of the late break, JD−2,450,000.

[c]The late linear slope in mag per 100 days.

Table 6: Parameters Obtained Fitting with Mean Template

| | Mean Template-Fitted $uvw1$ Parameters | | $t_B - t_{uvw1}$ | |
|---|---|---|---|---|
| SN | $t^a_{uvw1}$ | $uvw1^b_{\max}$ | Function Fit[c] | Template Fit[c] |
| (20) | (21) | (22) | (23) | (24) |
| 2005am | 3433.8 | 15.32(06) | 2.2 | 3.7 |
| 2005cf | 3532.4 | 15.08(07) | 3.0 | 1.8 |
| 2005df | 3597.7 | 13.83(07) | 0.7 | 0.4 |
| 2005hk | — | — | 5.6 | — |
| 2005ke | — | — | 1.0 | — |
| 2006dm | 3926.3 | 17.70(09) | 2.1 | 2.0 |
| 2006ej | 3972.9 | 17.05(08) | — | — |
| 2007S | — | — | 2.3 | 2.5 |
| 2007af | 4171.7 | 14.84(07) | 1.2 | 1.5 |
| 2007co | 4264.7 | 18.75(15) | 1.0 | 0.4 |
| 2007cv | 4289.1 | 16.95(08) | 1.7 | 1.1 |
| 2007on | — | — | 4.1 | — |
| 2008Q | 4502.9 | 14.92(05) | 3.5 | 2.6 |
| 2008ec | 4671.6 | 17.32(11) | 3.1 | 0.8 |
| | | Mean $t_B - t_{uvw1}$ = | 2.22±1.10 | 1.68±1.06 |

[a]The date of the $uvw1$-band peak magnitude, JD−2,450,000.

[b]Uncertainties in units of 0.01 mag.

[c]Time delay between peak magnitude and late break in days.

Table 7: $R_{UV} - R_v$ Values from Extinction Corrections

| SN | $E(B-V)$ [mag][a] | $R_{uvw1} - R_v$ [mag] | $R_u - R_v$ [mag] | $R_{uvw2} - R_v$ [mag] |
|---|---|---|---|---|
| 2006X | 1.32 | 1.92 | 2.17 | 1.63 |
| 2007S[b] | 0.45 | 1.63 | 0.81 | 1.20 |
| 2007co[b] | 0.26 | 1.09 | 0.95 | 1.53 |

[a]See Tables 1 and 2 for reddening references.

[b]Broader-peaked optical light curves than low-extinction sample.

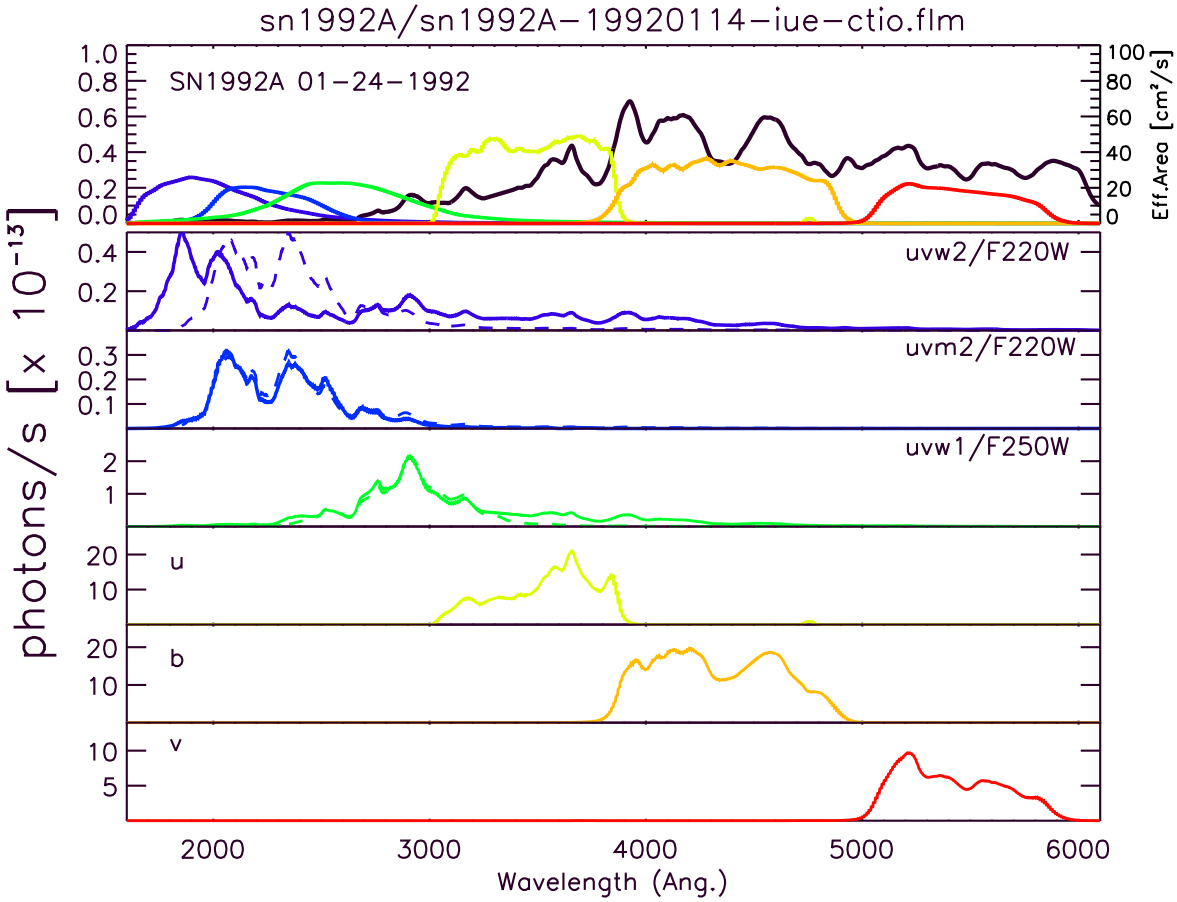


Fig. 1.— The six UVOT filter transmission curves folded through the *HST*/CTIO spectrum of SN 1992A (Kirshner et al. 1993). In the top panel, the spectrum is shown in black, compared to the transmission curves for the six UVOT filters. The next six panels show the SN spectrum folded through the UVOT transmission curves (solid lines), as well as the *HST* $F220W$ and $F250W$ filters (dashed lines).

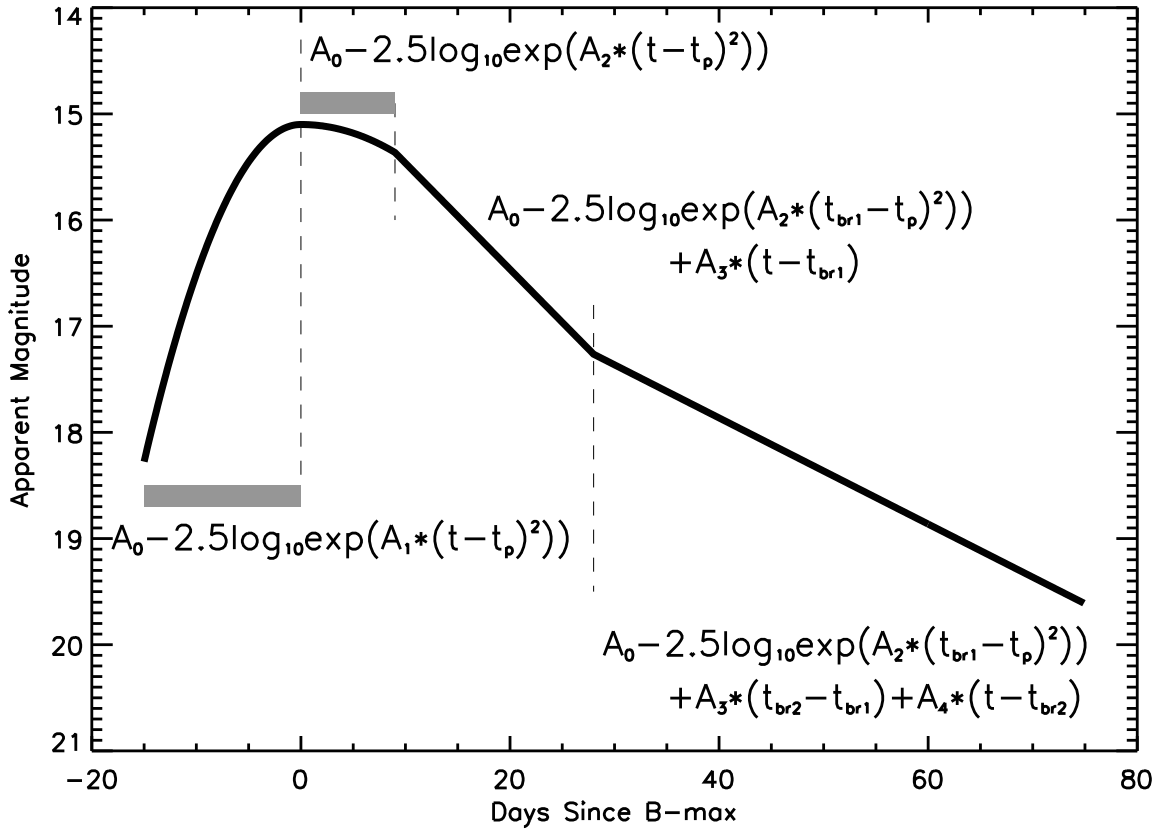


Fig. 2.— A schematic of the function fit to the SN light curves. The function is characterized by eight parameters: $A_0 - A_4$, $t_p$, $t_{br1}$, and $t_{br2}$.

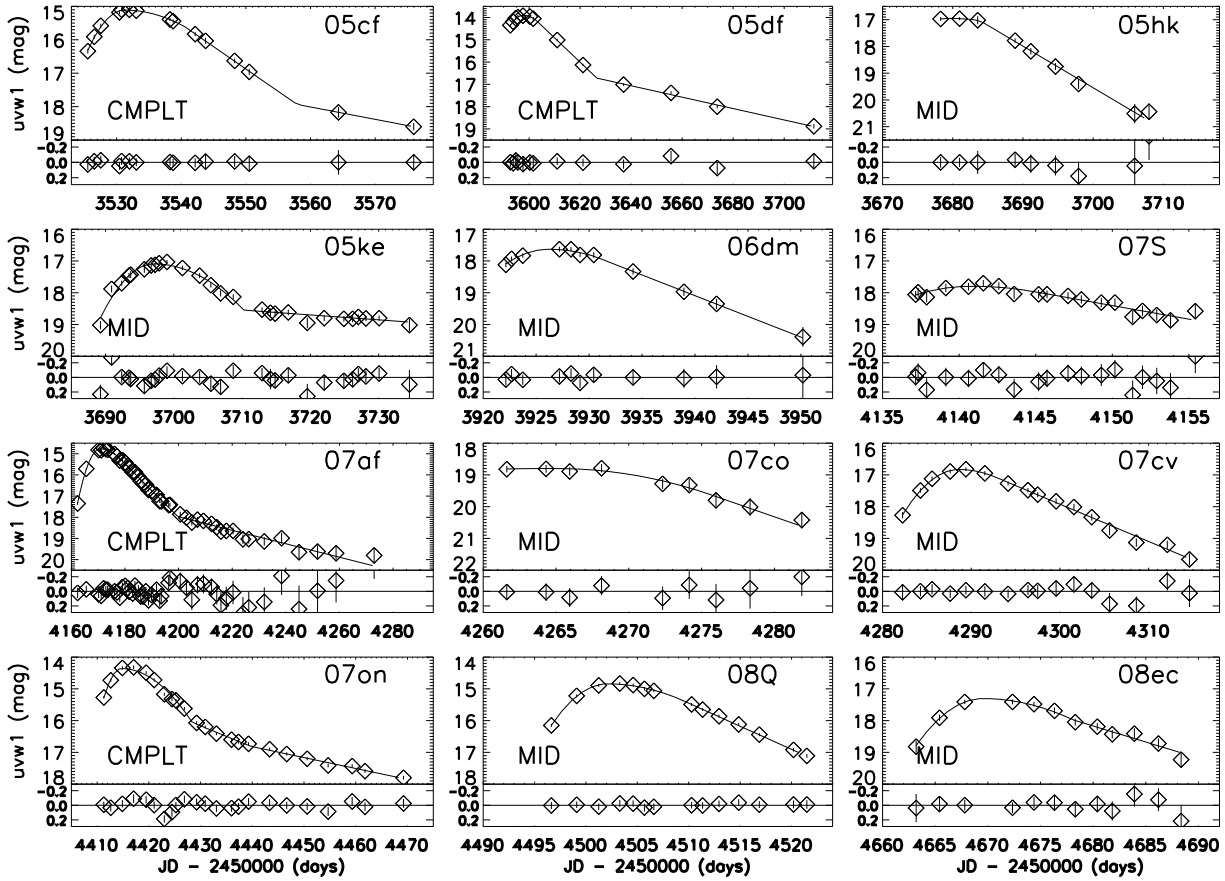


Fig. 3.— *uvw*1-band light curves of twelve SNe Ia observed near peak, fitted with a multi-component function, with residuals. The dataset for SN 2005ke was trunctated to allow fitting. See Fig. 12 for later-epoch data.

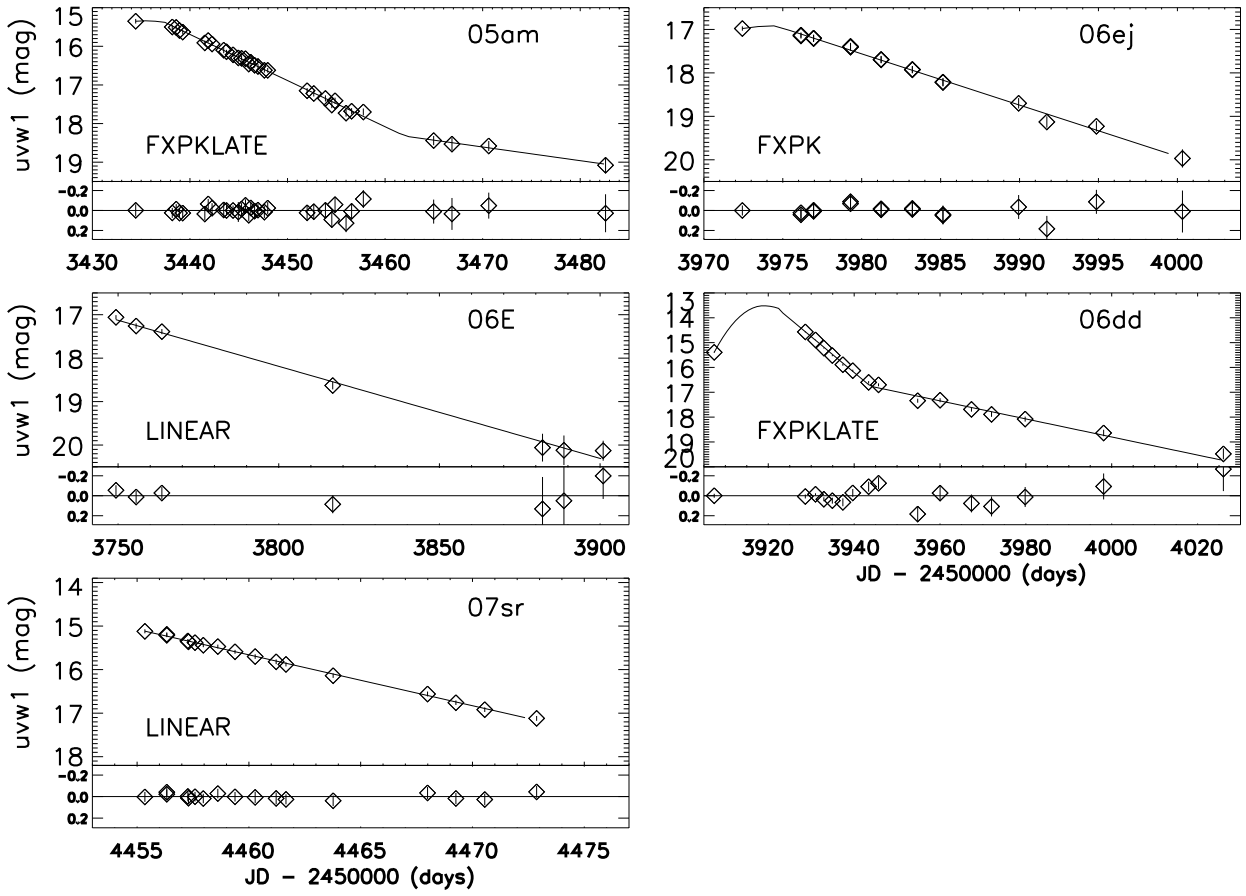


Fig. 4.— *uvw*1-band light curves of five SNe Ia not observed during the peak phase. Light curves were fitted with a model that fixed the Gaussian rise and decline constants.

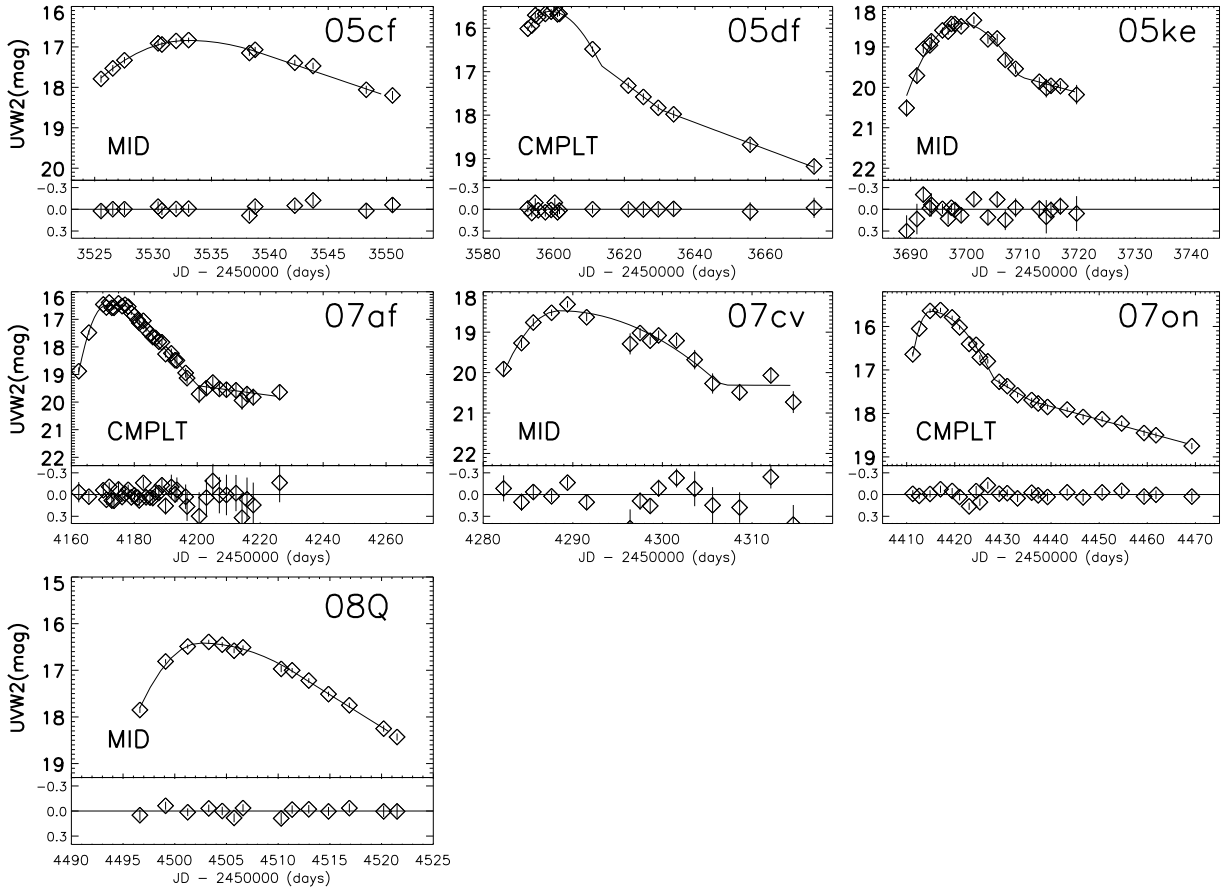


Fig. 5.— *uvw*2-band light curves of seven SNe Ia, fitted with a multi-component function, with residuals. The dataset for SN 2005ke was truncated, as in Fig. 3.

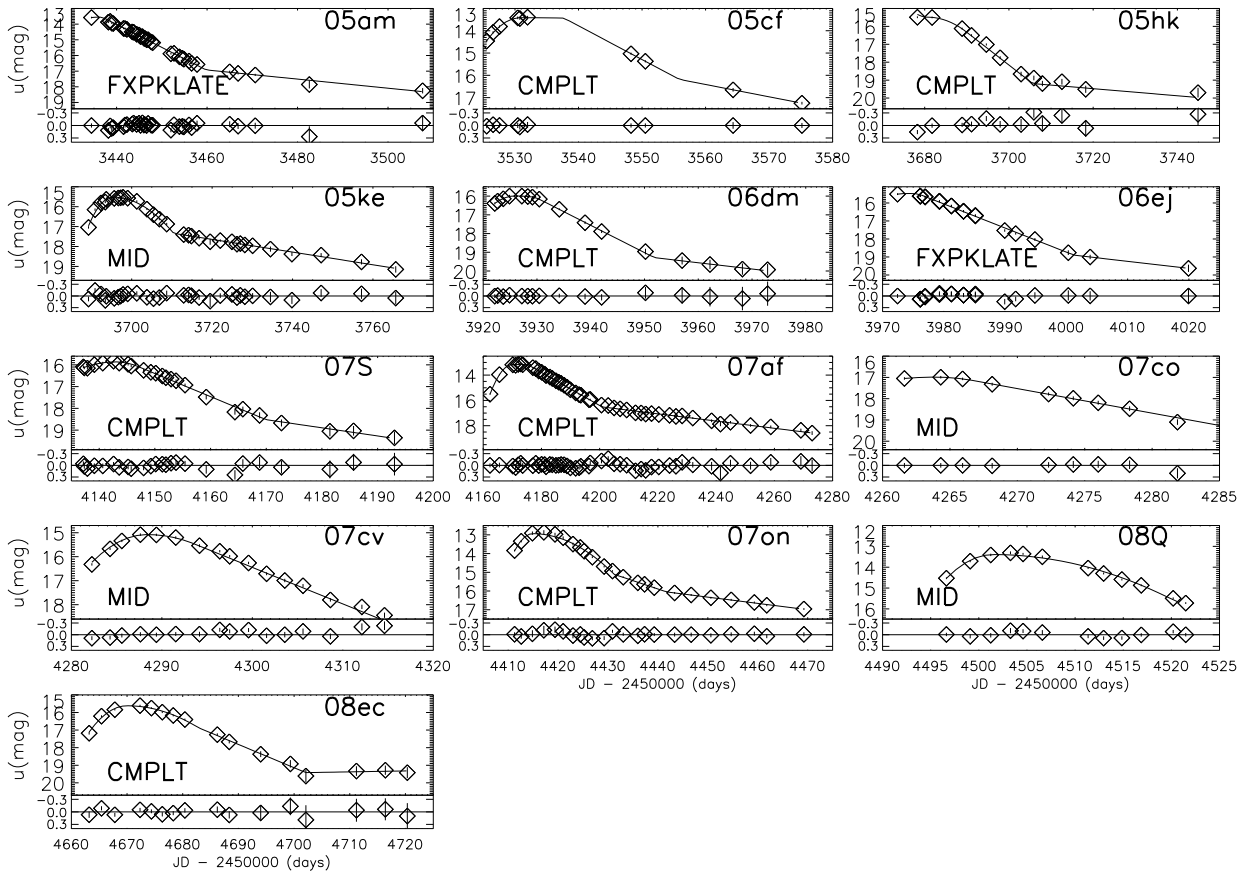


Fig. 6.— $u$-band light curves of ten SNe Ia, fitted with a multi-component function, with residuals. The dataset for SN 2005ke was truncated, as in Fig. 3.

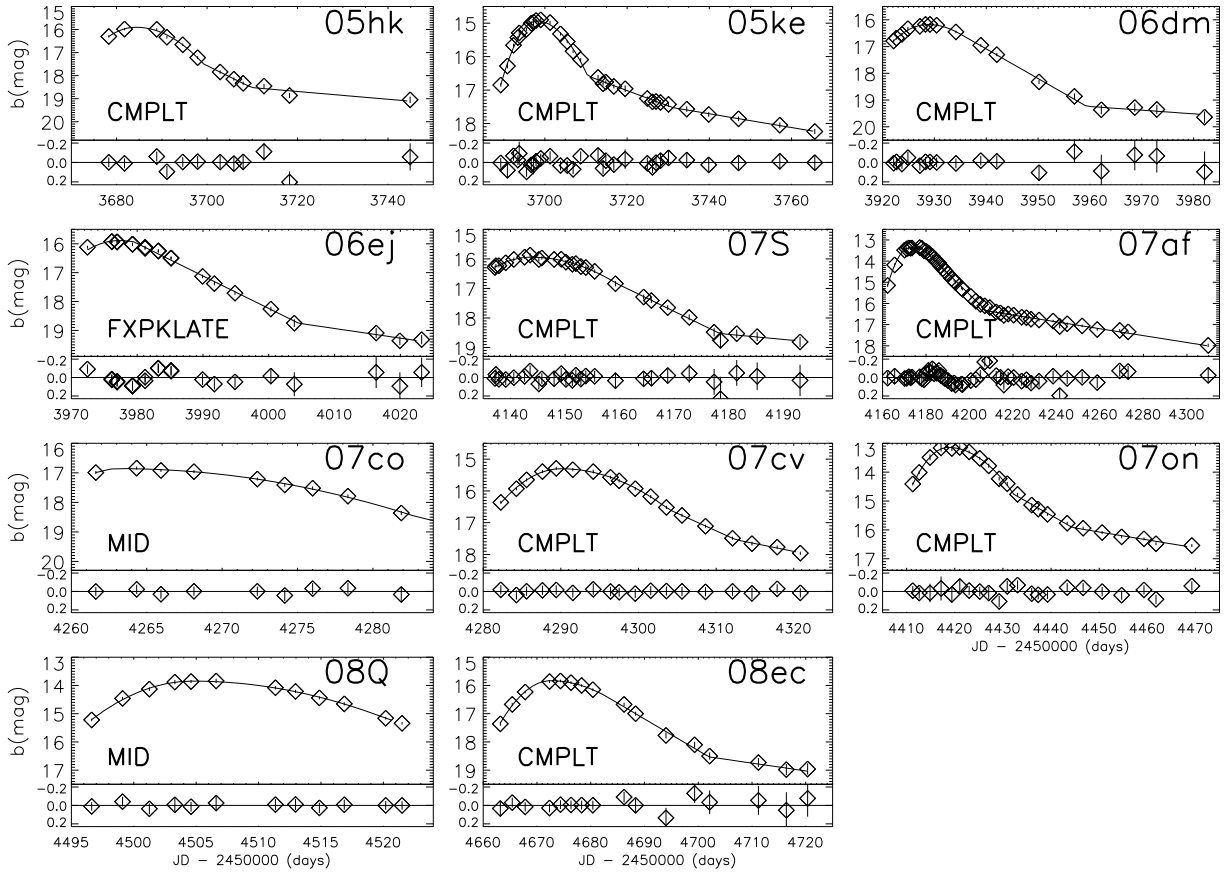


Fig. 7.— *b*-band light curves of ten SNe Ia, fitted with a multi-component function, with residuals. The dataset for SN 2005ke was truncated, as in Fig. 3.

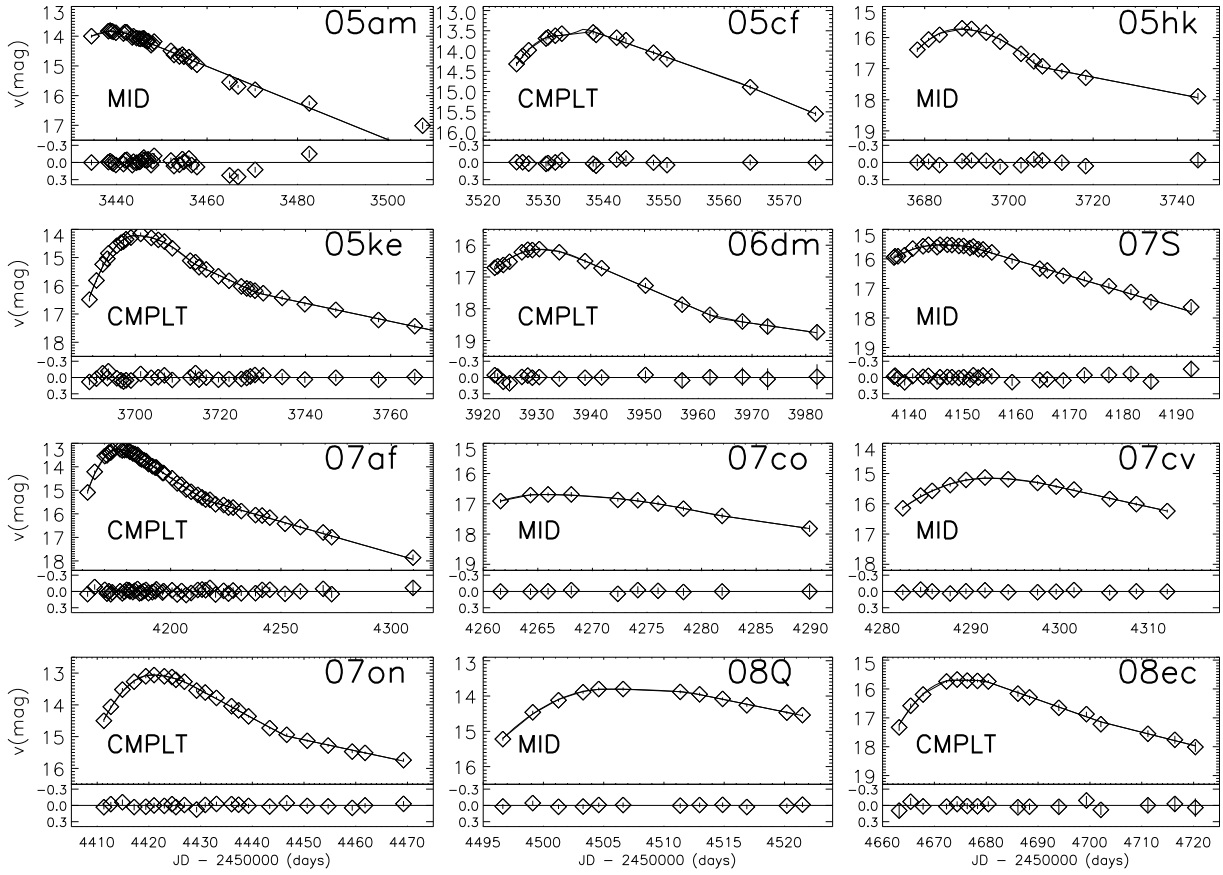


Fig. 8.— $v$-band light curves of twelve SNe Ia, fitted with a multi-component function, with residuals. The dataset for SN 2005ke was truncated, as in Fig. 3.

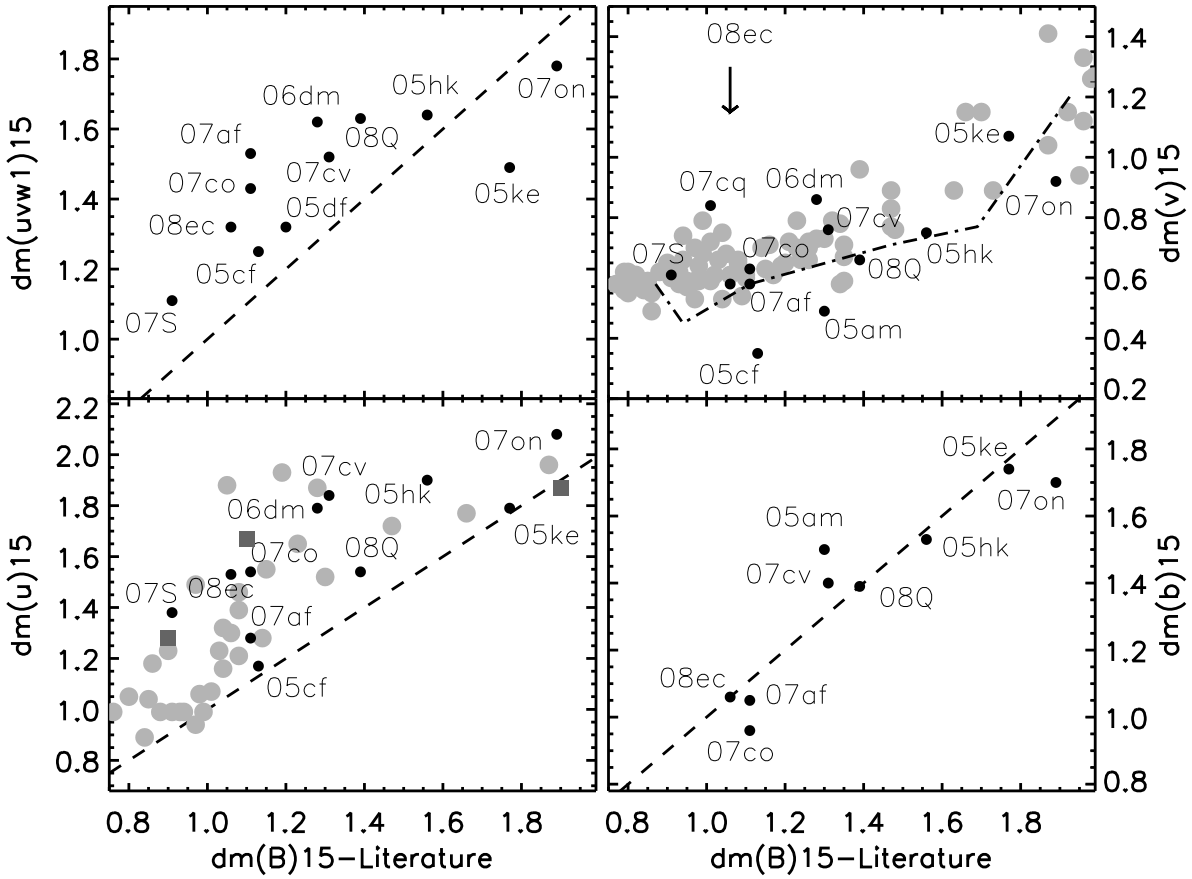


Fig. 9.— 15-day decline rates for UVOT data. The $uvw1$-band decline rates are compared to the $B$-band rates (upper-left panel), the $u$-band rates are compared to the $B$ band (lower-left panel), and the $v$-band rates are compared to the $B$ band (upper-right panel). UVOT $b$-band rates are compared to ground-based $B$-band values for the same SNe (lower-right panel); the dashed line indicates equality. The dot-dashed line shows values for SN Ia templates (Hamuy et al. 1996). Values of $\Delta m_{15}(U)$, $\Delta m_{15}(B)$, and $\Delta m_{15}(V)$ from 101 SNe Ia in the CfA3 study are shown as grey circles. Values of $\Delta m_{15}(U)$ versus $\Delta m_{15}(B)$ for the overluminous, normal and subluminous templates from Nugent are shown as grey squares.

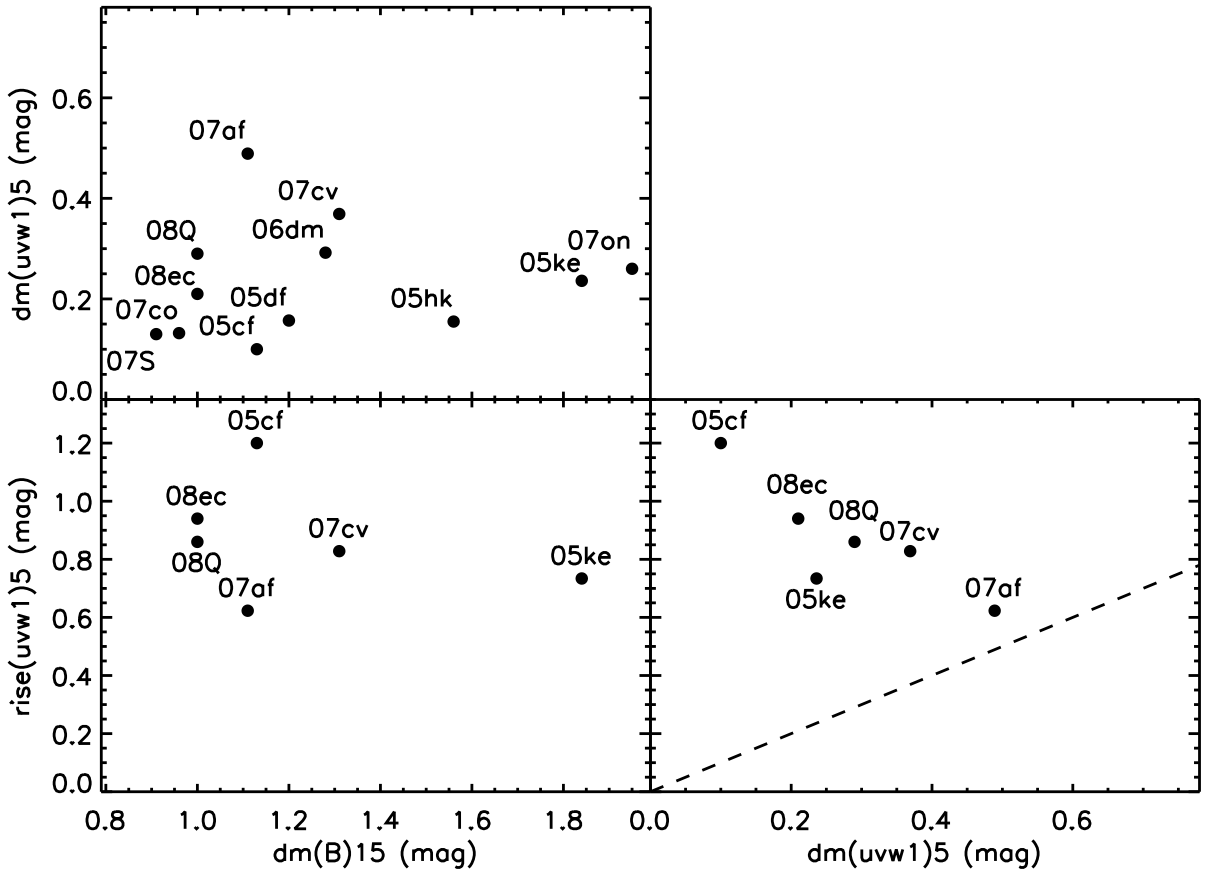


Fig. 10.— The 5-day rise (lower left) and 5-day declines (upper left) of the $uvw1$ emission from twelve SNe Ia. Six SNe Ia had measurements for both parameters, which are plotted against each other in the lower-right panel. The light curves rise to the peak more steeply than they decline from the peak. Values of $\Delta m_{15}(B)$ are taken from Tables 1 and 2.

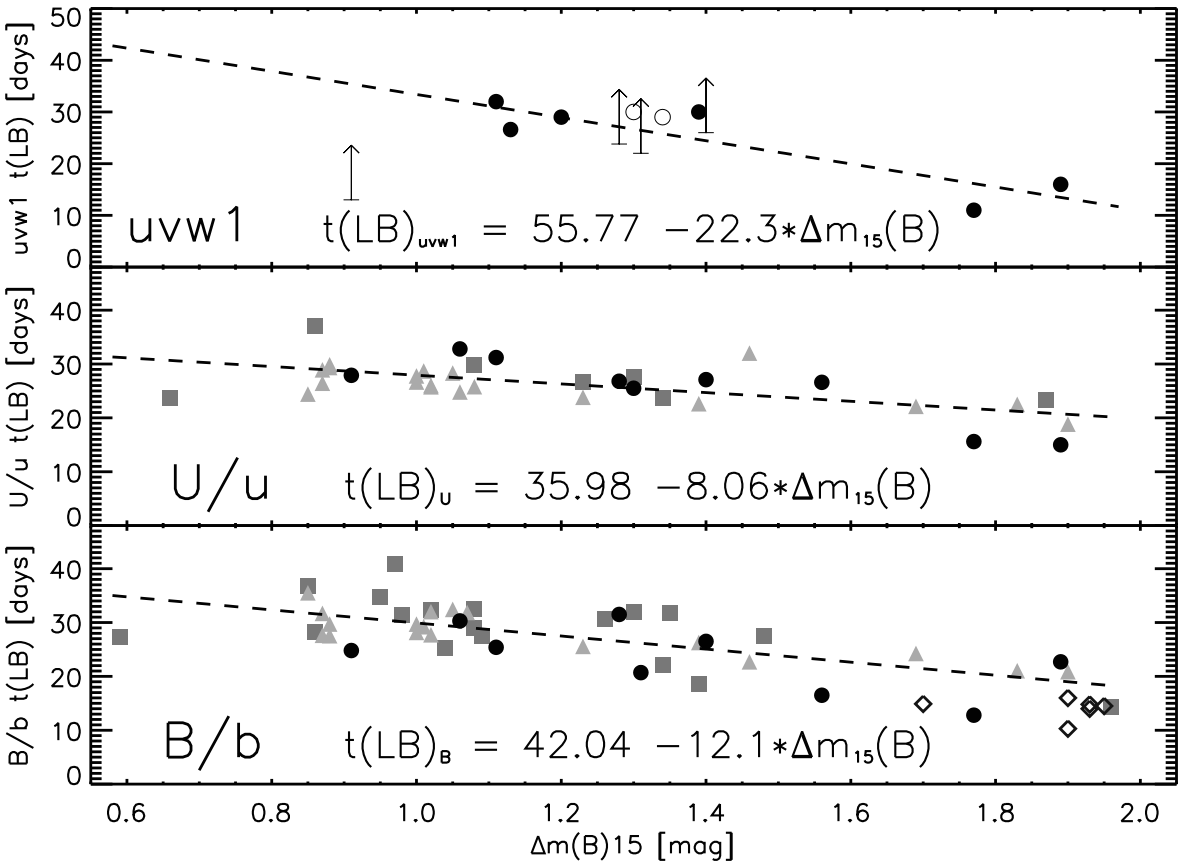


Fig. 11.— Late-time light-curve breaks in the $uvw1$ band (upper panel), $U$ and $u$ bands (middle panel), and $B$ and $b$ bands (lower panel) for 53 SNe Ia shown as a function of $\Delta m_{15}(B)$. UVOT SNe with well-defined peak dates are shown as filled circles, poorly defined peak dates are shown as open circles, lower limits as arrows. CfA2 SNe Ia are shown as grey triangles, and CfA3 SNe Ia are shown as grey squares. Subluminous SNe Ia from Kasliwal et al. (2008) are shown as open diamonds. The subluminous SNe Ia break sooner than do the normal SNe Ia. Each filter is fitted with a dashed line, following the function listed.

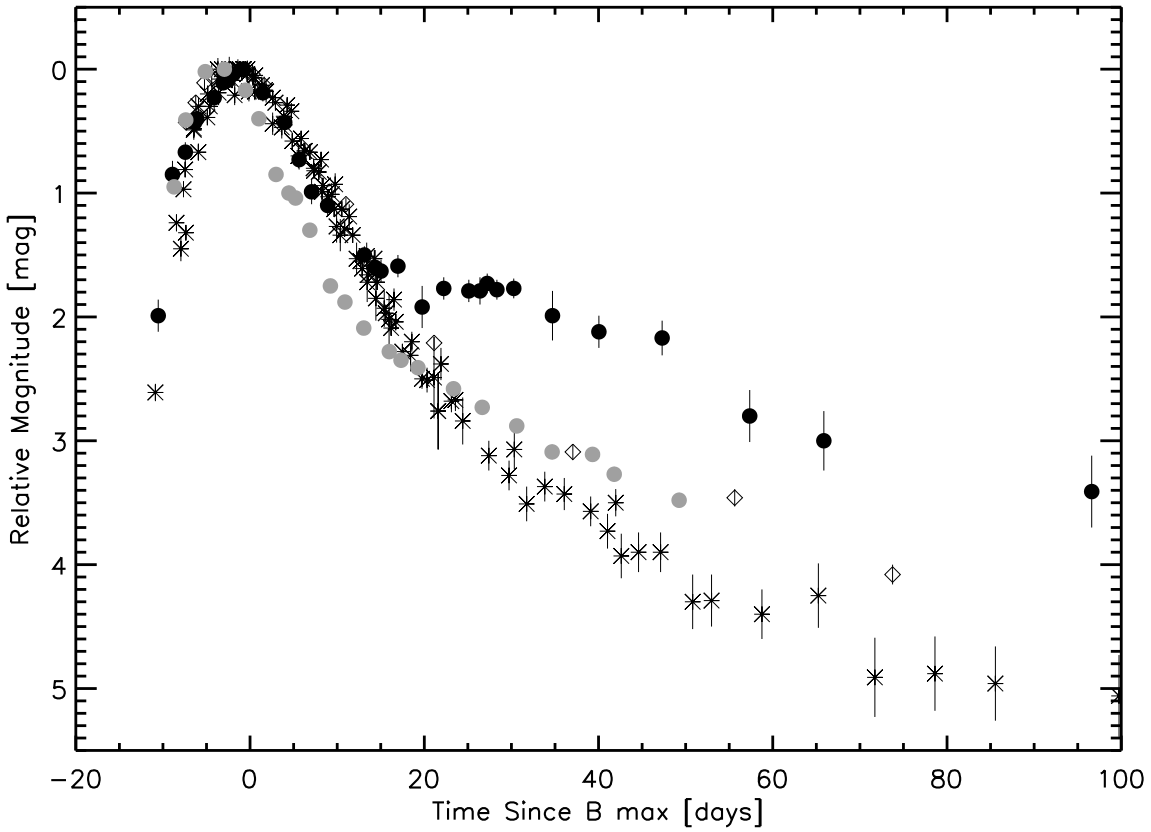


Fig. 12.— $uvw1$-band light curves of SNe Ia aligned by peak magnitude. Seven normal SNe Ia (asterisks/open diamonds) are shown compared to two subluminous SNe Ia (SNe 2005ke and 2007on). SN 2005ke (dark filled circles) breaks to a bright plateau, while SN 2007on (grey filled circles) breaks at an early epoch, but to a flat decline fainter than that of SN 2005ke. SN 2005df, a normal-luminosity SN Ia (open diamonds), features an early-time light curve similar to that of the other normal SNe Ia, but breaks at a late epoch to a very shallow decline.

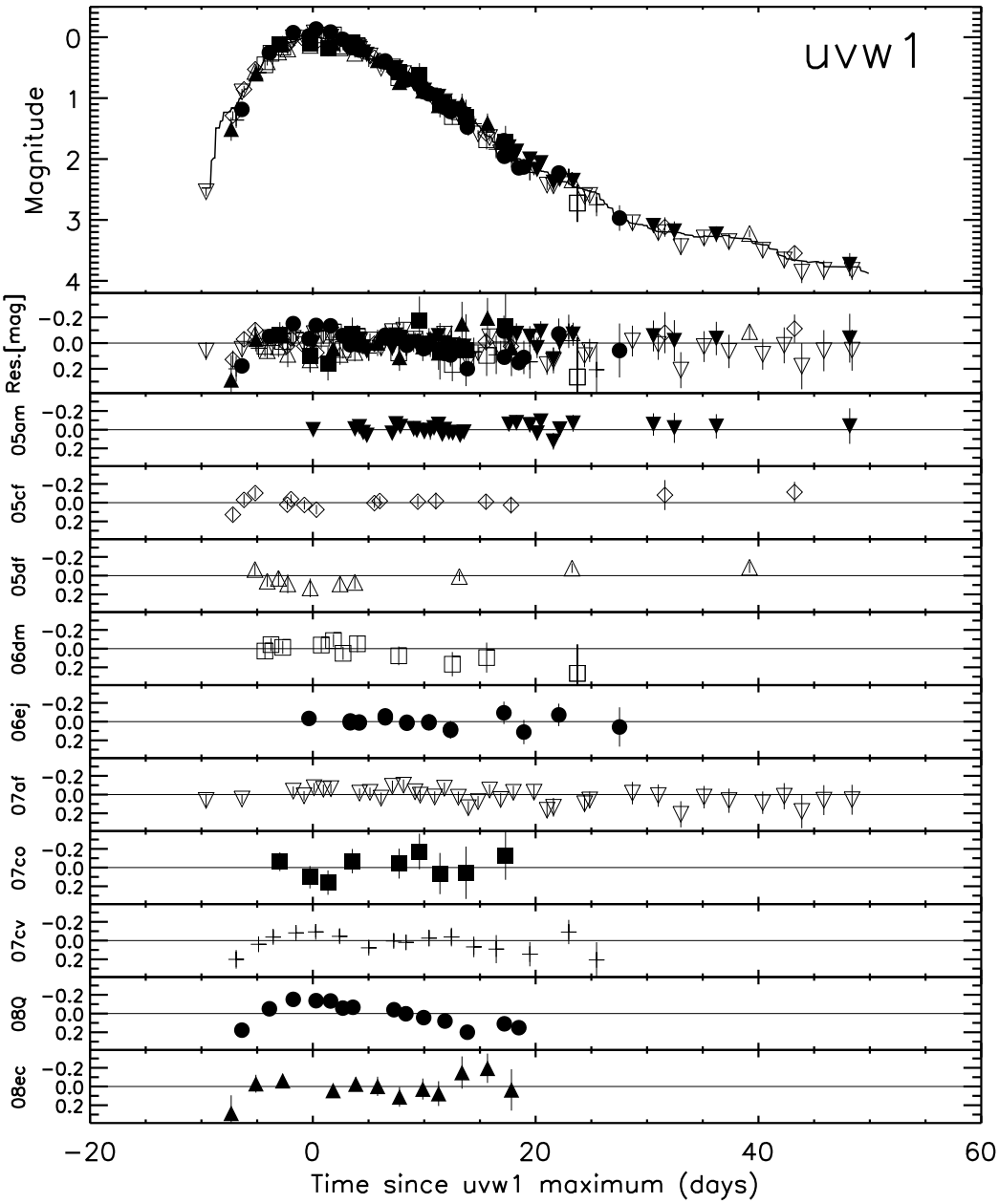


Fig. 13.— Mean template of eight SNe Ia in the *uvw*1 filter. The light curves were shifted in time and magnitude to produce the mean template (upper panel). The residuals of individual SNe relative to the mean template are shown in the lower panels. The template was calculated from −12 to +50 days relative to *uvw*1 maximum.

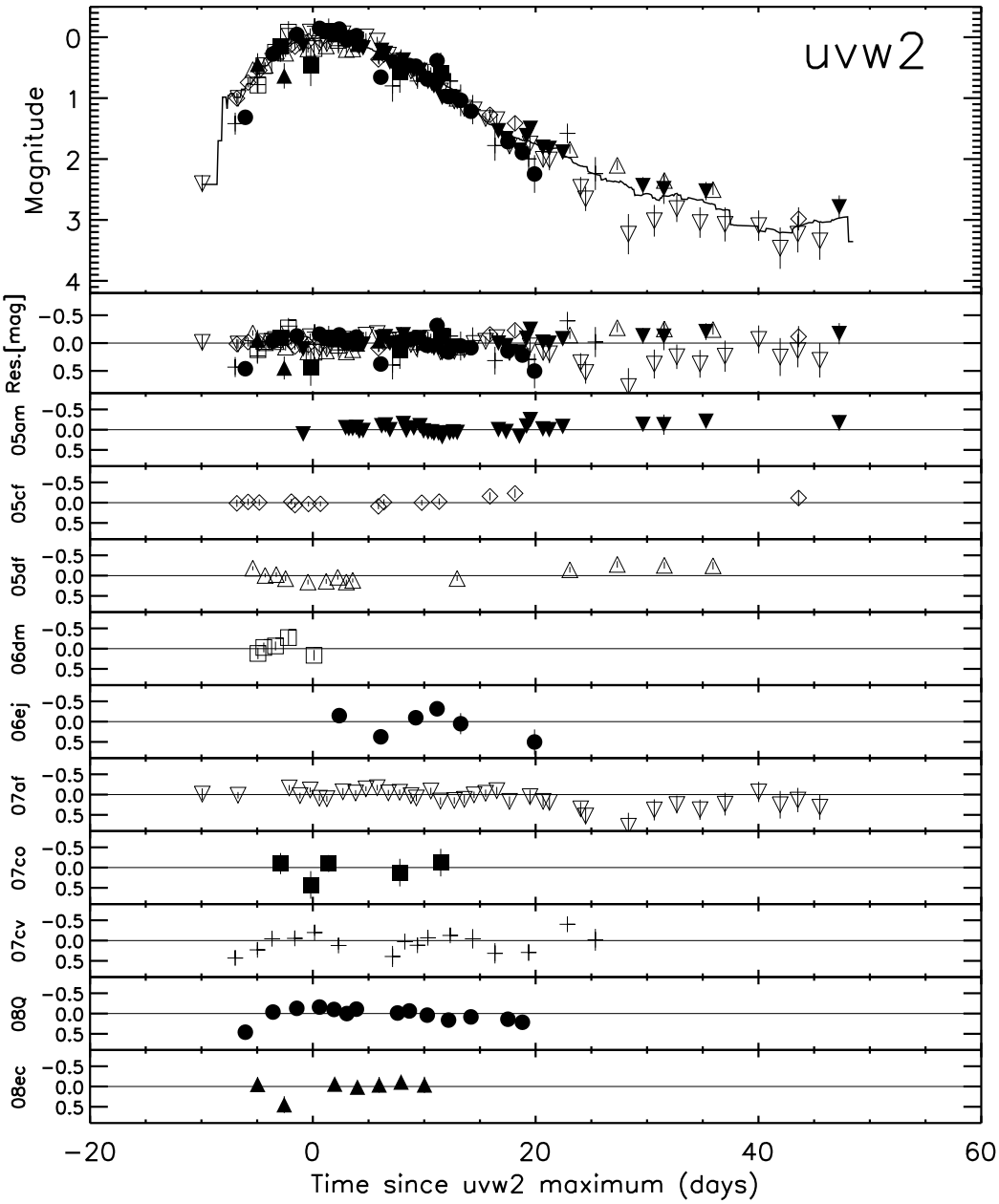


Fig. 14.— Mean template of eight SNe Ia in the $uvw2$ filter. The mean template is shown in the upper panel, while the residuals of individual SNe relative to the mean template are shown in the lower panels. The template was calculated from −12 to +50 days relative to $uvw2$ maximum.

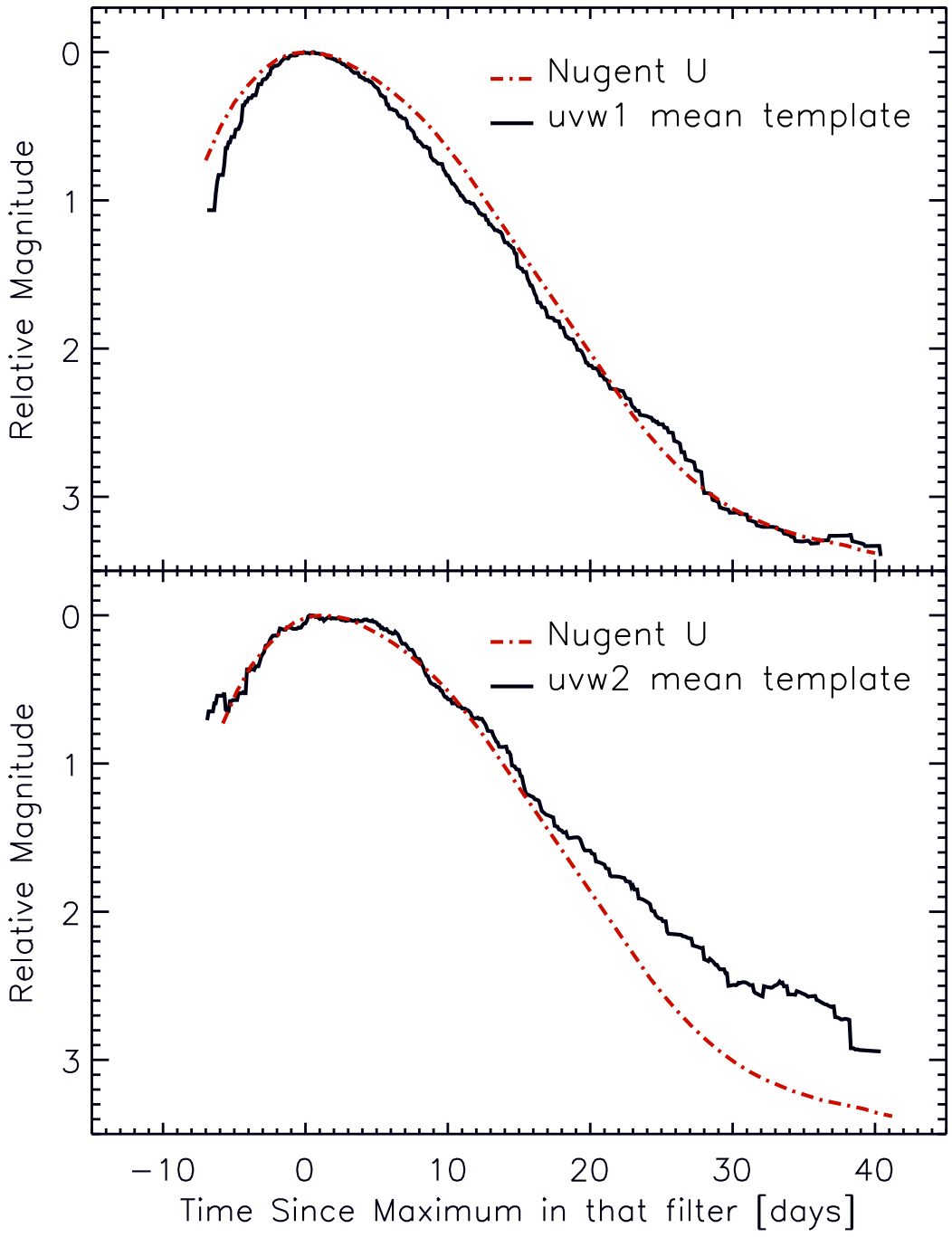


Fig. 15.— $uvw1$ and $uvw2$ mean templates compared to the normal $U$-band template from P. Nugent (2009, private communication). The $uvw1$ template (upper panel) rises more steeply to peak, and is somewhat faster than the $U$-band template in the initial decline, coming to better agreement at late times. The $uvw2$ template (lower panel) roughly matches the $U$-band template until +15 days, remaining brighter at later epochs.

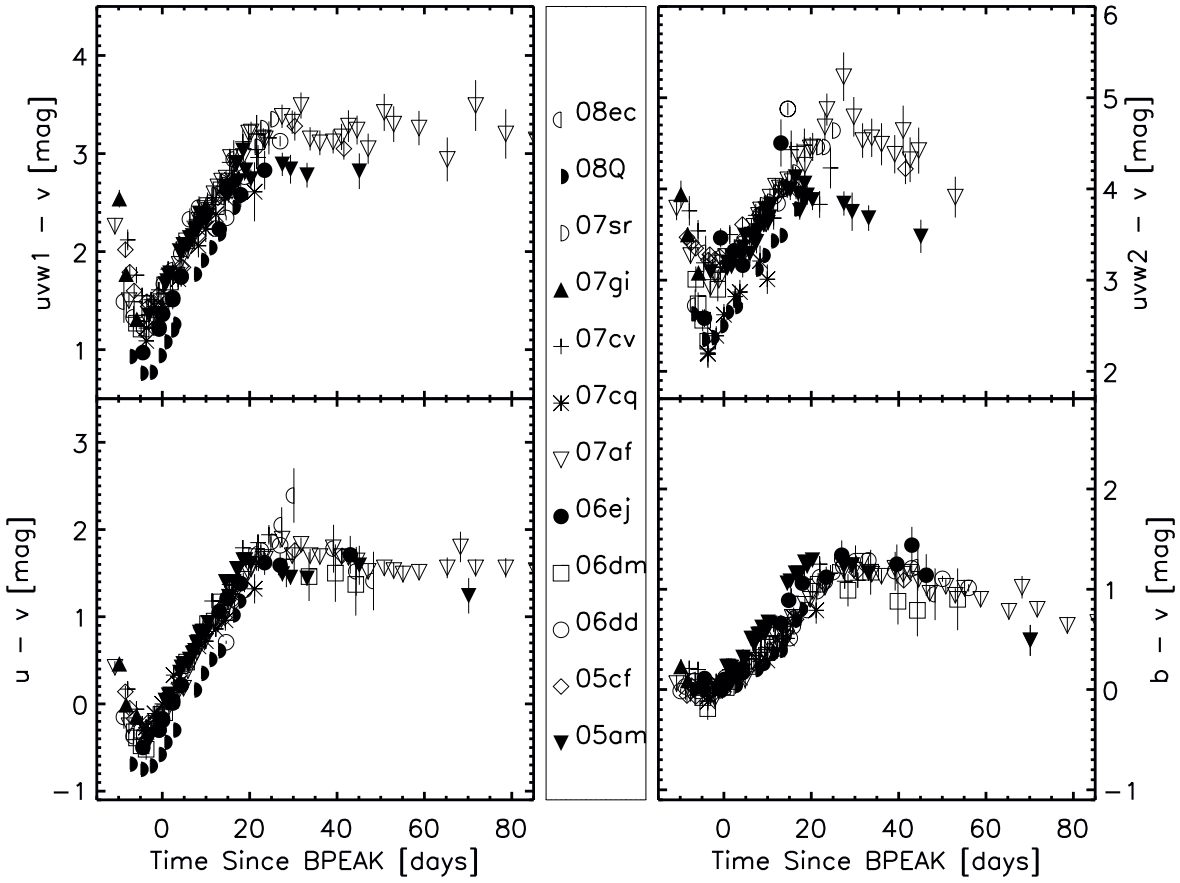


Fig. 16.— Colors of twelve normal SNe Ia relative to the $v$ band. There is a high degree of homogeneity in these SNe out to +25 days.

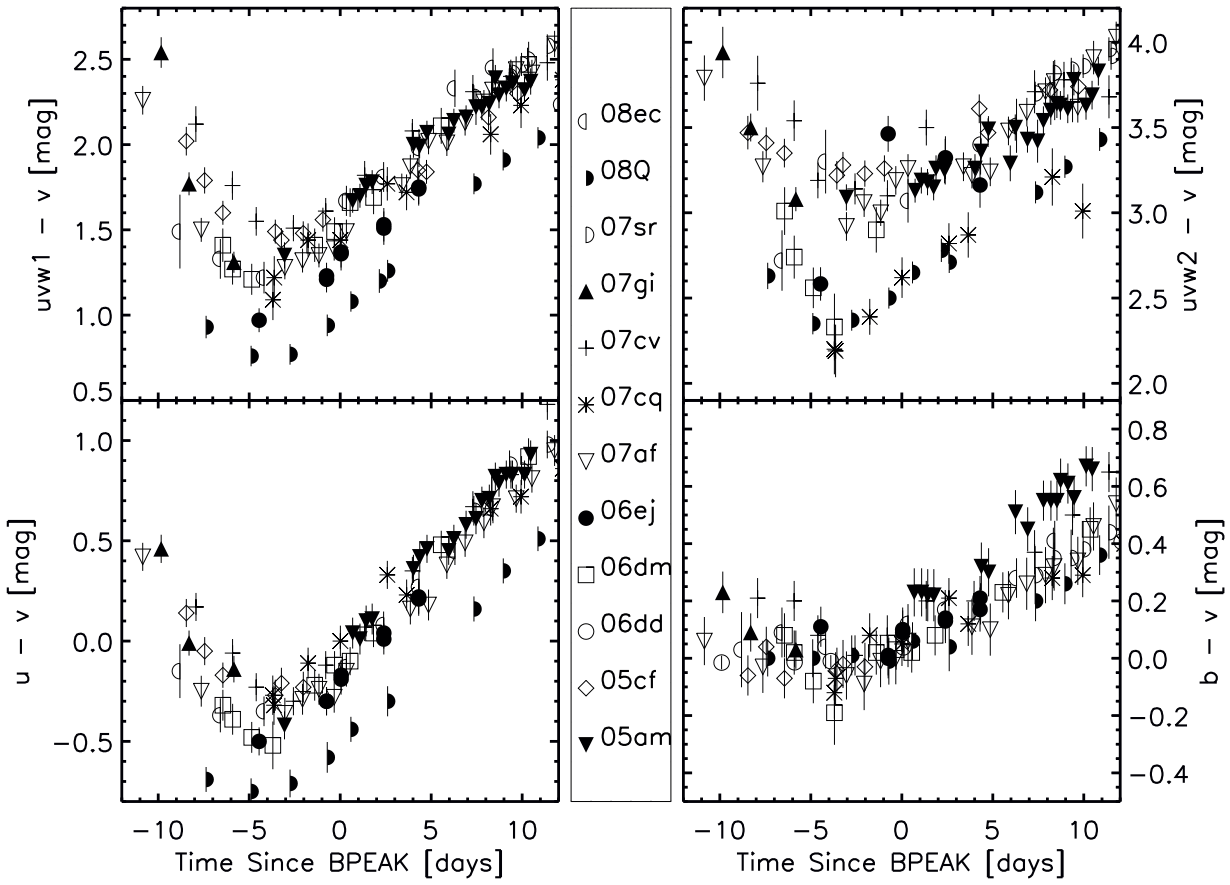


Fig. 17.— Near-peak colors of twelve normal SNe Ia compared to the $v$ band. When concentrating upon the near-peak epoch, variations between individual events are apparent. The variations of the "blue peak" are as small as $\sim$0.2 mag in $u - v$, but over 1.0 mag in $uvw2 - v$.

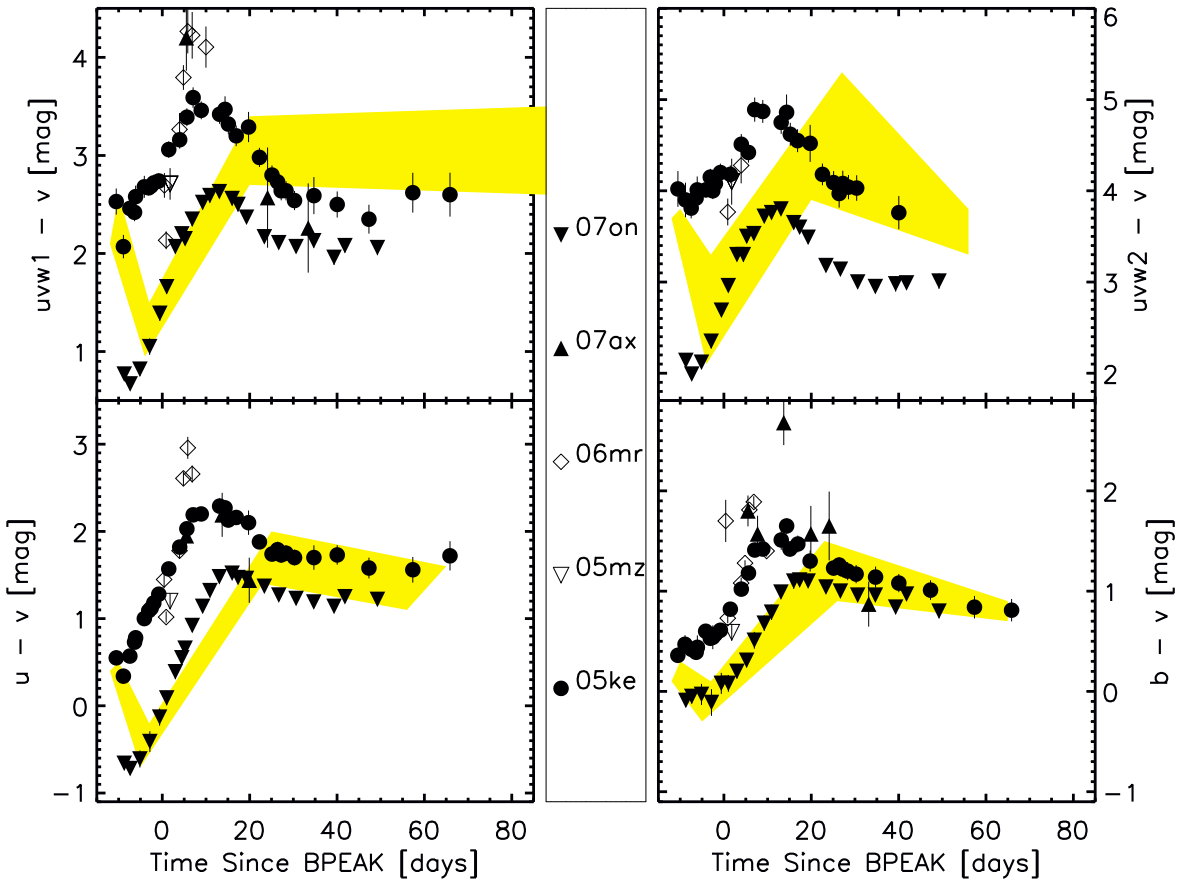


Fig. 18.— Colors of four subluminous SNe Ia compared to the $v$ band. In each panel, the range of colors of the normal SNe Ia is shown as the shaded region. The colors of the subluminous SNe Ia differ appreciably from those of the normal SNe Ia.

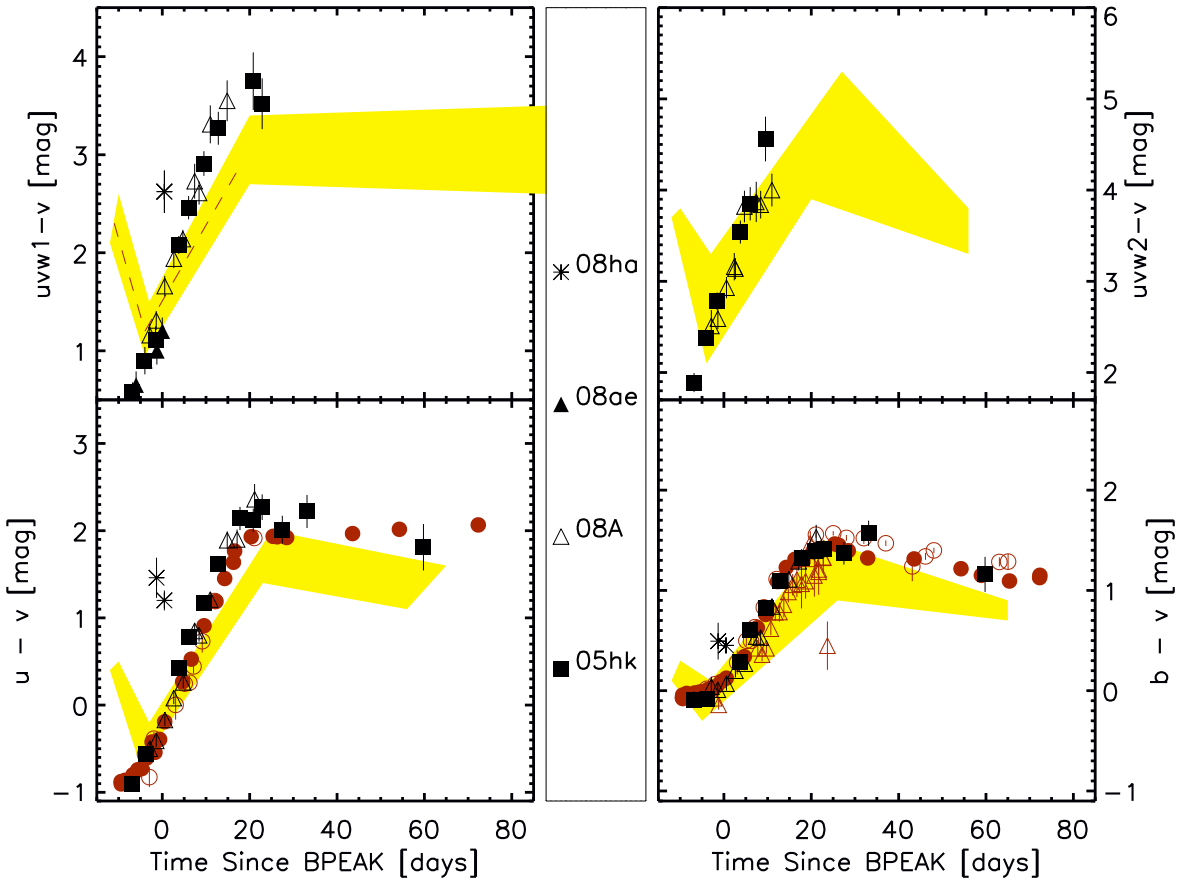


Fig. 19.— Colors of four SN 2002cx-like SNe Ia compared to the $v$ band. In each panel, the range of colors of the normal SNe Ia is shown as the shaded region. SN 2008ha UVOT photometry is from Foley et al. (2009). Ground-based $UBV$ observations of SN 2002cx (Phillips et al. 2007, open triangles) and SN 2005hk (Sahu et al. 2008, open circles; Stanishev et al. 2008, filled circles) confirm the trends seen in the UVOT photometry. The colors of the SN 2002cx-like SNe Ia are initially bluer than the normal SNe Ia, but become redder with a steeper slope than seen for the normal SNe Ia.

.

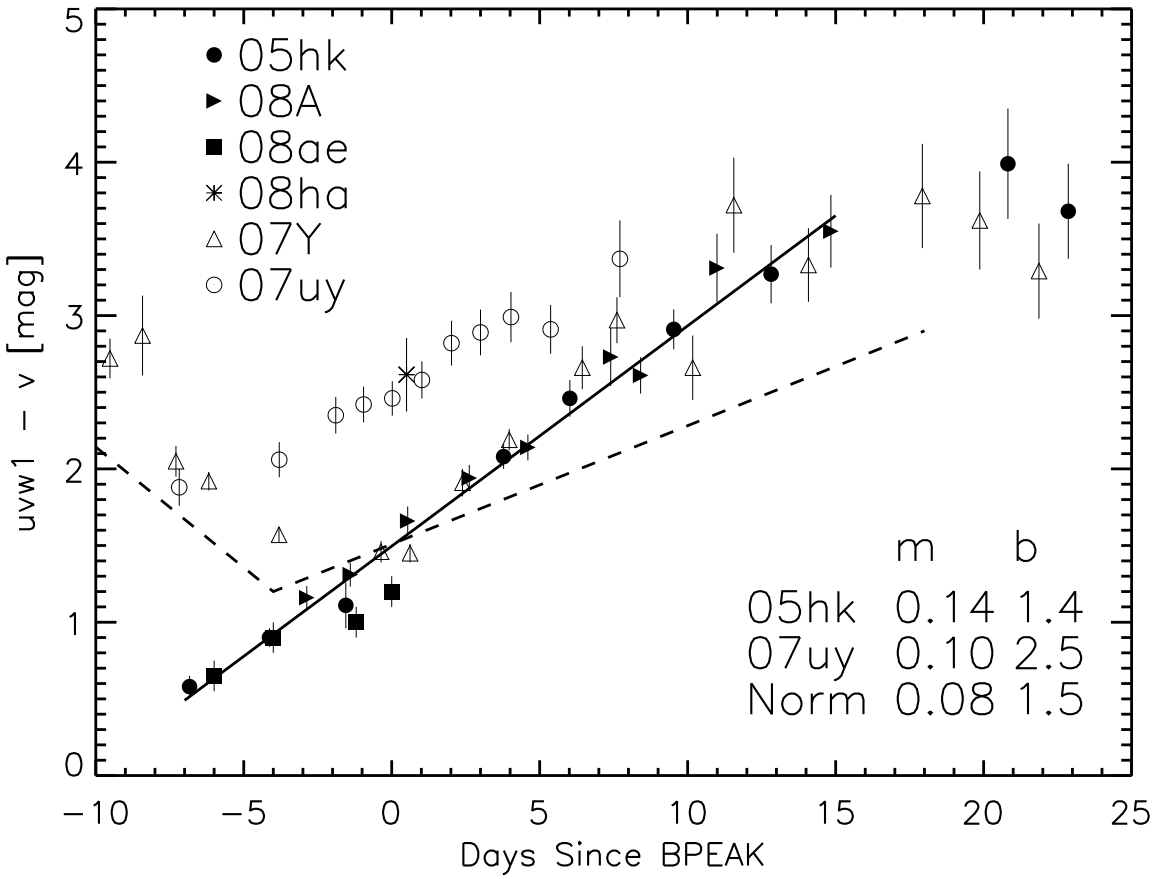


Fig. 20.— $uvw1 - v$ color curves for four SN 2002cx-like SNe Ia compared with normal SNe Ia and two SNe Ib/Ic. The solid line is a linear fit to the SN 2005hk data, and the dashed line is a two-line fit to the twelve normal SNe Ia shown in Fig. 16. Data for SN 2007Y (open triangles) and SN 2007uy (open circles) are from Brown et al. (2009). The three SN 2002cx-like SNe Ia have color evolution consistent with a linear evolution out to +13 days, with a slope which is steeper than that seen in the normal SNe Ia.

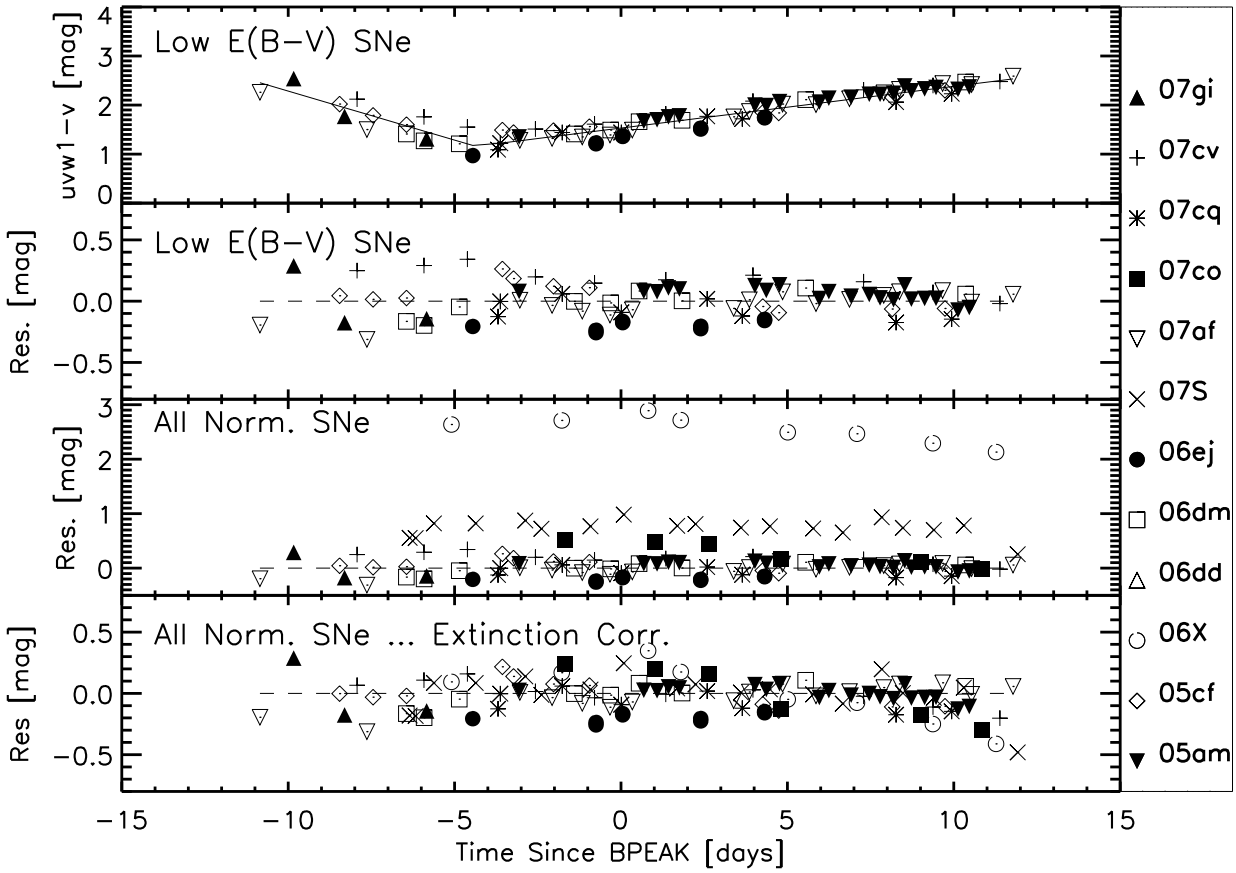


Fig. 21.— $uvw1 - v$ colors as a function of extinction. The $uvw1 - v$ colors of nine low-extinction, normal SNe Ia are shown fitted with a two-line function (upper panel), along with the resulting residuals (second panel). The residuals increase when higher-extinction SNe are added (third panel), but applying a reddening correction decreases the residuals (fourth panel). SN 2008Q was not included in this preliminary exploration of a reddening correction, as it appears to be an anomalously blue SN Ia.

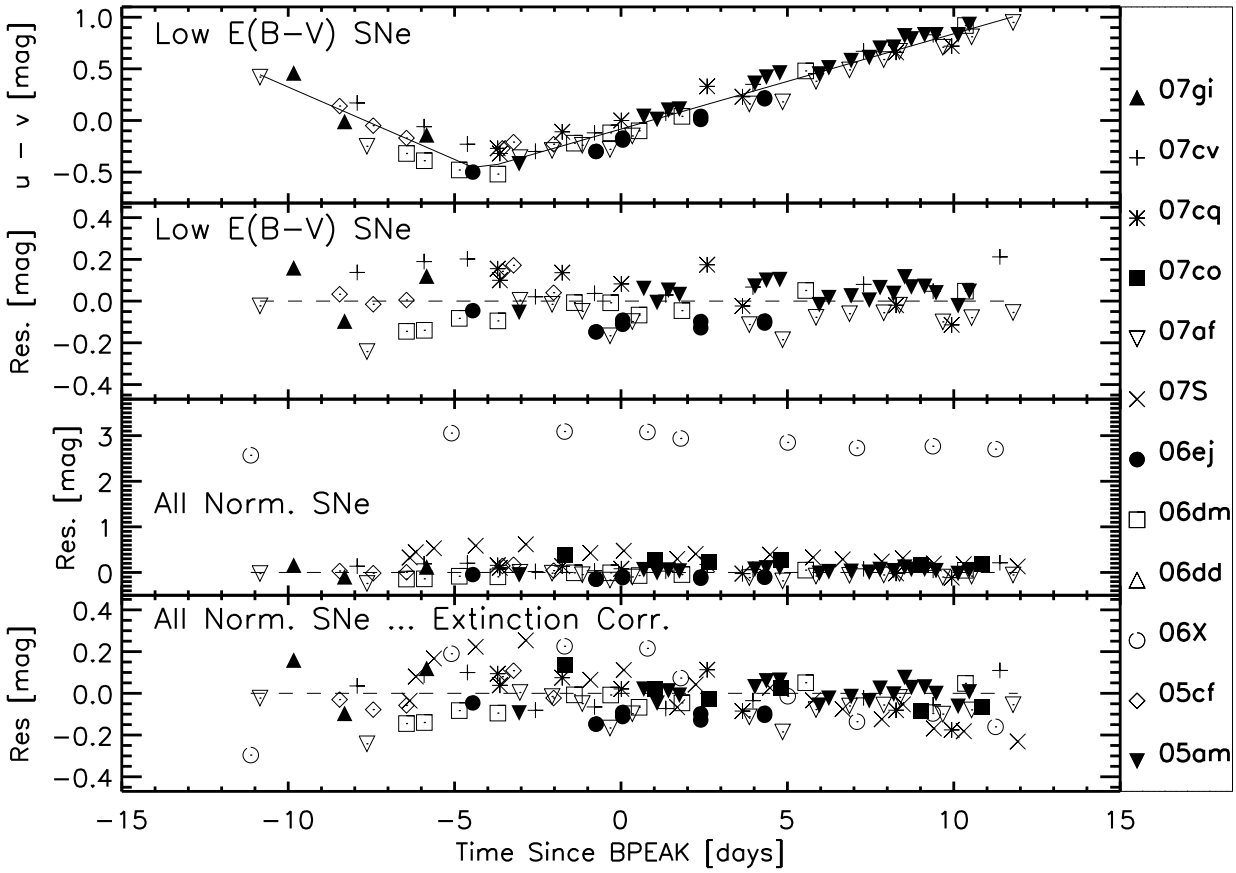


Fig. 22.— $u - v$ colors as a function of extinction. The panels are the same as in Fig. 21.

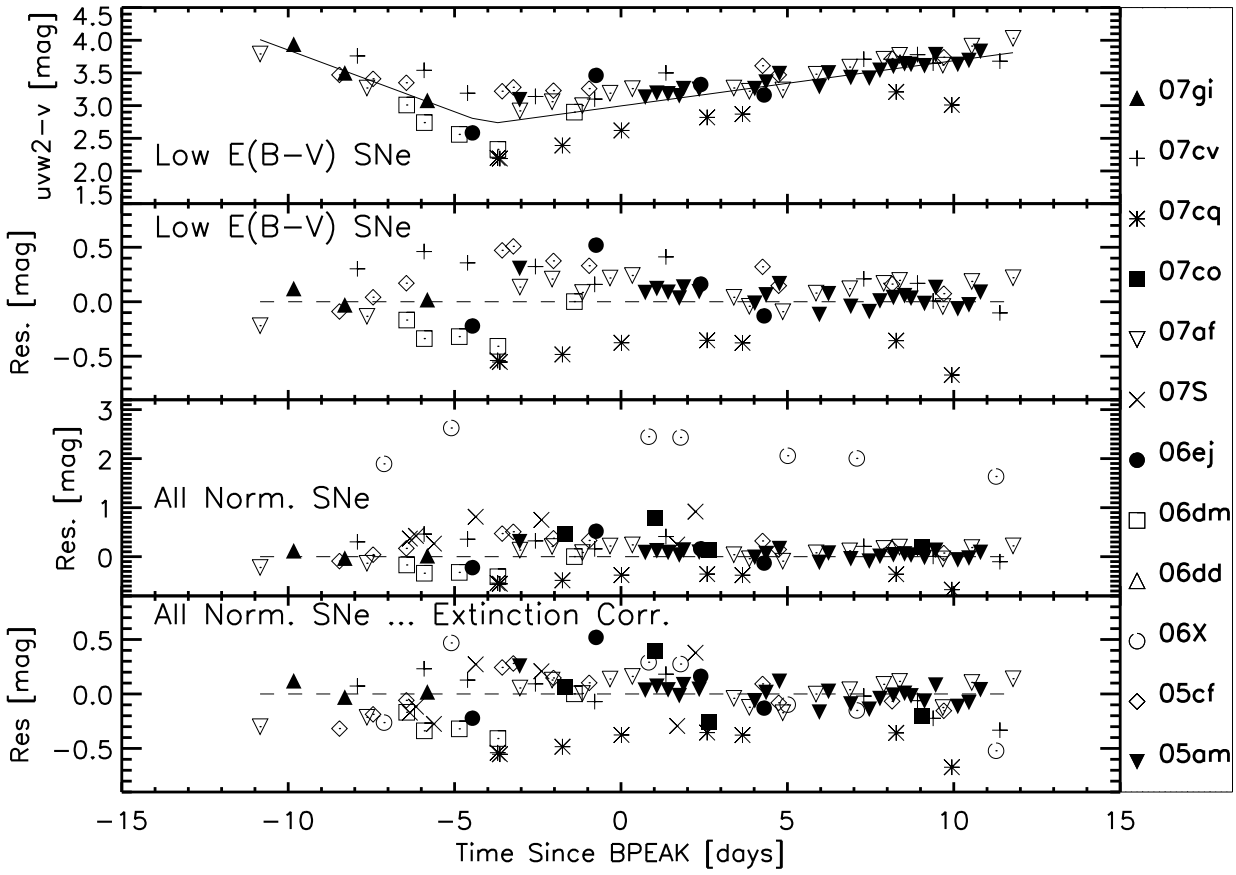


Fig. 23.— $uvw2 - v$ colors as a function of extinction. Symbols are the same as in Fig. 21. The color curves appear to deviate from the two-line fit during the near-peak epoch, with some bluer than the lines and some redder than the lines.

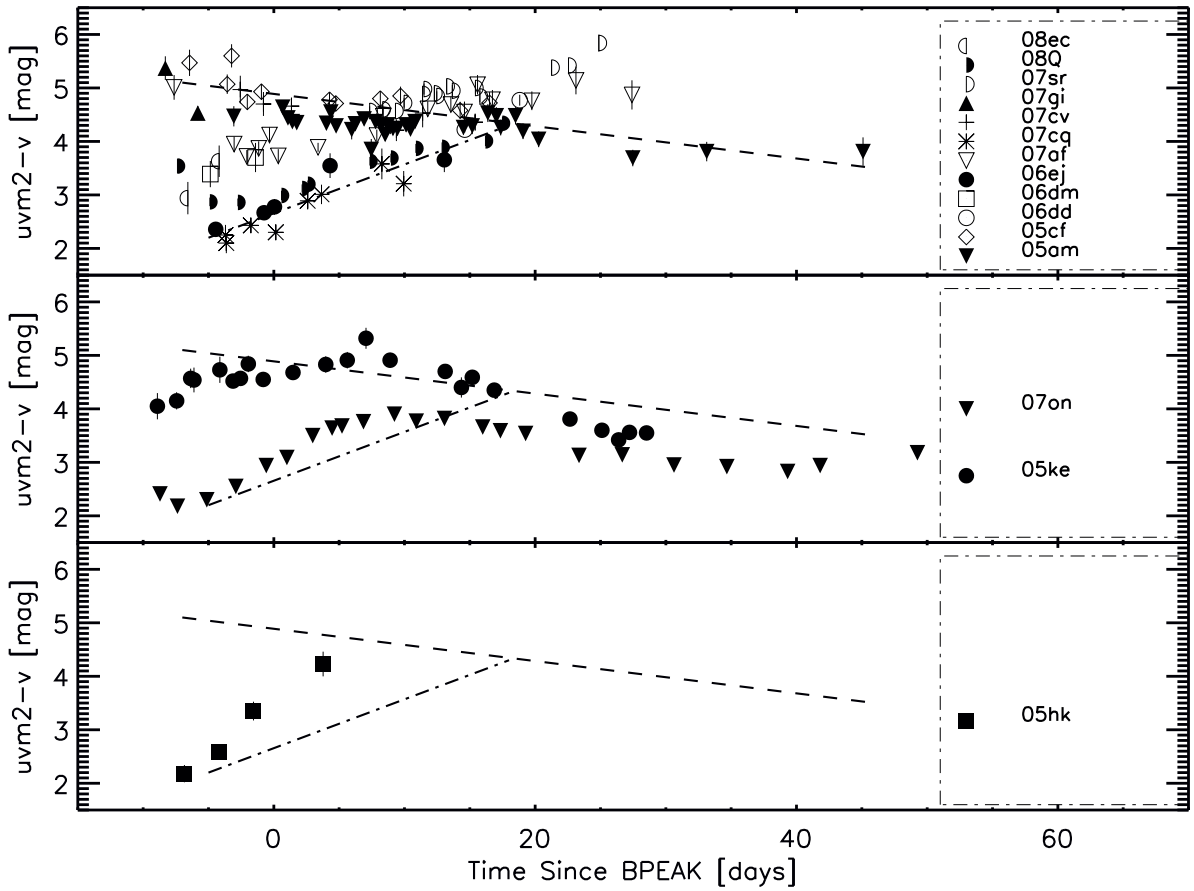


Fig. 24.— $uvm2 - v$ colors of 15 SNe Ia. Twelve normal SNe Ia are shown in the upper panel, the subluminous SNe 2005ke and 2007on in the middle panel, and the SN 2002cx-like SN 2005hk in the lower panel. The normal SNe Ia exhibit two branches of color-curve shape, while SNe 2005ke, 2007on, and 2005hk appear to follow the general evolution as seen for those SNe in the $uvw1 - v$ and $uvw2 - v$ color curves.

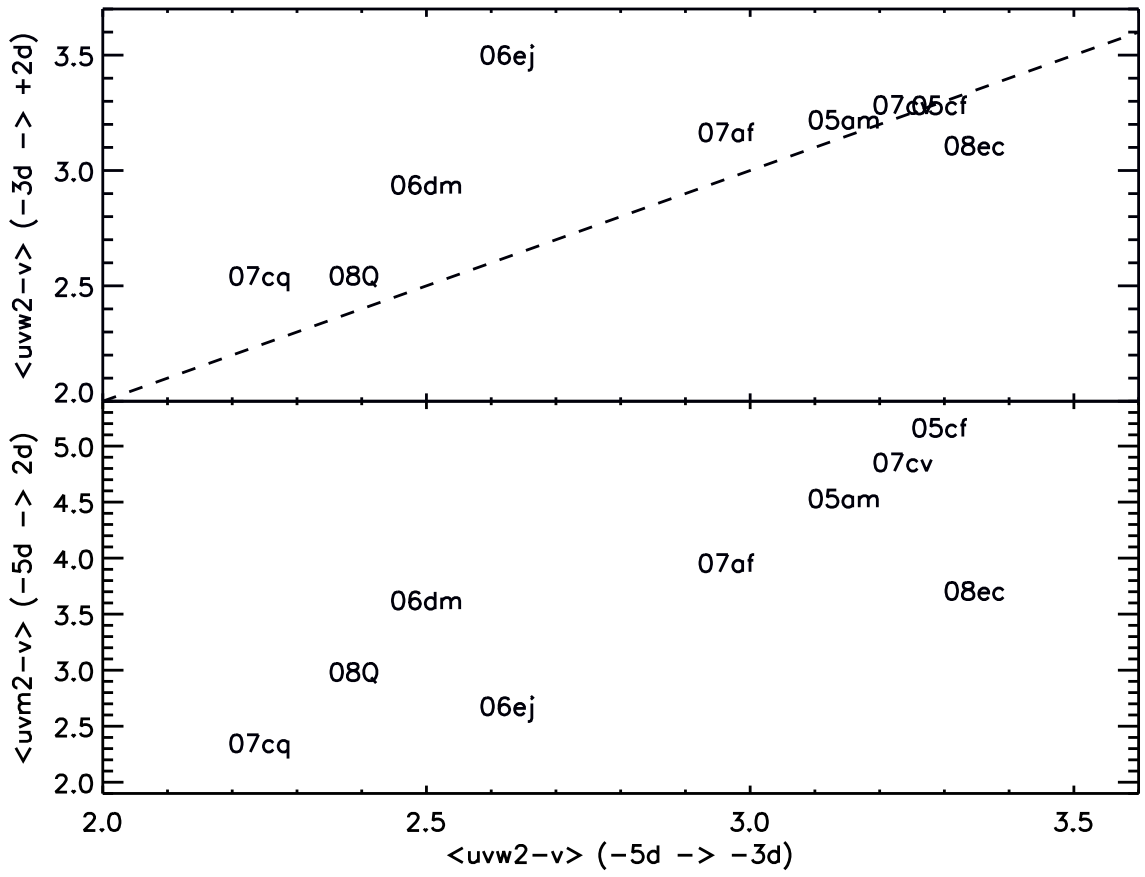


Fig. 25.— Color-color plots for normal SNe Ia. The mean $uvw2-v$ color during the epoch from $t=-5$ to $-3$ days relative to $B$ maximum is compared to the mean $uvw2-v$ color during the epoch $t=-3$ to $+2$ days (upper panel). Similarly, the mean $uvw2-v$ color during the epoch $t=-5$ to $-3$ days is compared to the mean $uvm2-v$ color during the epoch $t=-5$ to $+2$ days (lower panel). The general tendency for SNe Ia with red $uvw2-v$ color to also have a red $uvm2-v$ color is apparent.

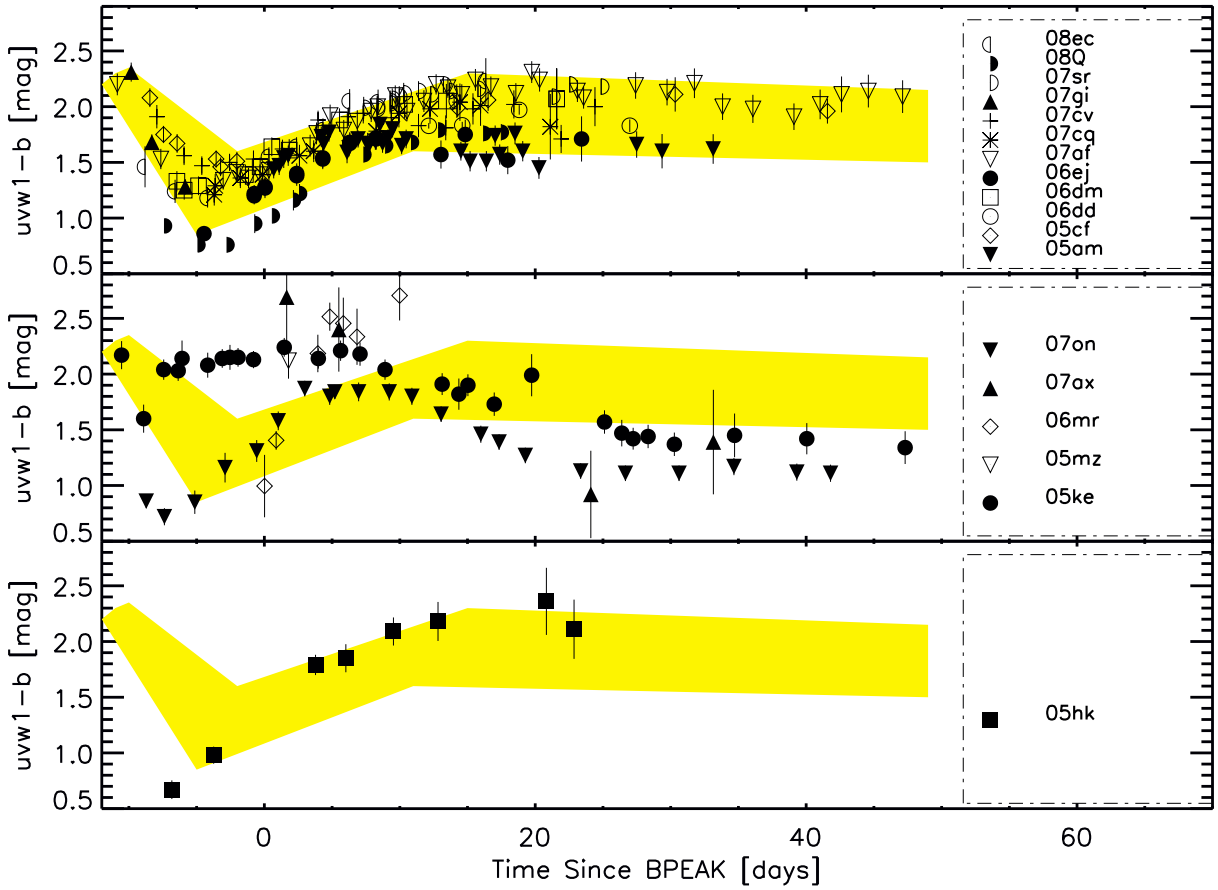


Fig. 26.— $uvw1 - b$ colors of 18 SNe Ia. Twelve normal SNe Ia are shown in the upper panel, five subluminous SNe Ia in the middle panel, and the SN 2002cx-like SN 2005hk in the lower panel. The range of the normal SNe Ia is shown as a shaded region.

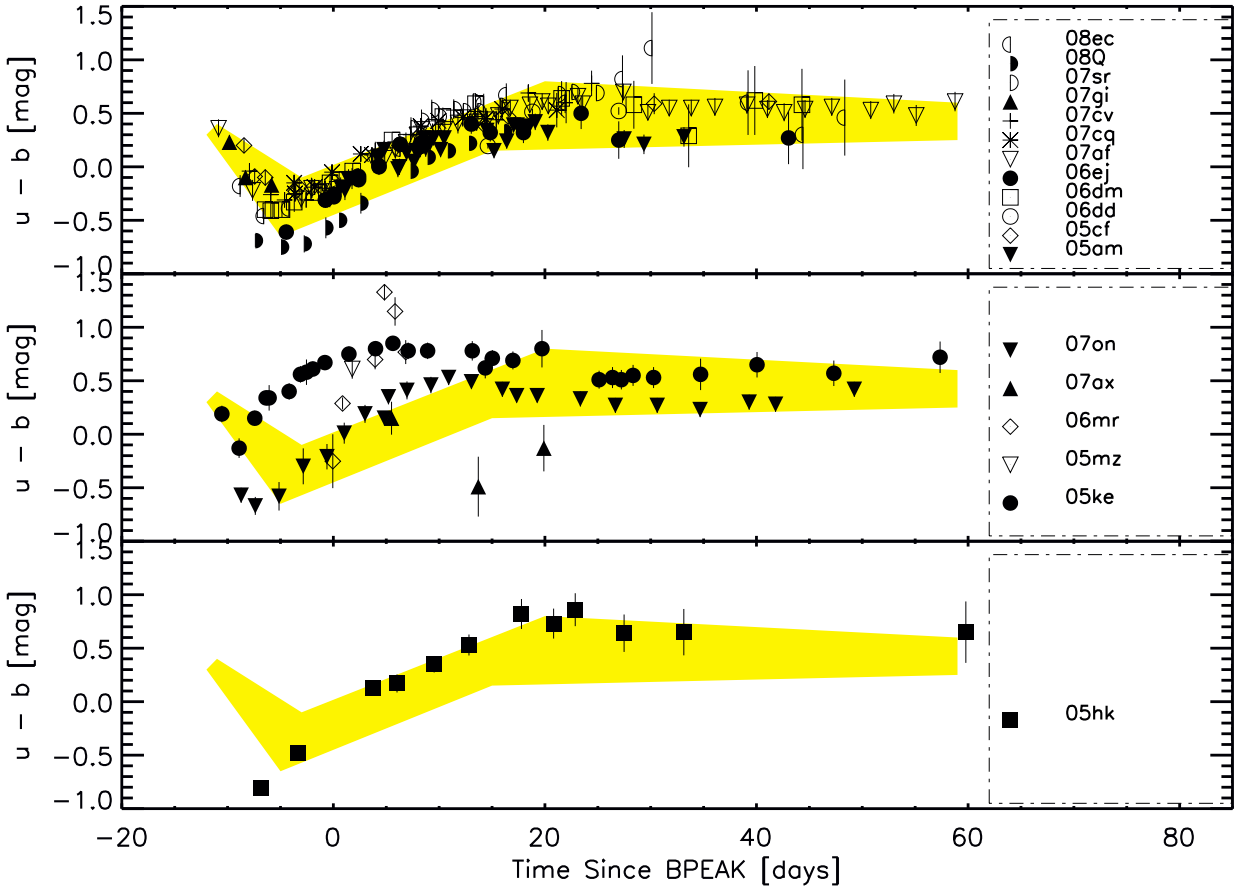


Fig. 27.— $u - b$ colors of 18 UVOT-observed SNe Ia. Twelve normal SNe Ia are shown in the upper panel, five subluminous SNe Ia in the middle panel, and the SN 2002cx-like SN 2005hk in the lower panel. The range of the normal SNe Ia is shown as a shaded region.

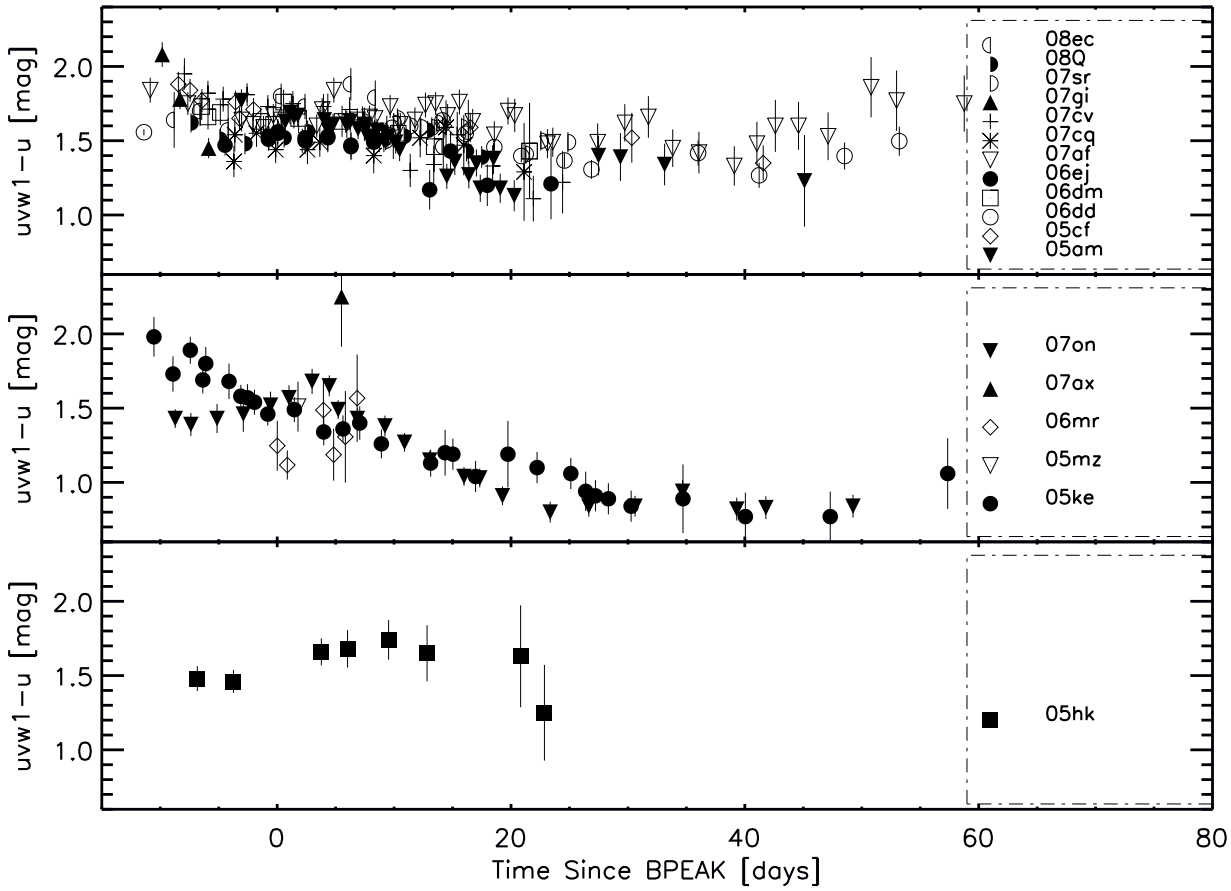


Fig. 28.— $uvw1 - u$ colors of 18 SNe Ia. Twelve normal SNe Ia are shown in the upper panel, three subluminous SNe Ia in the middle panel, and the SN 2002cx-like SN 2005hk in the lower panel. The normal SNe Ia gradually become bluer from the earliest epochs to +20 days. The subluminous SNe Ia appear to rapidly become bluer for all observed epochs. There is no clear trend in the SN 2002cx-like SN Ia.

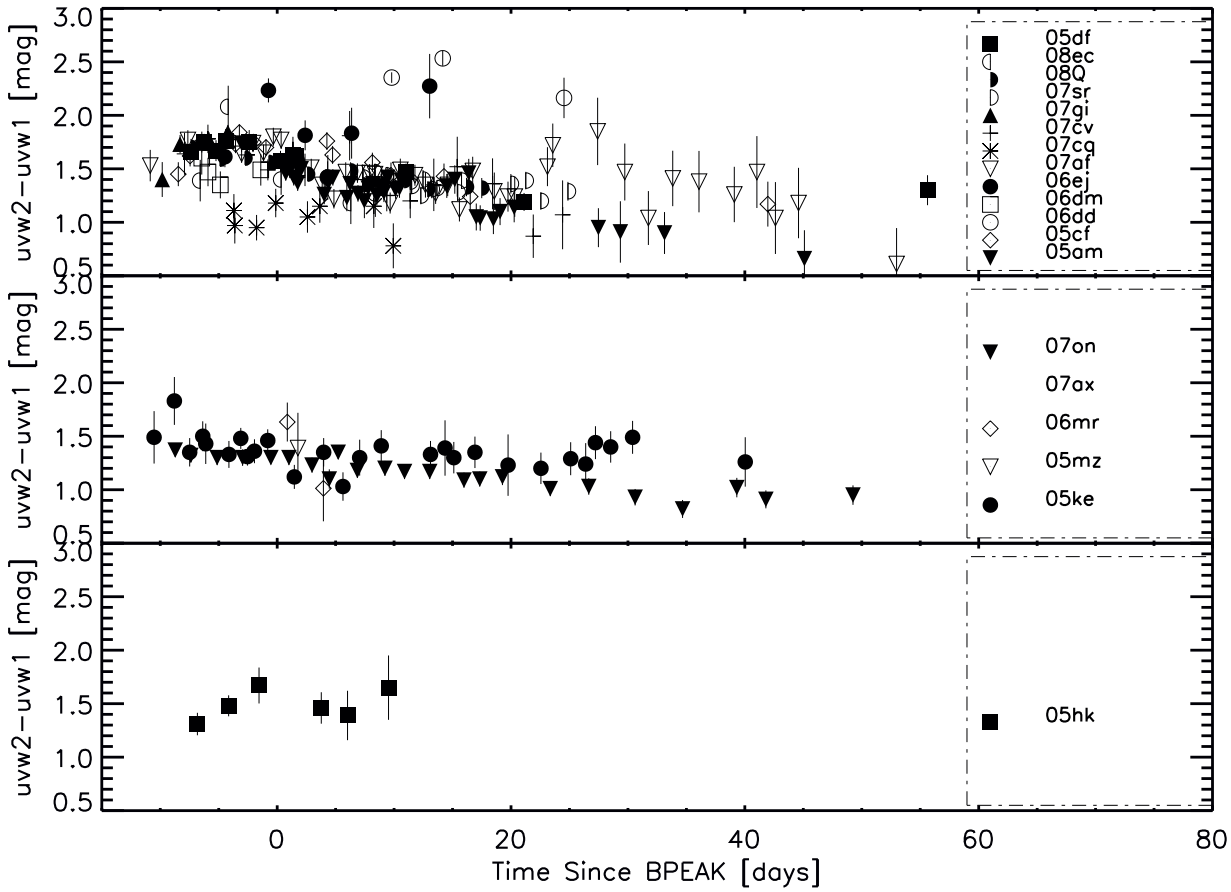


Fig. 29.— $uvw2 - uvw1$ colors of 16 SNe Ia. Nine normal SNe Ia are shown in the upper panel, three subluminous SNe Ia in the middle panel, and the SN 2002cx-like SN 2005hk in the lower panel.

## REFERENCES

Benetti, S., et al. 2004, MNRAS, 348, 261

Benetti, S., et al. 2005, ApJ, 623, 1011

Bloom, J. S., et al. 2006, in Astronomical Data Analysis Software and Systems XV, ed. C. Gabriel, et al. (San Francisco: ASP, Vol. 351), 751

Branch, D., & Venkatakrishna, K. L. 1986, ApJ, 306, L21

Brown, P. J., et al. 2005, ApJ, 635, 1192

Brown, P. J., et al. 2009, AJ, 137, 4517

Brown, P. J., et al. 2010, ApJ, accepted (B10)

Bufano, F., et al. 2009, ApJ, 700, 1456

Chornock, R., Filippenko, A. V., Branch, D., Foley, R. J., Jha, S., & Li, W., 2006, PASP, 118, 722

Contardo, G., Leibundgut, B., & Vacca, W. D., 2000, A&A, 359, 876

Feldmeier, J. J., Jacoby, G. H., & Phillips, M. M. 2007, ApJ, 657, 76

Filippenko, A. V., et al. 1992a, ApJ, 384, L15

Filippenko, A. V., et al. 1992b, AJ, 104, 1543

Filippenko, A. V. 1997, ARA&A, 35, 309

Filippenko, A. V., Li, W., Treffers, R.R., Modjaz, M. 2001, ASPC, 246, 121

Filippenko, A. V. 2003, in *From Twilight to Highlight: The Physics of Supernovae*, ed. W. Hillebrandt & B. Leibundgut (Berlin: Springer-Verlag), 171

Filippenko, A. V. 2005, in White Dwarfs: Cosmological and Galactic Probes, ed. E. M. Sion, S. Vennes, & H. L. Shipman (Dordrecht: Springer), 97

Fisher, A., Branch, D., Nugent, P., & Baron, E. 1997, ApJ, 481, L89

Foley, R. J., Filippenko, A. V., & Jha, S.W. 2008b, ApJ, 686, 467

Foley, R. J., et al. 2009, AJ, 138, 376

Folatelli, G., et al. 2010, AJ, 139, 120

Freedman, W. L., et al. 2001, ApJ, 553, 47

Gay-Yam, A., et al. 2008, ApJ, 685, L117

Garnavich, P. M., et al. 2004, ApJ, 613, 1120

Gehrels, N., et al. 2004, ApJ, 611, 1005

Gezari, S., et al. 2008, ApJ, 683, L131

Goldhaber, G., et al. 2001, ApJ, 558, 359

Hachinger, S., Mazzali, P. A., Tanaka, M., Hillebrandt, W., & Benetti, S. 2008, MNRAS, 389, 1087

Hachinger, S., Mazzali, P. A., Taubenberger, S., Pakmor, R., & Hillebrandt, W. 2008, MNRAS, 399, 1238

Hamuy, M., Phillips, M. M., Suntzeff, N. B., Schommer, R. A., Maza, J., & Aviles, R. 1996, AJ, 112, 2391

Hamuy, M., Phillips, M. M., Suntzeff, N. B., Schommer, R. A., Maza, J., Smith, R. C., Lira, P., & Aviles, R. 1996, AJ, 112, 2438

Hamuy, M., et al. 2006, PASP, 118, 2

icken, M, Wood-Vasey, W.M., Blondin, S.,

Hicken, M., Granavich, P., Prieto, J., Blondin, S., DePoy, D., Kirshner, R., Parrent, J. 2007, ApJ, 669, 17 Challis, P., Jha, S., Kelly, P.L., Rest, A., Kirshner, R. 2009, ApJ, 700, 1097

Höflich, P., Khokhlov, A., Wheeler, J. C., Phillips, M. M., Suntzeff, N. B., & Hamuy, M. 1996, ApJ, 472, L81

Howell, D. A., Höflich, P., Wang, L., & Wheeler, J. C. 2001, ApJ, 556, 302

Howell, D. A., et al. 2006, Nature, 443, 308

Immler, S., et al. 2006, ApJ, 648, L119

Immler, S., et al. 2007, ApJ, 664, 435

Jeffery, D. J., Leibundgut, B., Kirshner, R. P., Benetti, S., Branch, D., & Sonneborn, G. 1992, ApJ, 397, 304

Jha, S., et al. 2006a, AJ, 131, 527

Jha, S., et al. 2006b, AJ, 132, 189

Jha, S., et al. 2007, ApJ, 659, 122

Kasliwal, M., et al. 2008, ApJ, 683, L29

Kirshner, R. P., et al. 1993, ApJ, 415, 589

Krisciunas, K., Hastings, N. C., Loomis, K., McMillan, R., Rest, A., Riess, A. G., & Stubbs, C. 2000, ApJ, 539, 658

Krisciunas, K., Phillips, M. M., & Suntzeff, N. B. 2004, ApJ, 602, L81

Krisciunas, K. et al. 2009, AJ, 138, 1584

Leibundgut, B., et al. 1993, AJ, 105, 301

Lentz, E. J., Baron, E., Branch, D., & Haushildt, P. H. 2001, ApJ, 557, 266

Li, W., et al. 2001, PASP, 113, 1178

Li, W., et al. 2003, PASP, 115, 453

Lira, P. 1995, Masters thesis, Univ. Chile

Mazzali, P. A., Cappellaro, E., Danziger, I. J., Turatto, M., & Benetti, S. 1998, ApJ, 499, L49

Mazzali, P. A. 2000, A&A, 363, 705

Mazzali, P. A., Nomoto, K., Cappellaro, E., Nakamura, T., Umeda, H., & K. Iwamoto 2001, ApJ, 547, 988

Mazzali, P. A., et al. 2005, ApJ, 623, L37

Mazzali, P. A., Sauer, D.N., Pastorello, A., Benetti, S., Hillebrandt, W. 2008, MNRAS, 386, 1897

Milne, P.A., The, L. S., & Leising, M.D. 2001, ApJ, 559, 1019

Nugent, P., Phillips, M., Baron, E., Branch, D., & Hauschild, P. H. 1995, ApJ, 455, L147

Panagia, N. 2007, in Supernova 1987A: 20 Years After, ed. S. Immler, K. Weiler, & R. McCray (New York: AIP, Vol. 937), 236

Pauldrach, A. W. A., Duschinger, M., Mazzali, P.A., Puls, J., Lennon, M., Miller, D.L. 1996, A&A, 312, 525

Pastorello, A., et al. 2007, MNRAS, 376, 1301

Perlmutter, S., et al. 1999, ApJ, 517, 565

Phillips, M. M. 1993, ApJ, 413, L105

Phillips, M. M., Lira, P., Suntzeff, N. B., Schommer, R. A., Hamuy, M., & Maza, J. 1999, AJ, 118, 1766

Phillips, M. M., et al. 1987, PASP, 99, 592

Phillips, M. M., et al. 1992, AJ, 103, 1632

Phillips, M. M., et al. 2007, PASP, 119, 360

Pinto, P. A., & Eastman, R. G., 2000, ApJ, 530, 757

Poole, T., et al. 2008, MNRAS, 383, 627

Pskovskii, Yu. P., 1984, Soviet Astron., 28, 658

Riess, A. G., Press, W. H., & Kirshner, R. P. 1996, ApJ, 473, 88

Riess, A. G., et al. 1998, AJ, 116, 1009

Riess, A. G., et al. 2005, ApJ, 627, 579

Riess, A. G., et al. 2009, ApJ, 699, 539

Roming, P. W. A., et al. 2005, Space Science Reviews, 120, 95

Roming, P. W. A., Gronwall, C., vanden Berk, D. E., Page, M. J., & Boyd, P. T. 2009, A&SS, 320, 203

Sahu, D. K., Tanaka, M., Anupama, G. C., Kawabata, K. S., Maeda, K., Tominaga, N., Nomoto, K., Mazzali, P. A., Prabhu, T. P., 2008, ApJ, 680, 580

Salvo, M. E., et al. 2001, MNRAS, 321, 254

Sauer, D. N., Mazzali, P. A., Blondin, S., Filippenko, A. V., Benetti, S., Stehle, M., Challis, P., Kirshner, R. P., & Li, W. 2008, MNRAS, 391, 1605

Schweizer, F., et al. 2008, AJ, 136, 1482

Simon, J. D., et al. 2007, ApJ, 671, L25

Sollerman, J., et al. 2004, A&A, 426, 547

Stanishev, V., et al. 2007, in The Multicolored Landscape of Compact Objects and Their Explosive Origins, ed. ed. T. Di Salvo, et al. (New York: AIP, Vol. 924), 336

Stanishev, V., et al. 2008, AIPC, 924, 336

Stritzinger, M., et al. 2002, AJ, 124, 2100

Suntzeff, N. B., 1996, in Supernovae and Supernova Remnants. ed. R. McCray & Z. Wang (Cambridge: Cambridge Univ. Press), p. 41

Valenti, S., et al. 2009,

Wang, L., Goldhaber, G., Aldering, G., & Perlmutter, S. 2003, ApJ, 590, 944

Wang, L., Strovink, M., Conley, A., Goldhaber, G., Kowalski, M., Perlmutter, S. & Siegrist, J. 2006, ApJ, 641, 50

Wang, X., et al. 2008, ApJ, 675, 626

Wang, X., et al. 2009a, ApJ, 697, 380

Wang, X., et al. 2009b, ApJ, 699, L139

Wood-Vasey, W. M., et al. 2008, ApJ, 689, 377

Yamanaka, M., et al. 2009, ApJ, 707, L118

Zhang, T. et al. 2010, PASP, 122, 1

## APPENDIX A: UVOT Photometry for 6 SNe Ia

Here we present UVOT photometry for six SNe Ia that were not included in the Brown et al. (2009) survey. The underlying galaxy light has been subtracted (Brown et al. 2009) and the magnitudes calibrated to the UVOT Vega system (Poole et al. 2008).

Table A-1: UVOT Photometry of Six SNe Ia

SN 2005mz

| JD−2,450,000 [days] | $uvw2$ [mag][a] | $uvm2$ [mag][a] | $uvw1$ [mag][a] | $u$ [mag][a] | $b$ [mag][a] | $v$ [mag][a] |
|---|---|---|---|---|---|---|
| 3742.43 | 20.18(19) | ... | ... | ... | ... | ... |
| 3747.74 | 20.67(30) | ... | 19.28(17) | 17.77(07) | 17.16(06) | 16.57(06) |

SN 2007on

| JD−2,450,000 [days] | $uvw2$ [mag][a] | $uvm2$ [mag][a] | $uvw1$ [mag][a] | $u$ [mag][a] | $b$ [mag][a] | $v$ [mag][a] |
|---|---|---|---|---|---|---|
| 4411.28 | 16.64(05) | 16.91(04) | 15.27(04) | 13.84(05) | 14.41(05) | 14.50(04) |
| 4412.62 | 16.05(04) | 16.24(04) | 14.73(05) | 13.34(06) | 14.01(06) | 14.06(04) |
| 4414.87 | 15.64(05) | 15.82(04) | 14.34(05) | 12.91(09) | 13.49(10) | 13.52(05) |
| 4417.04 | 15.62(05) | 15.82(04) | 14.32(06) | 12.86(11) | 13.16(13) | 13.27(06) |
| 4419.46 | 15.79(04) | 16.04(04) | 14.49(05) | 12.97(08) | 13.18(09) | 13.10(06) |
| 4421.00 | 16.02(05) | 16.15(05) | 14.72(05) | 13.15(07) | 13.14(07) | 13.06(05) |
| 4422.98 | 16.40(05) | 16.60(05) | 15.17(05) | 13.49(07) | 13.30(05) | 13.10(05) |
| 4424.45 | 16.42(07) | 16.76(011) | 15.32(06) | 13.67(04) | — | 13.12(04) |
| 4425.22 | 16.71(05) | 16.89(05) | 15.36(04) | 13.87(05) | 13.52(05) | 13.21(05) |
| 4426.86 | 16.80(05) | 17.03(05) | 15.62(05) | 14.19(05) | 13.78(07) | 13.27(05) |
| 4429.22 | 17.27(05) | 17.45(06) | 16.07(05) | 14.69(05) | 14.23(06) | 13.55(05) |
| 4430.90 | 17.37(05) | 17.38(06) | 16.20(05) | 14.93(04) | 14.40(06) | 13.61(05) |
| 4433.05 | 17.58(05) | 17.60(07) | 16.41(05) | 15.26(04) | 14.77(05) | 13.78(04) |
| 4435.98 | 17.69(05) | 17.70(06) | 16.60(05) | 15.56(04) | 15.14(06) | 14.04(05) |
| 4437.33 | 17.77(05) | 17.76(07) | 16.67(05) | 15.64(04) | 15.28(05) | 14.17(05) |
| 4439.27 | 17.85(06) | 17.90(08) | 16.73(05) | 15.82(04) | 15.46(05) | 14.36(04) |
| 4443.36 | 17.91(05) | 17.86(07) | 16.90(05) | 16.10(05) | 15.77(05) | 14.73(04) |
| 4446.66 | 18.08(06) | 18.08(08) | 17.05(05) | 16.21(05) | 15.94(05) | 14.94(04) |
| 4450.62 | 18.13(06) | 18.08(08) | 17.20(05) | 16.36(05) | 16.09(05) | 15.13(04) |
| 4454.67 | 18.23(06) | 18.20(09) | 17.41(06) | 16.47(05) | 16.24(05) | 15.28(04) |
| 4459.32 | 18.45(07) | 18.30(09) | 17.43(06) | 16.61(05) | 16.31(05) | 15.47(05) |
| 4461.80 | 18.50(06) | 18.45(09) | 17.59(06) | 16.76(05) | 16.48(05) | 15.51(04) |
| 4469.25 | 18.75(07) | 18.92(11) | 17.80(06) | 16.96(05) | 16.54(05) | 15.74(05) |

[a]Uncertainties are in units of 0.01 mag.

## APPENDIX B: ANU Photometry of SN 2005df

We present photometry and light curve fitting results for SN 2005df, as obtained with the Australian National University 2.3 m and 1 m telescopes at Siding Springs.

Table A-2: UVOT Photometry of 6 SNe Ia (continued)

| SN 2007sr | | | | | | |
|---|---|---|---|---|---|---|
| JD−2,450,000 [days] | $uvw2$ [mag][a] | $uvm2$ [mag][a] | $uvw1$ [mag][a] | $u$ [mag][a] | $b$ [mag][a] | $v$ [mag][a] |
| 4455.33 | 16.54(04) | 17.41(07) | 15.12(04) | 13.49(05) | 13.13(09) | 12.84(05) |
| 4456.33 | 16.68(04) | 17.46(07) | 15.21(04) | 13.64(05) | 13.21(09) | 12.86(05) |
| 4456.34 | — | — | 15.19(04) | — | — | — |
| 4457.27 | 16.80(04) | 17.53(07) | 15.36(04) | 13.84(04) | 13.31(09) | 12.96(05) |
| 4457.30 | — | — | 15.34(04) | — | — | — |
| 4457.96 | 16.83(04) | 17.69(07) | 15.38(04) | 13.82(05) | 13.35(08) | 12.97(05) |
| 4457.98 | — | — | 15.44(04) | — | — | — |
| 4458.61 | — | — | 15.47(04) | — | — | — |
| 4459.38 | 16.97(04) | 17.90(08) | 15.59(04) | 13.99(04) | 13.45(08) | 13.01(05) |
| 4459.62 | 16.93(06) | 17.99(09) | — | — | — | — |
| 4460.29 | — | 18.01(13) | 15.70(05) | 14.11(04) | 13.59(05) | 13.11(04) |
| 4460.66 | 17.10(07) | 17.96(08) | — | — | — | — |
| 4461.23 | 17.13(06) | 18.14(14) | 15.82(05) | 14.23(04) | 13.62(05) | 13.11(04) |
| 4461.66 | 17.20(05) | 18.15(10) | 15.88(04) | 14.26(04) | 13.74(06) | 13.20(04) |
| 4463.09 | — | 18.35(11) | — | — | — | — |
| 4463.77 | 17.53(06) | 18.19(11) | 16.14(05) | 14.55(04) | 13.98(05) | 13.35(04) |
| 4467.99 | 17.92(07) | 18.71(17) | 16.56(05) | — | — | — |
| 4469.26 | 18.15(06) | 19.07(14) | 16.76(05) | 15.35(04) | 14.67(04) | 13.69(04) |
| 4470.55 | 18.12(06) | 19.08(014) | 16.92(05) | 15.42(04) | 14.72(04) | 13.66(04) |
| 4472.87 | 18.41(07) | 19.61(018) | 17.12(05) | 15.63(04) | 14.94(04) | 13.77(04) |

| SN 2008A | | | | | | |
|---|---|---|---|---|---|---|
| JD−2,450,000 [days] | $uvw2$ [mag][a] | $uvm2$ [mag][a] | $uvw1$ [mag][a] | $u$ [mag][a] | $b$ [mag][a] | $v$ [mag][a] |
| 4473.11 | 19.26(16) | 19.25(21) | 17.91(07) | 16.25(04) | 16.79(05) | 16.75(08) |
| 4474.60 | 19.24(10) | 19.24(13) | 17.96(07) | 16.24(04) | 16.66(04) | 16.65(05) |
| 4476.58 | 19.39(11) | 19.78(17) | 18.18(08) | 16.30(04) | 16.54(04) | 16.47(05) |
| 4478.12 | 19.45(16) | — | — | — | — | — |
| 4478.62 | 19.43(11) | 19.66(17) | 18.23(08) | 16.37(04) | 16.49(04) | 16.29(05) |
| 4480.60 | 20.09(19) | 20.04(21) | 18.41(08) | 16.53(04) | 16.54(04) | 16.27(05) |
| 4483.40 | 20.06(25) | — | 18.92(18) | 17.04(07) | 16.73(05) | 16.19(06) |
| 4484.42 | 20.07(16) | 20.81(35) | 18.84(11) | 17.03(05) | 16.76(04) | 16.23(05) |
| 4486.99 | 20.26(20) | — | 19.57(22) | 17.47(06) | 17.10(05) | 16.26(05) |
| 4490.84 | — | 21.00(34) | 20.02(24) | 18.36(08) | 17.58(06) | 16.47(06) |
| 4493.12 | — | — | — | 18.64(10) | 18.03(07) | 16.74(06) |
| 4494.86 | — | — | — | 18.71(19) | 18.07(13) | — |
| 4497.13 | — | — | — | 19.35(17) | 18.52(10) | 16.99(08) |

[a]Uncertainties are in units of 0.01 mag.

Table A-3: UVOT Photometry of 6 SNe Ia (continued)

SN 2008Q

| JD−2,450,000 [days] | $uvw2$ [mag][a] | $uvm2$ [mag][a] | $uvw1$ [mag][a] | $u$ [mag][a] | $b$ [mag][a] | $v$ [mag][a] |
|---|---|---|---|---|---|---|
| 4496.63 | 17.85(06) | 18.76(14) | 16.15(04) | 14.53(04) | 15.22(04) | 15.22(04) |
| 4499.11 | 16.81(04) | 17.33(07) | 15.22(04) | 13.71(05) | 14.46(05) | 14.46(04) |
| 4501.25 | 16.49(04) | 16.98(06) | 14.89(04) | 13.41(05) | 14.13(05) | 14.12(04) |
| 4503.29 | 16.39(04) | — | 14.83(04) | 13.31(06) | 13.88(07) | 13.89(04) |
| 4504.59 | 16.45(05) | 16.79(08) | 14.88(04) | 13.36(04) | 13.86(05) | 13.80(04) |
| 4505.74 | 16.58(05) | 16.92(06) | 15.00(05) | — | — | — |
| 4506.60 | 16.51(04) | 17.00(05) | 15.06(04) | 13.50(06) | 13.84(07) | 13.80(04) |
| 4510.29 | 16.97(07) | — | 15.49(04) | — | — | — |
| 4511.35 | 17.00(04) | 17.51(07) | 15.65(04) | 14.04(04) | 14.08(05) | 13.88(04) |
| 4512.96 | 17.22(05) | 17.64(07) | 15.86(04) | 14.30(04) | 14.21(05) | 13.95(04) |
| 4514.87 | 17.51(05) | 17.95(07) | 16.12(04) | 14.59(04) | 14.44(05) | 14.08(04) |
| 4516.88 | 17.75(05) | 18.15(08) | 16.44(04) | 14.87(04) | 14.65(05) | 14.26(04) |
| 4520.20 | 18.25(06) | 18.48(09) | 16.92(05) | 15.49(04) | 15.16(04) | 14.47(04) |
| 4521.50 | 18.43(07) | 17.11(05) | — | 15.72(04) | 15.34(04) | 14.54(04) |

SN 2008ec

| JD−2,450,000 [days] | $uvw2$ [mag][a] | $uvm2$ [mag][a] | $uvw1$ [mag][a] | $u$ [mag][a] | $b$ [mag][a] | $v$ [mag][a] |
|---|---|---|---|---|---|---|
| 4663.19 | — | — | 18.82(19) | 17.18(07) | 17.36(07) | 17.33(12) |
| 4665.41 | 19.30(18) | 19.52(36) | 17.91(10) | 16.21(05) | 16.67(05) | 16.58(07) |
| 4667.81 | 19.49(21) | 19.82(36) | 17.41(07) | 15.84(05) | 16.23(05) | 16.19(06) |
| 4672.34 | 18.81(13) | — | 17.41(07) | 15.61(05) | 15.86(05) | 15.74(05) |
| 4674.38 | 18.97(14) | — | 17.48(08) | 15.75(05) | 15.84(05) | 15.67(05) |
| 4676.33 | 19.11(20) | — | 17.69(10) | 15.98(05) | 15.90(05) | 15.71(06) |
| 4678.30 | 19.23(18) | — | 18.05(11) | 16.17(05) | 16.00(05) | 15.72(05) |
| 4680.40 | 19.46(20) | — | 18.19(11) | 16.40(05) | 16.15(05) | 15.74(05) |
| 4681.81 | — | — | 18.43(13) | — | — | — |
| 4683.91 | — | — | 18.41(17) | — | — | — |
| 4686.21 | — | — | 18.72(16) | 17.26(07) | 16.67(06) | 16.16(11) |
| 4688.35 | — | — | 19.23(22) | 17.67(09) | 17.00(07) | 16.29(06) |
| 4694.00 | — | — | — | 18.37(17) | 17.77(11) | 16.65(12) |
| 4699.33 | — | — | — | 18.92(21) | 18.10(11) | 16.87(08) |
| 4702.12 | — | — | — | 19.61(35) | 18.50(13) | 17.22(10) |
| 4711.20 | — | — | — | 19.33(27) | 18.73(16) | 17.55(12) |
| 4716.39 | — | — | — | 19.28(26) | 18.98(20) | 17.76(14) |
| 4720.34 | — | — | — | 19.42(31) | 18.96(20) | 18.01(17) |

[a]Uncertainties are in units of 0.01 mag.

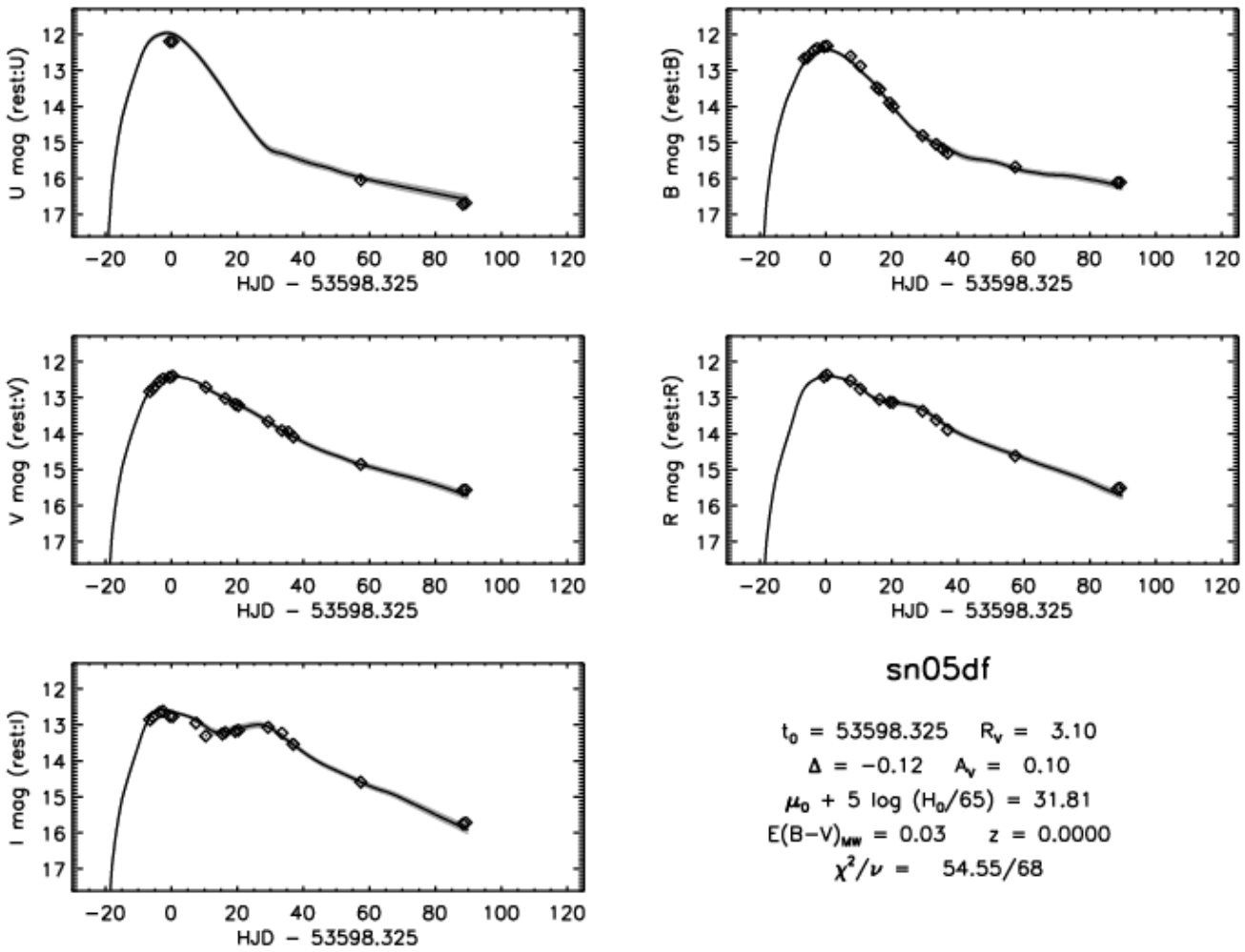


Fig. B-1.— $UBVRI$ light curves of SN 2005df. The light curves were fitted with the MLCS2k2 routine to estimate the date of maximum brightness peak magnitude ($B_{\rm peak}$), extinction, and $\Delta$ value, as shown.

Table B-1: ANU Photometry of SN 2005df

| MJD [days] | Phase[a] [days] | $U$ [mag] | $B$ [mag] | $V$ [mag] | $R$ [mag] | $I$ [mag] | Inst. |
|---|---|---|---|---|---|---|---|
| 53591.79 | -7 | — | 12.68(0.04) | 12.82(0.02) | — | 12.82(0.01) | 1m+SITE |
| 53592.76 | -6 | — | 12.65(0.02) | 12.73(0.01) | — | 12.75(0.01) | 1m+SITE |
| 53594.75 | -4 | — | 12.45(0.02) | 12.54(0.01) | — | 12.63(0.01) | 1m+SITE |
| 53595.75 | -3 | — | 12.39(0.01) | 12.47(0.01) | — | 12.59(0.01) | 1m+SITE |
| 53597.79 | -1 | 12.24(0.02) | 12.33(0.03) | 12.42(0.02) | 12.41(0.02) | 12.72(0.02) | 2.3m+Im |
| 53598.70 | 0 | 12.24(0.03) | 12.32(0.02) | 12.39(0.01) | 12.36(0.01) | 12.73(0.01) | 2.3m+Im |
| 53605.79 | 7 | — | 12.60(0.04) | — | 12.53(0.01) | 12.93(0.01) | 1m+WFI |
| 53608.76 | 10 | — | 12.89(0.02) | 12.70(0.02) | 12.75(0.02) | 13.30(0.02) | 2.3m+Im |
| 53613.72 | 15 | — | 13.46(0.01) | — | — | 13.27(0.01) | 1m+WFI |
| 53614.63 | 16 | — | 13.52(0.02) | 13.02(0.01) | 13.05(0.01) | 13.24(0.01) | 1m+WFI |
| 53617.68 | 19 | — | 13.88(0.02) | 13.20(0.01) | 13.11(0.01) | 13.20(0.01) | 1m+WFI |
| 53618.66 | 20 | — | 14.00(0.05) | 13.25(0.01) | 13.12(0.01) | 13.17(0.01) | 1m+WFI |
| 53627.62 | 29 | — | 14.79(0.01) | 13.71(0.01) | 13.34(0.00) | 13.09(0.01) | 1m+WFI |
| 53631.78 | 33 | — | 15.04(0.03) | 13.96(0.01) | 13.59(0.01) | 13.26(0.01) | 1m+WFI |
| 53633.76 | 35 | — | 15.11(0.04) | 14.06(0.05) | — | — | 1m+SITE |
| 53635.25 | 36 | — | 15.22(0.05) | 14.19(0.02) | 13.88(0.01) | 13.59(0.03) | 1m+SITE |
| 53655.72 | 57 | 16.05(0.05) | 15.72(0.04) | 14.86(0.01) | 14.62(0.01) | 14.58(0.01) | 2.3m+Im |
| 53686.68 | 88 | 16.72(0.04) | 16.14(0.03) | 15.60(0.04) | 15.56(0.03) | 15.78(0.02) | 2.3m+Im |
| 53687.51 | 89 | 16.70(0.05) | 16.14(0.05) | 15.59(0.03) | 15.54(0.03) | 15.75(0.01) | 2.3m+Im |
| 53742.60 | 144 | 18.07(0.05) | — | 16.72(0.07) | 17.08(0.04) | 17.27(0.05) | 2.3m+Im |
| 53773.44 | 174 | — | 15.72(0.04) | 17.46(0.03) | — | 17.64(0.03) | 2.3m+Im |
| 53831.86 | 233 | — | — | 18.08(0.04) | 18.45(0.06) | — | 2.3m+Im |

[a]Phase relative to the fitted $B_{\rm peak}$.